Polarisation Resolved Ultrafast Spectroscopic Investigation of Photoinduced Structural Dynamics in DCM dye

A thesis submitted for the degree of

Doctor of Philosophy

by

David McDonald

Centre for Atom Optics and Ultrafast Spectroscopy

Faculty of Engineering and Industrial Sciences

Swinburne University of Technology

Melbourne, Australia

November 27, 2013

"If you get there before me, could you save me a seat?"

— John Darnielle, Shadow Song

"You can know the name of a bird in all the languages of the world, but when you're finished, you'll know absolutely nothing whatever about the bird. So let's look at the bird and see what it's doing - that's what counts"

— Richard Feynman, The Pleasure of Finding Things Out

Declaration

I, David Luke McDonald, declare that this thesis entitled:

"Polarisation Resolved Ultrafast Spectroscopic Investigation of Photoinduced Structural Dynamics in DCM dye"

is my own work and has not been submitted previously, in whole or in part, in respect of any other academic award.

David McDonald

Centre for Atom Optics and Ultrafast Spectroscopy
Faculty of Engineering and Industrial Sciences
Swinburne University of Technology
Melbourne, Australia

Dated this day, November 27, 2013

Abstract

This thesis reports on the results of steady-state, polarisation and time-resolved spectroscopic investigations of the excited-state configurational dynamics of the well-known donor-acceptor dye molecule DCM. The aim of this study was to investigate the structural configuration of the excited-state or DCM and add to the discussion about the proposed, but controversial, existence of a twisted intramolecular charge transfer (TICT) state in this molecule.

Using a suite of purpose built laser spectroscopy experiments, the spectral dynamics of DCM and a planar, conformationally-restricted analogue molecule were probed. Steady-state, time-resolved fluorescence and pump-supercontinuum-probe measurements were made on the molecules in a range of solvents. Further information was obtained by analysing the polarisation-dependence of these signals in order to determine the time-dependent anisotropy $r(t)$ - a parameter that has features and dynamics determined by the transition dipole moment of the probe molecule and the rotational diffusion of the molecules in solution.

By performing a number of different solvent dependent measurements focussing on various solvent parameters, the dynamics and the features seen were attributed to the viscosity, dielectric constant and dipole moment of the solvent. The de-convoluted dynamics were then compared with that of the planar twist-restricted molecule, DCJ.

Analysis of the data, produced strong evidence to support the formation of

an intramolecular charge transfer (ICT) state after photoexcitation. However, the results indicate that the ICT state of DCM does not involve a twisting conformation about the dimethylamino bond, despite this being the twist position most often cited in the literature with regards to a TICT in this molecule.

Acknowledgements

The preparation of this thesis has been a long journey for me. I began my PhD research project as a humble chemistry graduate and was told that learning the ins and outs of ultrafast laser spectroscopy would involve a very steep learning curve. It did indeed. Despite the intervening time, sidetracks and the stress that this work has caused me over the years, I did gain a lot of valuable knowledge, maturity and confidence. There are many people who supported me on this crusade of scientific endeavour.

A PhD candidate's life can seem a solitary one. When one cannot communicate to the lay person of the frustration when an obscure experiment doesn't work without first teaching them the fundamentals of molecular spectroscopy, such frustrations are often left unspoken. Nevertheless, the people around me supported my efforts by sharing good times, good beers and just generally being good friends. Without the assistance of my fellow PhD candidates and the support of my family and wonderful friends I don't think I would have stuck it out and completed this document. I would therefore like to take this opportunity to recognise their contribution.

I'd first like to thank my supervisors Professor Lap Van Dao and Professor Peter Hannaford from the Centre for Atom Optics and Ultrafast Spectroscopy (CAOUS) at Swinburne University for introducing me to the extremely interesting world of ultrafast lasers and chemical physics. These were not easy concepts to grasp but Lap and Peter gave me invaluable assistance in learning the necessary skills and theory to accomplish my project.

My friends, peers and colleagues at CAOUS were always willing to help with

technical know-how, advice and the sharing of highly caffeinated drinks during late night experimental runs in the lab. The members of the ultrafast group - Tra My Do, Xiao Min Wen, Chris Hall and Craig Lincoln - were particularly helpful.

I would particularly like to acknowledge the help and support of Dr. Jeff Davis for many patient and fruitful discussions as my experimental work progressed, assistance in the the collating and analysis of data and the frank suggestions about the viability of the various explanations of my data that I proposed.

Also huge thanks must go to my good friends and colleagues Daniel White, Michael Volk and Annelene Dethlefsen for good times at Haddons bar on Fridays after those long weeks in the lab, for countless conversations about my work and for encouragement and the gentle nudge and reminders I needed along the way.

I would like to thank my mum, dad, siblings and their partners for all their support, love and encouragement. Thank you for believing in me!

Finally, I would like to thank my amazing and wonderful wife Sarah for her unwavering support, persistence and patience with me as I spent much of my time in the study poring over graphs, figures and techno-babble buzzwords that she didn't understand. Despite this inability to communicate what it is I was writing day-in, day-out, this whole process would have been so much harder without you here. You are the best! Thank you and I love you!

David Luke McDonald
Melbourne, Australia
November 27, 2013

Contents

List of Figures

List of Tables

Chapter 1

Introduction

The photochemistry and photophysics of molecules has been a topic of interest for many years. The understanding of the processes that underlie photosynthesis in plants [1], the design of more efficient organic displays [2, 3, 4] and solar cells [5, 6] and the development of chemistries for meta-materials with novel optical properties requires an intimate knowledge of the events that occur when the system absorbs (or emits) a photon. Study of the photo-excitation and subsequent relaxation of molecules also gives fundamental insights into the mechanisms and variables that affect these processes. By exploiting this knowledge, new compounds can be designed with specific photochemical properties.

Many of the important photochemical and photophysical processes occur on extremely fast time scales. One reason for this is that many photochemical reactions are unimolecular i.e. they do not rely on chance collisions between reactants. The timescales involved thus depend on the very fast rearrangement of electrons and (sometimes) atoms. Reactions that occur on these timescales are difficult to analyse using steady-state absorption and fluorescence spectroscopy, as short-lived intermediates states only have a small contribution to the time-integrated spectrum.

The development of ultrashort high repetition rate pulsed lasers allows direct spectroscopic observation of dynamics on extremely short time-scales. With the current generation of lasers now capable of producing pulses of visible light with a duration of just a few femtoseconds [7], where 1 fs is equal to 10^{-15} s, the range of phenomena that can be studied is growing all the time. Femtosecond laser systems are now relatively common-place in research labs around the world and their use and application to the study of chemical and material dynamics has become widespread.

The interest in femtosecond pulsed lasers in the chemistry community is due to the fact that the dynamics associated with electronic transitions, atomic vibrations and the relaxation of excited-states within molecules occur on this timescale. Femtosecond time-resolved spectroscopy is thus the ideal technique to study the very fast initial processes that occur in photochemical reactions such as those involved in photosynthesis and fundamental details on the energetics and motion of molecules in excited-states.

Donor-acceptor molecules are compounds that contain both electron-donor and electron-acceptor groups. When promoted to the excited-state, a charge migrates to (or towards) the acceptor creating a charge separated zwitterion or a highly polar state. One goal of developing these compounds is to extend the lifetime of the charge separated state in order to use it to do useful work such as producing an electrical current for organic solar cells [8].

The objective of this project is to study transient **configurational changes** in the substituted stilbenoid dye DCM [9] in order to better understand the dynamics and mechanisms of processes leading to emission. In particular, the thesis aims to investigate evidence for the popular, but controversial, twisted intramolecular charge transfer (TICT) model [10, 11, 12] for excited-state charge transfer in conjugated aromatic donor acceptor compounds, and whether it is a valid explanation for the excited-state of DCM.

In order to address this question, the study incorporates results from various spectroscopic methods based on a pulsed femtosecond laser system. These include polarisation resolved streak camera time-resolved fluorescence and pump-supercontinuum-probe, as well as steady-state absorption and fluorescence measurements.

The thesis will present a progression of experiments designed to examine the strong effect of solvent environment on the excited-state of DCM. An overview of the thesis chapters and the logical steps followed is shown below:

After a review of the literature regarding DCM and similar TICT compounds, this study has been undertaken to provide further evidence to resolve the controversy [13, 14, 15] about the TICT model in DCM.

Chapter 4 presents data on DCM dissolved in methanol to highlight the features seen with each experiment described in chapter 3. Methanol is a common and well understood solvent to use for solvation studies [16, 17, 18] and previous studies of DCM have tended to use methanol as a solvent [19, 20, 21]. This data provides a baseline for the comparative study against the parameters investigated in the later results chapters. Some ambiguities about the origin of certain spectral and time-resolved features were discovered in this initial data-set and subsequent experiments were designed to determine the processes that cause them by eliminating variables in a systematic manner.

Chapter 5 is focussed on the effect of solvent viscosity on the features from the methanol chapter. An increase in viscosity slows diffusion rates of solvent and solute within the sample volume. The aim of this chapter is to characterise which excited-state relaxation processes are diffusion dependent in order to account for the effect of viscosity when the other parameters were studied.

This leads into chapter 6, in which the effect of solvent dipole moment and dielectric properties is determined. The dipole moment of a solvent directly

determines its ability to stabilise highly polar excited-state such as the one proposed for DCM. Thus the solvent polarity dependence allows control over the extent to which charge transfer can occur.

Chapter 7 concludes the results section with a comparison between the excited-state of DCM and an analogue compound, DCJ. DCJ has a structure which restricts the rotation of the bond commonly associated with the TICT mechanism in DCM. One would thus expect the dynamics to be quite different in the two compounds. Some interesting results were found.

Chapter 8 concludes the thesis by summarising the results of the data analysis, stating the conclusions of the study and giving some suggestions for further work that could be done to clarify points that were beyond the scope of this work.

Portions of this work were presented at the 8th Femtochemistry and Femtobiology conference in Oxford, UK [22] and the 15th International Conference on Ultrafast Phenomena [23].

Chapter 2

Background

2.1 DCM

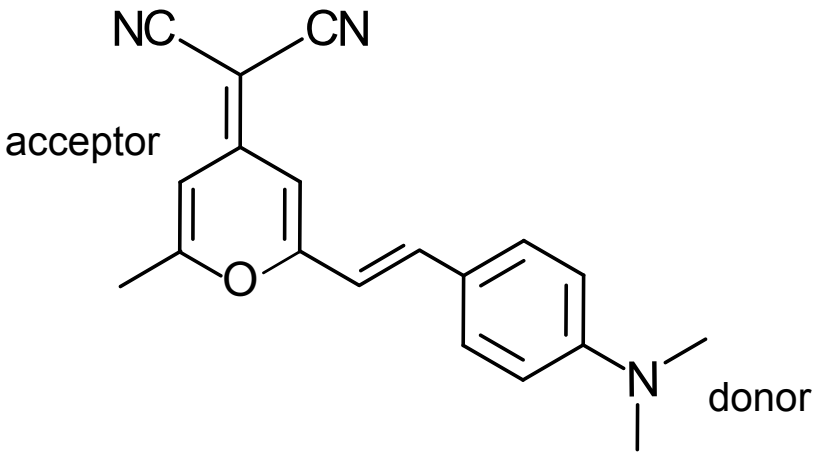

Figure 2.1: *Chemical structure of fluorescent dye DCM*

DCM or 4-(dicyanomethylene)- 2-methyl-6-(p-dimethylaminostyryl)-4H-pyran is a fluorescent dye that was developed by the Eastman-Kodak company in the mid-1970s by Webster et al. [9] to extend the tunable range of dye lasers into the red range of the visible spectrum. When dissolved in a polar solvent such as methanol and excited with light of the appropriate energy, its spectral

properties are characterised by a highly efficient [24, 25], broad fluorescence band, a relatively long excited-state lifetime [19] and a large solvent dependent Stokes shift [11] (the energy difference between absorption and fluorescence). This molecule has experienced considerable interest in the research community regarding the energy, molecular configuration and dynamics of the excited-states that give rise to the emission.

DCM is an example of a donor-π-bridge-acceptor molecule. It consists of an electron-donating dimethylamino group and an electron-accepting dicyano group, separated by a conjugated bridge (Fig 2.1)[9]. Such systems are expected to undergo photoinduced intramolecular charge transfer (ICT), in which the excited free electron migrates from the donor to acceptor (Fig 2.2) before relaxing back to a less polar ground-state.

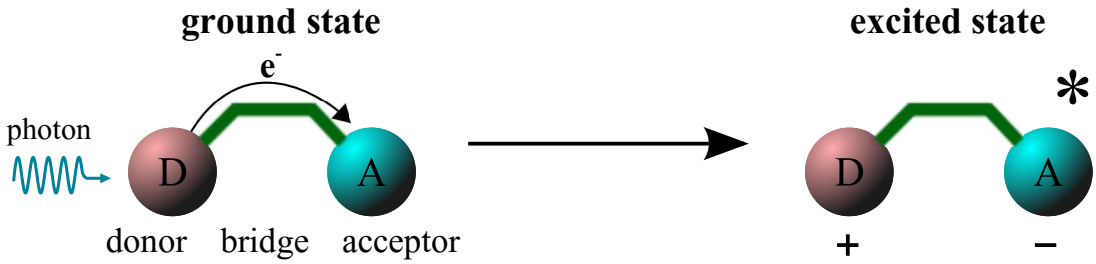

Figure 2.2: *Photoinduced intramolecular charge transfer (ICT) in a donor-acceptor molecule*

The intramolecular charge transfer is mediated by the conjugated bridge. The bridge is composed of two aromatic rings and alternating single and double bonds that extend all the way from the donor to the acceptor. Conjugation gives rise to a π molecular orbital that extends from the donor to the acceptor by overlapping of the p-orbitals from the constituent carbon atoms or from lone pairs. As seen in figure 2.3, the simple 4-carbon conjugated molecule 1,3-butadiene has a series of π molecular orbitals that are delocalised along the length of the molecule [26, 27, 28].

In the ground-state of a conjugated system, the highest occupied molecular

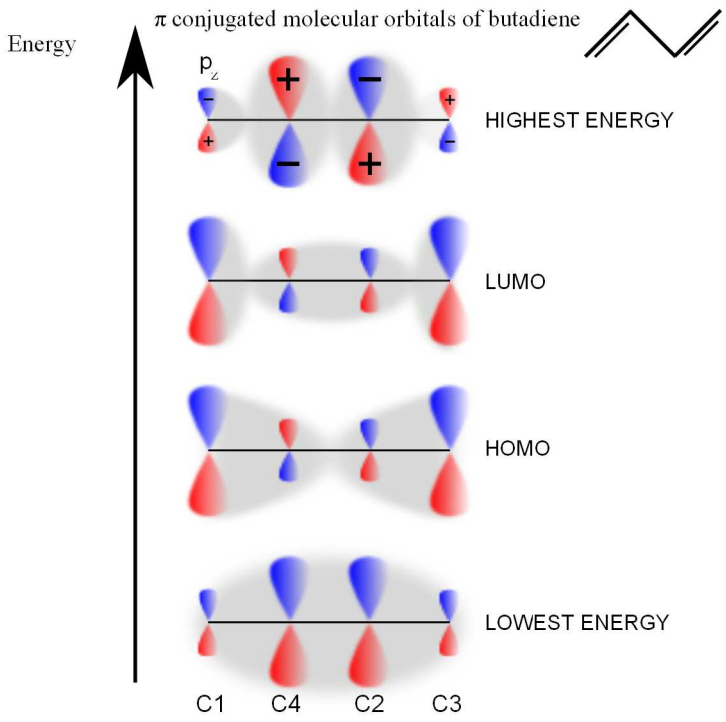

Figure 2.3: *The π molecular orbitals of butadiene showing delocalisation due to conjugation*

orbital (HOMO) is fully occupied and electrons cannot move. However, if an electron from the donor group is excited into the lowest unoccupied molecular orbital (LUMO) state, it is free to migrate along the delocalised orbital.

The energy separation of the π-orbitals of a conjugated system can be modelled by a 1-dimensional "particle-in-a-box" where the electrons are essentially confined to an infinite potential well [29]. The solutions of Schrödinger's equation for such a system give rise to energy levels whose separation is proportional to the length of the well (figure 2.4). In a conjugated system this is defined by the distance over which the delocalised π orbital extends and is referred to as the conjugation length [30, 31, 32].

As mentioned above, the formation of the delocalised molecular orbitals of a conjugated system requires the p-orbitals of the atoms that form it to overlap.

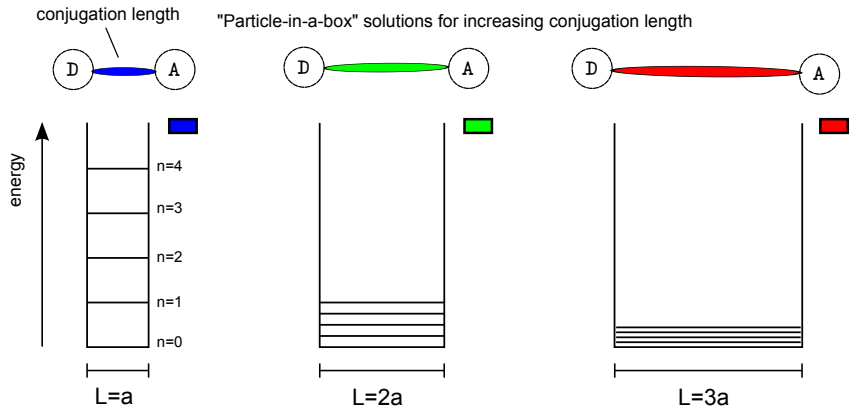

Figure 2.4: *Particle in a box energy levels for the molecular orbitals in a conjugated donor-acceptor system*

The p-orbitals that form π-orbitals have lobes that extend perpendicularly to the carbon chain in a defined direction and the extent of overlap of adjacent p-orbitals depends on the angle between them as shown in figure 2.5. Thus the conjugation length is highly dependent on the relative angles between the p-orbitals of the atoms within the molecule.

The amino nitrogen in the donor group of DCM is expected to have orbitals that are in between pure sp^3 and sp^2 hybrid orbitals. This is due to resonance structures that involve delocalisation of the lone pair to the aromatic ring [33]. In aliphatic amines, the lone pair resides in one of four sp^3 hybrid orbitals but in aromatic amines, the orbitals are closer to sp^2 and the amino group takes on a more planar conformation with respect to the ring and the lone pair resides in a p-orbital [34]. The overlap between the lone pair orbital and the π orbitals in the aromatic ring determines the ability of the lone pair to delocalise; thus the sp^2 hybridisation is preferable for charge-transfer to occur [35, 36, 37].

In DMABN, one of the lone-pair electrons in the non-bonding (n) orbital of the dimethylamine donor group is excited to the unoccupied π^* orbital in the aromatic ring [10, 38]. The charge from the lone pair orbital is then free to migrate towards the acceptor cyano group on the pyran ring. This polar excited-

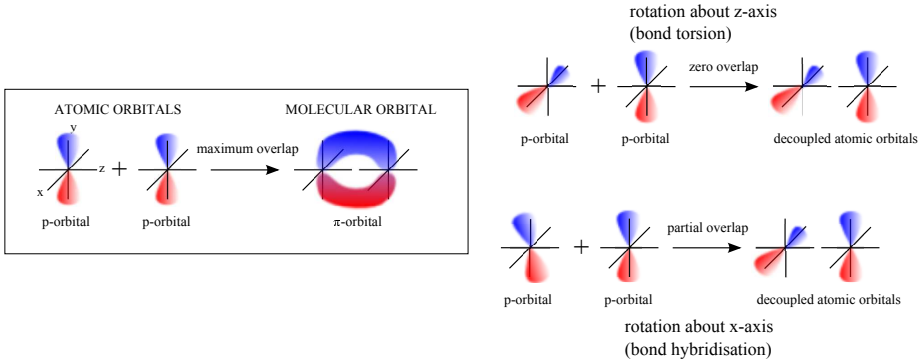

Figure 2.5: *The influence of the relative angle of adjacent p-orbitals on the formation of a π molecular orbital. The figure shows the effect of bond-torsion about the z-axis (twisting) and bond-angle about the x-axis (due to orbital hybridisation and/or steric interactions) on the extent of overlap.*

state is referred to as a charge transfer state. As will be seen in section 2.1.1.2, the exact nature of this state for DCM and similar molecules is a subject of some controversy.

The existence of a charge transfer excited-state for DCM is supported experimentally by **solvatochromism** measurements, whereby the dependence of the Stokes shift on solvent dielectric properties can be used to calculate the change in the dipole moment between the ground and excited-state. Solvatochromism experiments performed by Meyer et al. [19], in which the Stokes shifts of DCM dissolved in a series of 25 solvents were measured and analysed with the Lippert-Mataga solvation theory [39, 40, 41], suggested an increase in the molecular dipole moment of 20.2 D with respect to the ground-state. The existence of a charge transfer (ICT) state is thus not in dispute but the nature of this CT state is.

2.1.1 The TICT theory

2.1.1.1 DMABN

The main source of controversy with regard to the ICT state of DCM has been the validity of the so-called twisted intramolecular charge transfer (TICT) model for this molecule. The TICT model was first proposed by Grabowski et al. [10] to account for the phenomenon known as "dual fluorescence" [39] in the donor-bridge-acceptor compound dimethylamino benzonitrile (DMABN). Figure 2.6 compares the structure of DCM to that of DMABN. As can be seen, both DCM and DMABN have a dimethylamino donor and nitrile acceptor separated by a conjugated bridge - the aromatic ring being a special example of a conjugated system. The trans ethene linkage separating the two aromatic rings in DCM extends the bridge and adds degrees of freedom for bond rotation not available to DMABN. Both trans-cis isomerisation around the central double bond [42, 19, 43] and rotation of the various single bonds can occur. Any rotation that changes the orientation of p-orbitals on the donor with respect to the acceptor can cause a decoupling of the conjugated molecular orbital [44] as already seen in figure 2.5 for bond-torsion. This decoupling is an important concept in the TICT model and will be a central theme of this thesis.

The dipole moment, μ, for two opposite charges of magnitude q separated by a distance r is given by:

$$\mu = q.r \tag{2.1}$$

Therefore a full charge transferred from donor to acceptor would give rise to a higher excited-state dipole moment in DCM than that of the charge transfer (CT) state in DMABN. Employing the theory of Lippert and Mataga that uses data from the solvent-dependent shift of the fluorescence band to estimate the

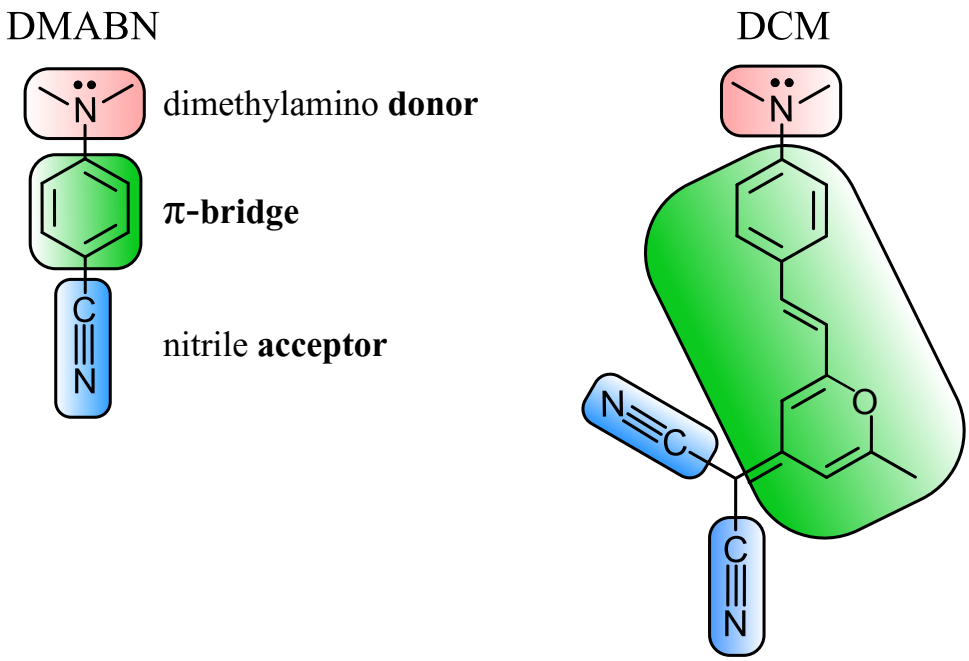

Figure 2.6: *The donor, bridge and acceptor groups in DMABN and DCM.*

excited-state dipole moment, Mialocq et al. [45] calculated that the excited-state of DCM in methanol had a dipole moment of 26.3 D.

DCM's excited-state dynamics are also complicated by the central double bond that can undergo trans-cis isomerisation [42]. However, this process is not very efficient in polar solvents due to lowering of the energy of the charge transfer state. As the isomerisation reaction has a barrier along the bond coordinate of the double bond half way between the trans and cis states, the lowering of the CT state effectively increases the height of the barrier to isomerisation [19].

2.1.1.2 Dual fluorescence

Part of the controversy arises because the tell-tale marker of twisted intramolecular charge transfer, the phenomenon of "dual fluorescence" [39], is noticeably absent in the fluorescence spectra of DCM. Dual fluorescence refers to the appearance of two distinct bands in the fluorescence spectrum of DMABN as in

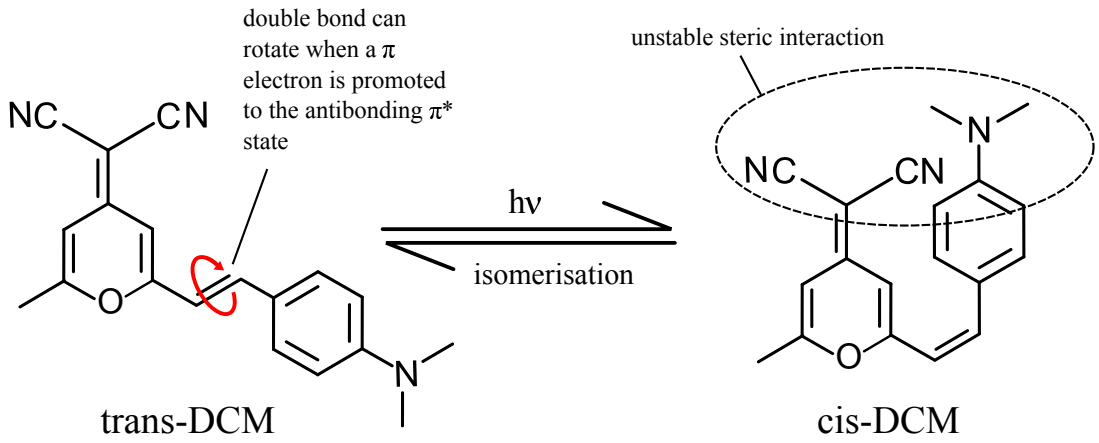

Figure 2.7: *The photoisomerisation of DCM is a possibility if it absorbs a photon that matches the energy of the $\pi \rightarrow \pi^*$ energy gap.*

figure 2.8, the relative intensities of which are highly dependent on the solvent polarity.

Grabowski's group [10] attributed these bands in DMABN's fluorescence spectrum to two excited-states associated with the orientation of the dimethylamino group with respect to the aromatic ring. In the TICT model, the high energy band is attributed to a planar state where the dimethylamino group is in the plane of the ring and is designated as the locally excited (LE) state. The low energy band is attributed to a state in which the dimethylamino group is twisted with respect to the ring and is accompanied by the transfer of a unit of charge from the dimethylamino nitrogen donor to the nitrile (-CN) group - the **TICT state**.

According to Grabowski's theory [10, 46, 47, 48], the locally excited-state should have a dipole moment that is similar to that of the ground-state whereas the twisted state decouples the molecular orbitals of the donor and acceptor, thus localising the charge separation and increasing the lifetime of the state by preventing recombination (see figure 2.9).

Since the TICT theory was first proposed, the phenomenon of dual fluo-

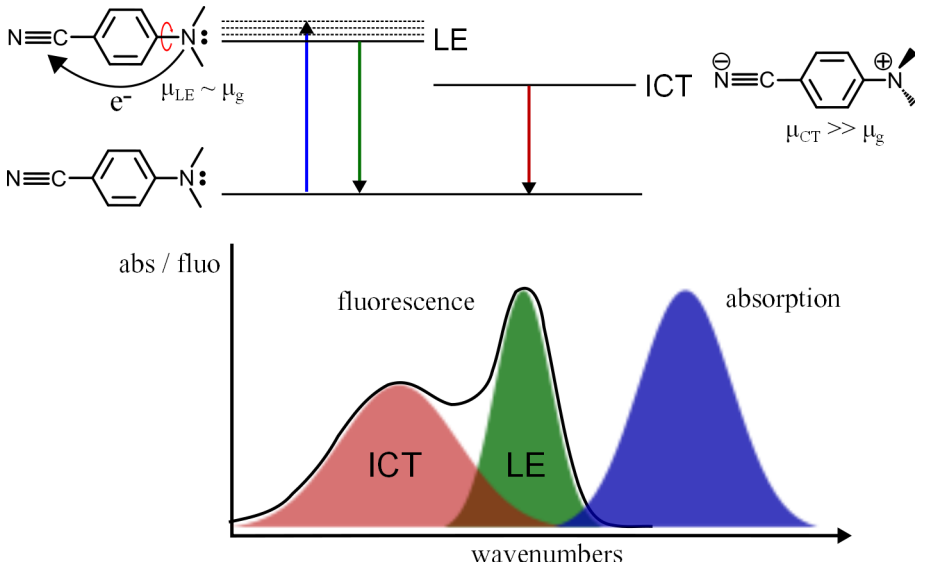

Figure 2.8: *Dual fluorescence in DMABN and the contribution from locally excited (LE) and twisted intramolecular charge transfer (TICT) states. μ_g, μ_{LE} and μ_{CT} refer to the magnitude of dipole moments of the ground, LE and TICT states.*

rescence in DMABN and other compounds has been extensively studied and reviewed [12]. A number of model compounds based on constricted planar and pre-twisted versions of DMABN have provided support for the TICT theory. It has been shown [12] that constricted planar versions exhibit only the band corresponding to the locally excited-state, whereas the pre-twisted molecule produces only emission attributed to the low energy TICT band. The TICT state in DMABN is still not fully understood and as of the submission date of this thesis there are still current articles addressing it [49, 50, 51].

Keeping in mind the structural similarities between DMABN and DCM (Fig 2.6), one would expect that the TICT state might also be valid for DCM. A majority of the spectroscopic studies of DCM, however, note the absence of dual-emission. An often cited exception is the work of Hsing-Kang et al. in 1985 [52]. Proponents for TICT state formation in DCM suggest that most of the emission occurs from the TICT state due to a very rapid decay [17] or strong coupling [53] of the LE state to the TICT accounting for the missing signature feature

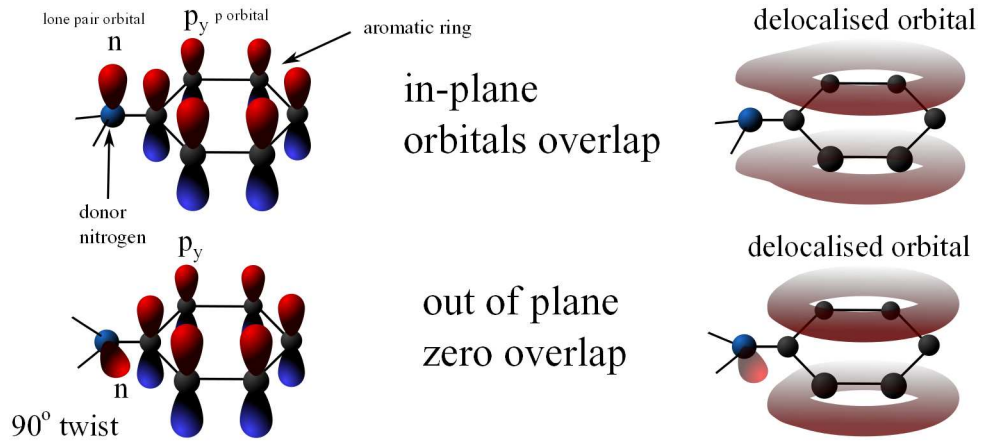

Figure 2.9: *The influence of dimethylamino twist angle on the delocalisation of non-bonding electrons to the aromatic π orbital.*

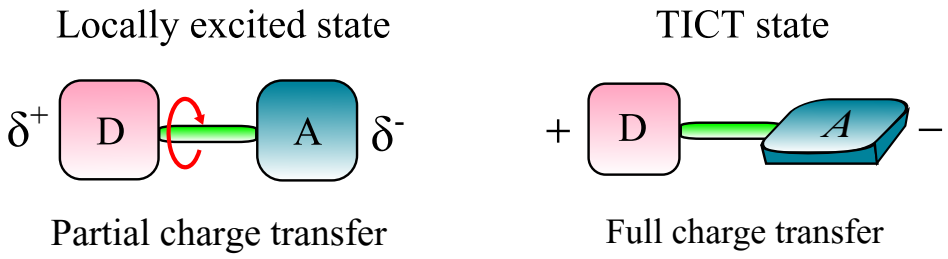

Figure 2.10: *The locally excited and TICT states in a donor-acceptor system*

of TICT. However, even in highly viscous environments, e.g. within artificial micelles, dual fluorescence is not seen - but the fluorescent state in these cases is still attributed to a twisted charge transfer state [54] as large, but slow, time-dependent Stokes shifts are still evident.

Extensive time-resolved investigations of DCM in the 1980s and 90s [43, 55, 14, 56, 15] attempted to aid the discussion about the nature of the excited-state but reached conflicting conclusions. DCM in polar solvents shows a time-dependent Stokes shift towards a **steady-state** fluorescence band-shape which has been attributed to the relaxation of solvent molecules to a configuration that accommodates the changed dipole moment of the excited-state - a process that

lowers the energy of the solute (DCM) and solvent system [57].

Meyer's study [19] found no direct evidence for fluorescence from a locally excited (LE) state in picosecond photon counting methods. The paper suggested that fluorescence occurs from a relaxed excited-state and a possible LE state would have a lifetime less than 100 picoseconds.

Theoretical simulations, by Marguet et al [13], of the energy of the first three singlet states (S_0, S_1 and S_2) of DCM versus the angle of the central double bond and dimethylamino group using quantum chemical calculations produced some interesting results. The simulations reproduced here in figure 2.11 showed that the ground singlet state (S_0) has a significant energy barrier along the isomerisation (double bond angle) coordinate as would be expected, whereas the S_1 and S_2 does not have this feature. Therefore the ground-state is stable to isomerisation and the trans-cis conversion may only occur via the photo-excited-states. More interestingly, the simulations showed that the S_2 state crosses the S_1 state at a double bond torsion angle of 45° when the dimethylamino angle is 90° to the plane of the ring. Marguet, attributed this to a TICT state.

Chang et al. [58] studied model analogues of DCM that have restricted rotation around the dimethylamino bond and found an order of magnitude increase in the lifetime of the assigned S_1 state compared with un-restricted DCM. The TICT state in this study was assigned to the S_2 state from Marguet's study.

This 90° twisted conformation of the dimethylamino group corresponds to the lowest S_2 state energy. As it is a lower energy than the S_1 state, it is argued that this prevents the trans-cis isomerisation. The calculated TICT state conformation was also found to have a large dipole moment, consistent with the previous experimental work and analysis of Meyer et al.

When studied in solution, the solvent has a role to play in the dynamics of

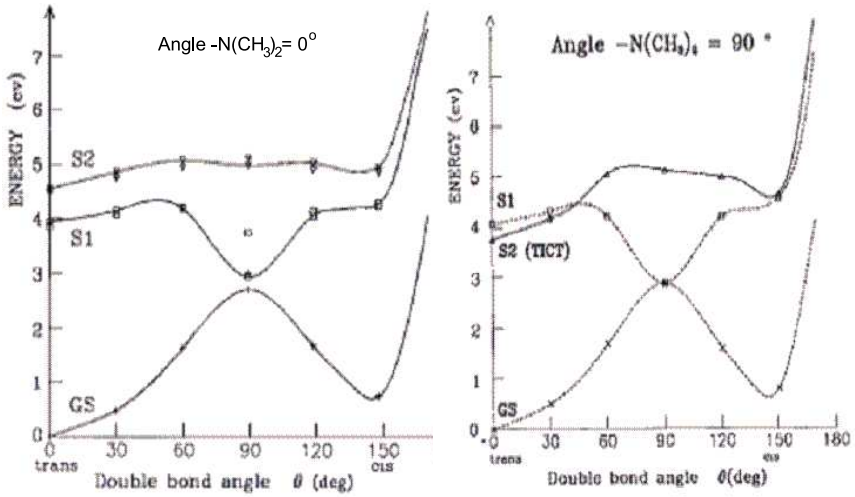

Figure 2.11: *Energy surface for planar and twisted dimethyl amine bond as the double bond rotates. Figure reproduced from: S. Marguet et al., J. Phys. Chem., 160:265279, 1992.*

the excited-state and the rate at which the CT state is formed. A highly polar solvent will stabilise the high dipole moment species of DCM and thus we expect the rate of formation to be fast. The size and therefore mobility of the solvent may also affect the rate of solvent reorganisation around the excited molecule and therefore formation of the CT state. The Stokes shift shows a dependence on the solvent polarity which gives further evidence for the presence of a charge transfer mechanism.

Some papers suggest alternative mechanisms for the time-dependent Stokes shift in DMABN that doesn't invoke a twisted single bond, such as planar charge-transfer states whose energy shifts during solvation [15, 17] or rehybridised intramolecular charge transfer (RICT) states where the reaction coordinate is the rehybridisation of the sp cyano carbon in the acceptor group to sp^2. Or the pseudo-Jahn-Teller ICT (PICT) model in which the charge separation of the donor and acceptor occurs by pyramidalisation of the sp^2 trigonal planar dimethylamino bond to a sp^3 orbital decoupling the donor and acceptor orbitals [59]. Even the bond that twists in the model compound DMABN is not fully

accepted [60].

Van Tassle et al [61] presented visible pump IR probe experiments performed on DCM and deuterated DCM. The group assigned an infrared band at 1495 cm^{-1}, which they assigned to a stretching mode of the N-C bond in a twisted conformation of the dimethylamino group, in agreement with the TICT mechanism. Van Tassle's analysis also precludes the RICT or PICT mechanisms in DCM.

So, the exact nature of DCM's excited-state is far from clear. This study presents new evidence to the discussion of DCM. The background and theory behind the spectroscopic methods used in this study will be introduced first before a discussion about the practical aspects of the experiments in chapter 3.

2.2 Photochemical processes in molecules

Elucidation of the excited-state structure of DCM is complicated by the dynamical processes dependent on many variables. This section outlines some of the processes that lead to the features seen in the steady-state and time-resolved experiments outlined in chapter 3.

2.2.1 Electronic transitions

When a molecule absorbs an ultraviolet or visible photon, it is perturbed from its ground-state into an energetic and transient excited-state whereby an electron is promoted to a higher molecular orbital. In order for the molecule to return to the ground-state, the extra energy must be dissipated. There are a number of processes that can achieve this.

In **spontaneous emission**, the excited-state molecule loses energy by emitting a photon with an energy that corresponds to the transition from the excited-state

to the ground-state (or lower excited-state). This process can occur from the initially excited-state, or from a state produced after a non-radiative relaxation process. A fluorescence spectrum records the energy of transitions that occur from the excited-state by measuring the number and wavelength of photons emitted by the excited molecule.

Stimulated emission is a process whereby a transition from an excited-state back to the ground-state can be stimulated by another photon of equivalent energy to the transition. This mode of emission is particularly important in the pump-probe measurements which will be discussed in chapter 3.

The **Franck-Condon principle** [62, 63] states that the nuclei within a molecule are essentially stationary during electronic transitions between molecular orbitals. Thus when vibrational potentials of molecular electronic states are plotted, transitions between electronic and vibrational levels (vibronic transitions) are represented as vertical lines (Figure 2.12). This is due to the faster motion of the much less massive electrons relative to the nuclei of the atoms.

Figure 2.12 shows the ground and excited electronic states of a molecule with harmonic potentials associated with the vibrational modes available in each state. The quantised vibrational levels and their probability distributions (coloured red) are also shown. The probability distributions for each vibronic state are given by the square of the wave function at the allowed levels of a harmonic oscillator. Vibronic transitions (between vibrational levels of two electronic states) occur with high probability when there is a large overlap between the wave function of the occupied vibrational level of the initial electronic state and that of the final electronic state [63]. As a consequence, photoexcitation from the excited-state often produces an electronic state in a vibrational level higher than the lowest available mode ($v' > 0$). The state produced by such transitions is known as a Franck-Condon state.

The excess vibrational energy generally relaxes very quickly to the $v' = 0$ state by collisions with surrounding molecules, i.e. the solvent. Relaxation to the ground electronic state will also occur from the vibrationally relaxed excited-state to the vibrational level that has the largest overlap. Thus, emission from this electronic level will be red-shifted (towards lower energy) with respect to the absorption transition by the combined energy difference between the Franck-Condon and lowest vibrational level in the excited-state (Fig 2.12a) and the difference between the vibrationally excited-state and the lowest vibrational level in the excited-state (Fig 2.12b).

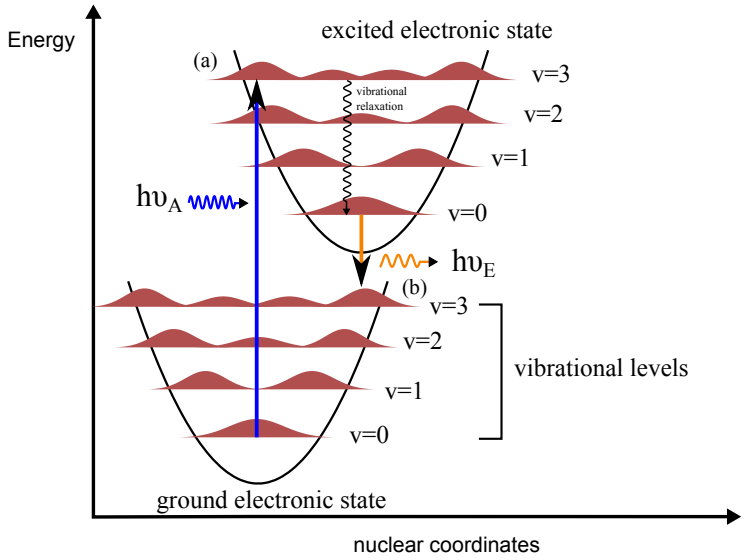

Figure 2.12: *Vibronic transitions in molecules demonstrating the Franck-Condon principle.*

2.2.2 Solvation

Solvation refers to the reorientation of solvent molecules to accommodate a changed charge or spatial distribution of a solute following photo-excitation. When there is a large difference in the dipole moments of the ground and excited-states $\Delta\mu = \mu_e - \mu_g$, this solvent reorganisation can significantly lower the energy of the excited-state [64].

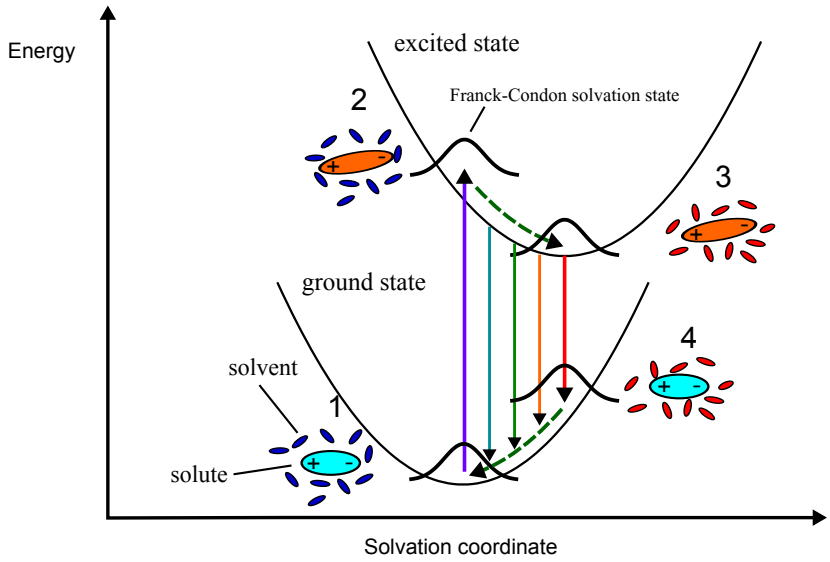

Figure 2.13: *Energy diagram illustrating the contribution of solvation to the Stokes shift of a photo-excited molecule. The structure of the solvent cage surrounding the molecule is essentially unchanged during electronic excitation.*

The Lippert-Mataga theory of solvation [39, 40, 41, 57] describes the energy shift in terms of the solvent refractive index (n) and dielectric constant (ϵ).

$$\overline{\nu}_A - \overline{\nu}_F = \frac{2}{hc}\left(\frac{\epsilon_0 - 1}{2\epsilon_0 + 1} - \frac{n^2 - 1}{2n^2 + 1}\right)\frac{(\mu_e - \mu_g)^2}{a^3} \tag{2.2}$$

where μ_g and μ_e are the dipole moments of the ground and excited-states, h is Planck's constant, c is the speed of light, a is the radius of a sphere that encloses the molecule and $\overline{\nu}_A$ and $\overline{\nu}_F$ are the absorption and fluorescence maxima (in cm^{-1}).

The term in the large brackets in equation 2.2 is known as the **orientational polarisability** of the solvent and is given the designation Δf.

$$\Delta f = f(\epsilon) - f(n) \tag{2.3}$$

This is derived from the high frequency or electronic polarisability $f(n)$, which is a function of the refractive index n and describes the instantaneous response of

electrons in the solvent to the dipole moment of a solvent molecule:

$$f(n) = \frac{n^2 - 1}{2n^2 + 1} \tag{2.4}$$

and the low frequency polarisability, which is a function of the solvent dielectric constant and takes into account the slower response of the orientational motion of solvent dipoles [37]:

$$f(\epsilon) = \frac{\epsilon - 1}{2\epsilon + 1} \tag{2.5}$$

Figure 2.14 highlights the origin of the components of the reaction field. The dipole-dipole interactions between solvent and solute stabilise polar excited-states, lowering their energy and therefore red-shifting the fluorescence band.

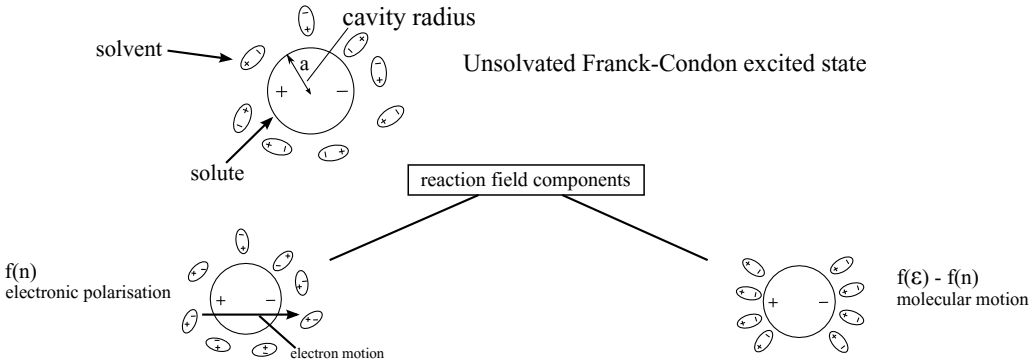

Figure 2.14: *The electronic and molecular motion components of the reaction field*

Due to the large number of solvent molecules and degrees of freedom of solvent configuration, the potential energy of a molecule versus solvent coordinate can be treated as a classical continuum rather than a quantised system. As with the Franck-Condon principle for vibronic transitions, electronic transitions occur essentially instantaneously with respect to solvent orientation (Fig 2.13). Thus the solvent is in a non-equilibrium configuration immediately following excitation and must reorganise into the lowest energy excited-state configuration as shown at figure 2.13: point 3. Relaxation of the vibronic state of the molecule again produces a non-equilibrium solvation configuration (figure

2.13: point 4) as the ground electronic state has a smaller dipole moment.

Because of this, in a time-resolved experiment one would expect to see a shift in the energy of the excited-state transitions (such as fluorescence and excited-state absorption - to be discussed in chapter 3) to the red within ones to tens of picoseconds [14]. Conversely, ground-state dynamics would be expected to shift to the blue as the solvent reorganises, thereby lowering the energy of the molecular ground-state-solvent system.

2.2.3 Polarisation Anisotropy

The direction of the electric field oscillation in a light beam defines its polarisation. The absorption of light by a sample can depend on the orientation of the absorbing species with respect to the direction of the light polarisation. If a sample exhibits a change in its optical response with the light polarisation, the optical response is said to be **polarised**.

For most cases of molecules dissolved in solvents, the optical response from a large sample of molecules is unpolarised or isotropic, i.e., the signal measured has no dependence on the angle of polarisation. An explanation for this, and how a polarised response can be induced in such samples, requires the introduction of two concepts - the **transition dipole** and a process known as **photoselection** [65, 57].

2.2.3.1 Photoselection

Molecular transitions occur via coupling of the electric field oscillation of a light wave to the **transition dipole moment**. The transition dipole moment from an initial state m to a final state n is defined as the sum over all the charge (electron and nuclei) positions in the two states, i.e., it is determined by the change in

charge distribution within the molecule before and after the transition.

$$\overrightarrow{\mu}_{nm} = e \int \Psi_n^* \sum Z_i \overrightarrow{r}_i \Psi_m d\tau \tag{2.6}$$

where e is the electron charge, Ψ_m and Ψ_n are the electron wave-functions of states m and n, $\mathbf{r}$ is the displacement vector of each particle and Z is the atomic number.

The square of μ_{nm} gives the probability of the transition $m \rightarrow n$ and the *direction of the vector* in the molecular framework gives the *polarisation* of the transition. The transition probability follows a cos^2 dependence with the angle θ between the excitation direction, given by the direction of oscillation of the electric field, and the orientation of the transition dipole moment:

$$P_{abs} \propto cos^2(\theta_{\mu,E}) \tag{2.7}$$

Molecules in a bulk solvent environment will in general have a random orientation such that the absorption transition dipoles will also be randomly distributed. As many molecules are sampled in a typical spectroscopy experiment, the polarisation dependence will be averaged out. Therefore, the signal will show an equal (isotropic) response at all detected polarisation directions. However, upon introduction of a linearly polarised excitation source, the molecules whose transition dipole moments are aligned with the polarisation of the light will be preferentially excited. This process is referred to as **photoselection**.

Figure 2.15 shows the orientational probability distribution of excited-state molecules produced by photoselection. In the figure, the probability of finding a molecule in the excited-state at each orientation is proportional to the length of the vector from the origin to the surface.

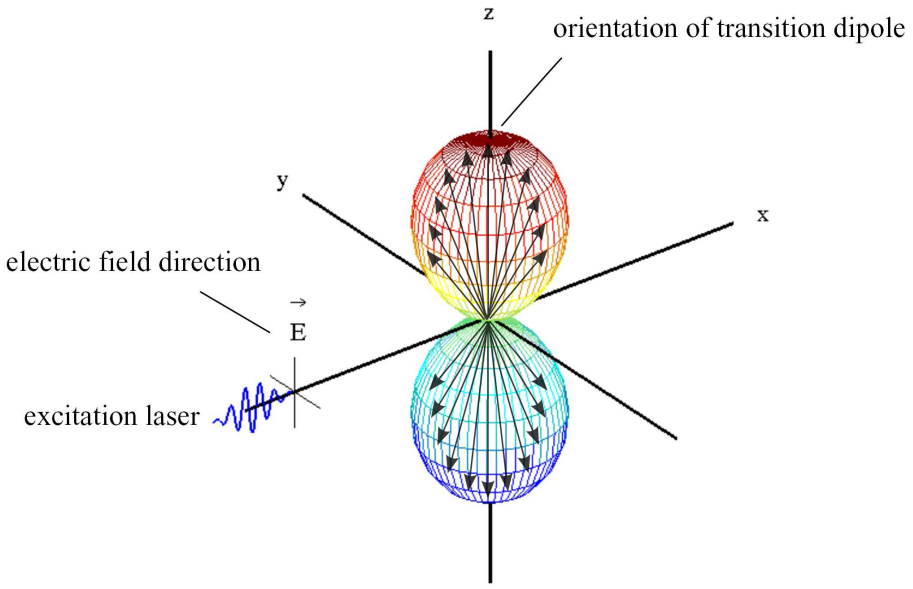

Figure 2.15: *Orientational probability distribution of excited molecules by photoselection*

2.2.3.2 Anisotropy

As can be seen, molecules whose transition dipoles are aligned with the electric field vector of the pump light ($\vec{E}$) absorb the light with maximum probability, while those at 90° remain in the ground-state. The photo-selected orientational distribution gives rise to an anisotropic response to optical measurements such as fluorescence and pump-probe spectroscopy.

The extent to which the optical response of the molecules is aligned to the polarisation of the excitation beam is often characterised by a number called the **anisotropy** (r). This parameter can be measured in the following example of a fluorescence anisotropy experiment (2.16).

In this example, the anisotropy is given by:

$$r = \frac{I_{\parallel} - I_{\perp}}{I_{\parallel} + 2I_{\perp}} \tag{2.8}$$

where $I_{\parallel}$ and $I_{\perp}$ represent the intensities of the fluorescence components that are

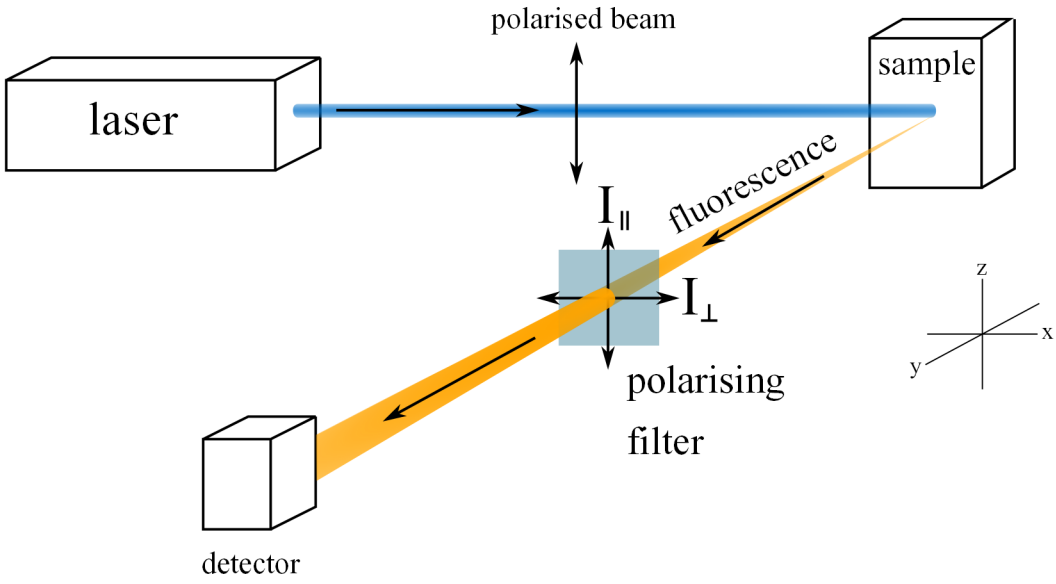

Figure 2.16: *How to measure fluorescence anisotropy.*

parallel and perpendicular with respect to the polarisation of the excitation light.

The total intensity is given by:

$$I_T = I_x + I_y + I_z \tag{2.9}$$

which can be thought of as the sum of one parallel and two perpendicular components:

$$I_{\parallel} + 2I_{\perp} \tag{2.10}$$

Thus the anisotropy is normalised by the total intensity.

In this study, the total (rotation independent) intensity was calculated from the parallel and perpendicular channels from equation 2.10. However, the total can be measured directly by analysing the signal at the polarisation direction known as the ”magic angle” [57]. At a polarisation angle of 54.7° with respect

to the excitation polarisation, the contributions of each emitted component (I_x, I_y and I_z) are equal. Thus, under these conditions the measured intensity is proportional to the total fluorescence intensity I_T and the time dependent intensity decays are independent of rotational motion of the solute.

Consider a single molecule with an emission dipole that is aligned to the polarisation of the excitation light source. In this case θ is 0 and r is equal to 1.0. This is also the case when a sample of molecules are all aligned so that their average θ is also 0. Randomly distributed molecules in a solvent, however, can never reach an anisotropy value of 1.0.

As indicated in equation 2.7, photoselection imposes a distribution of excited-state molecules within the excitation volume giving a distribution given by $cos^2\theta$.

For a sample in which the molecules are randomly oriented, the proportion of molecules within the range θ to $\theta + d\theta$ is given by $sin\theta d\theta$. When coupled with equation 2.7 this gives the following formula for the distribution of molecules produced by photoselection in an isotropically oriented sample.

When considering photoselection in a sample of molecules with a random orientational distribution, the probability that a molecule is aligned to the polarisation vector of the excitation light field is given by:

$$f(\theta)\,d\theta = cos^2\theta sin\theta\,d\theta \tag{2.11}$$

When the absorption and emission dipoles are collinear, the average value of $cos^2\theta$ is given by:

$$< cos^2\theta >= \frac{\int_0^{\pi/2} cos^2\theta\, f(\theta)\,d\theta}{\int_0^{\pi/2} f(\theta)\,d\theta} \tag{2.12}$$

Substituting equation 2.11 into 2.12 gives a $< cos^2\theta >$ of 3/5 for collinear

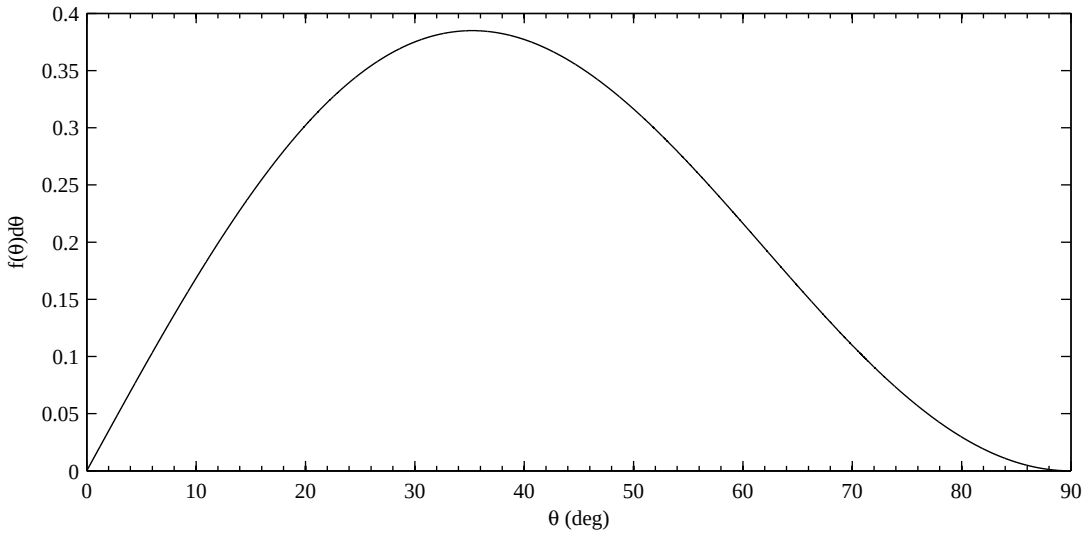

Figure 2.17: *The probability distribution of molecules, in an isotropic solution, that they will be aligned with the electric field vector of linearly polarised light.*

absorption and emission transition dipoles.

If the absorption and emission dipoles are not collinear, the anisotropy depends on the angle β between them and is given by:

$$r = \frac{2}{5}\left(\frac{3cos^2\beta - 1}{2}\right) \tag{2.13}$$

For parallel transition dipoles this gives an anisotropy of 0.4 and for perpendicular transition dipoles a value of -0.2.

β (degrees)	r
0	0.40
54.7	0.00
90	-0.20
45	0.10

Table 2.1: Anisotropy values

Thus, the anisotropy can give detailed information about the orientation and

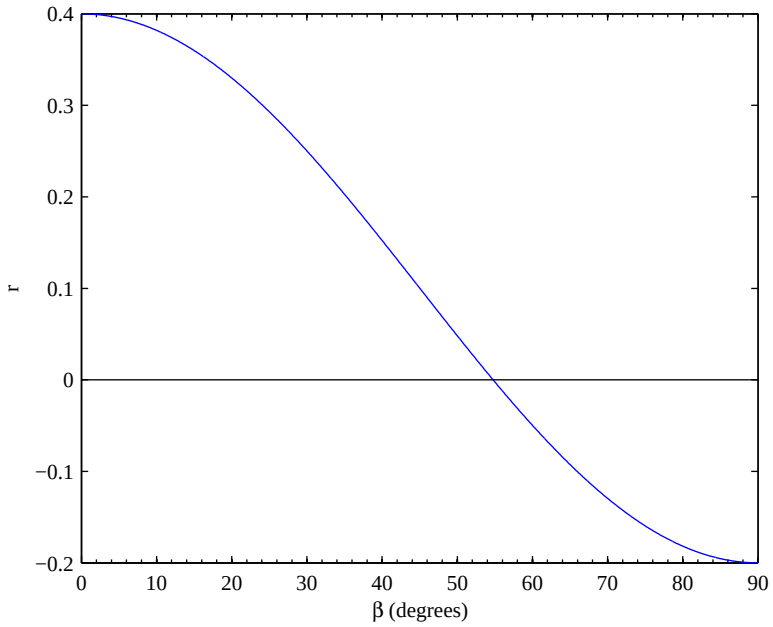

Figure 2.18: *The influence of the angle between* $\mu_{\mathbf{fluo}}$ *and* $\mu_{\mathbf{abs}}$ *on the measured anisotropy*

dynamics of the transition dipole. If the fluorescence transition dipole moment changes its orientation with time, which might occur during formation of a TICT state, it should be reflected as a change in the measured anisotropy.

2.2.3.3 The polarisation response and the magic angle

As mentioned in a previous section, the magic-angle, with a value of approximately 54.7° is the polarisation detection angle, relative to the excitation or pump beam, at which the measured signal is independent of rotation of the sample molecule(s). Under these conditions, the total measured signal is composed of a mixture of the parallel and perpendicular signals $S_{\parallel}$ and $S_{\perp}$ in a proportion of 1:2 i.e.

$$S_T = S_{\parallel} + 2S_{\perp} \tag{2.14}$$

as the parallel component given by $\cos^2 57.4$ will be 0.333 and the perpendicular component given by $\sin^2 57.4 = 0.667$.

By combining the parallel and perpendicular components of the signal in 1:2 proportion, the magic angle equivalent signal can be calculated rather than needing to measure it independently. This method was used in the experiments described in chapter 3.

2.2.3.4 Time dependent anisotropy

Our previous discussions about anisotropy assume that the molecule remains static in the excited-state. In a solvent, this is not true. If a photo-selected distribution of molecules is dissolved in a solvent, the molecules will lose any preferential orientation in time due to the process of rotational diffusion. Thermal motion of the molecules causes them to rotate, so that the transition dipoles become randomly oriented with respect to the axis defined by the maximum of the probability distribution. The value of the anisotropy, therefore, decays during this process with a characteristic time(s).

The time-dependent anisotropy $r(t)$ of a sample of spherical molecules that can freely diffuse is given by:

$$r(t) = r_0 e^{-t/\tau_{rot}} \tag{2.15}$$

where r_0 is the initial anisotropy created by photoselection and τ_{rot} is the rotational diffusion time given by the Stokes-Einstein-Debye (SDE) [66, 67, 68] relation:

$$\tau_{rot} = \frac{\eta V}{k_B T} \tag{2.16}$$

where η is the solvent viscosity, V is the volume of the rotating molecule, T is the temperature (Kelvin) and k_B is the Boltzmann constant.

Rotational diffusion of non-spherical particles is considerably more complex [69] and involves a number of axes of rotation with distinct rotational correlation times giving a multi-exponential decay

$$r(t) = r_1 e^{-t/\tau_1} + r_2 e^{-t/\tau_2} + r_3 e^{-t/\tau_3} ... \tag{2.17}$$

A modified version of the SDE relation takes into account the shape of the molecule S and introduces a friction coefficient F which defines the boundary condition between the solvent and the rotating solute:

$$\tau_{rot} = \frac{\eta V F}{k_B T S} \tag{2.18}$$

The frictional factor F can range from 0 to 1. A value of zero is known as the **slip** boundary condition where there is no direct interaction between the solvent and the solute. A value of one corresponds to the **stick** boundary condition in which a layer of solvent molecules sticks to the rotating solute.

The shape factor S for a symmetrical ellipsoid depends on the ratio of the length and width of the ellipse and the axes on which the rotation occurs.

The hydrodynamic volume is defined as:

$$V_{hydro} = \frac{VF}{S} \tag{2.19}$$

Dielectric friction, which is the effect of the solvent reaction field on rotation of the solute in a polar solvent is also a possible complicating factor in interpreting anisotropy decays - contributing an extra component to the rotational correlation time:

$$\tau_{rot} = \tau_{SDE} + \tau_{dielectric\,friction} \tag{2.20}$$

At this stage it is simply worth noting that the rotational correlation time

depends on solvent viscosity and the shape of the molecule. The viscosity dependence of rotational diffusion will be exploited in chapter 5 with fixed temperature measurements. This will be used to determine whether a change in the atomic configuration of DCM due to TICT (or other processes) can be observed by their effect on diffusion rates.

The time-dependent anisotropy can be a difficult parameter to interpret and there are many factors that can determine how it changes and/or decays. This study attempts to disentangle some of these factors by comparing the anisotropy of DCM in various solvents and with its model compound DCJ.

Chapter 3 will introduce the practical aspects of the experiments described above.

Chapter 3

Experimental techniques

The experimental data used in this thesis were obtained from a variety of techniques. The steady-state absorption spectra were obtained with a traditional commercial bench-top UV-Vis spectrometer (Shimadzu UV 1601 CE). All other measurements were made using a commercial ultrafast laser system with experimental setups that were custom built by the author and colleagues.

The steady-state fluorescence was excited by a pulsed laser source and collected by focussing the emitted light with a 3" aperture lens onto a spectrometer with a 1024-pixel CCD detector.

Time-resolved measurements were made using two methods: time-resolved fluorescence using an optical streak camera and and a pump-supercontinuum-probe setup. All time-resolved measurements were polarisation-resolved in that the parallel and perpendicular components of the signal with respect to the excitation laser polarisation were detected simultaneously in order to determine the time-dependent **anisotropy**.

This chapter will describe the methods, some theory and practical issues involved with making the measurements mentioned above - including the

generation of ultrashort pulses.

3.1 Steady-state spectroscopy

In this work, the term **steady-state spectroscopy** will refer to the time-integrated absorption and fluorescence spectra. These techniques give information about the states that can be excited by optical transitions and the radiative transitions that can occur from these excited-states. In the UV and visible range (wavelengths from 200-700 nm), absorption transitions correspond to the promotion of a ground-state electron to a higher molecular orbital and fluorescence transitions correspond to the electron returning to a lower energy excited-state or back to the ground-state.

In absorption spectroscopy a sample of molecules absorbs photons from a white light excitation source that correspond to the energy difference between the ground and allowed excited-states. The absorbance is defined as the logarithm of the ratio of the light before and after the sample (figure 3.1).

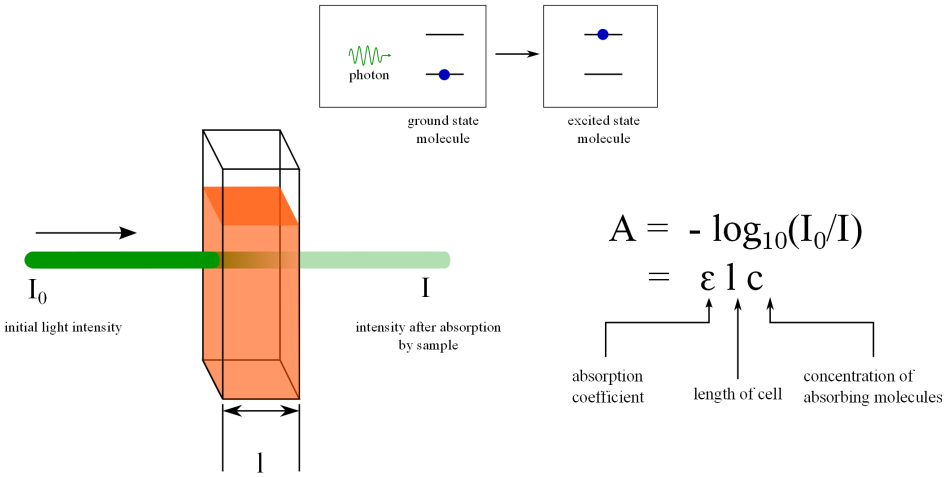

Figure 3.1: *Absorption of light by a chemical sample.*

The measured absorbance as a function of light frequency ($A(\nu)$) depends on the frequency-dependent molar absorption coefficient ϵ ($M^{-1}.cm^{-1}$), which is a measure of the strength or probability of a transition occurring, the concentration or number of absorbing species c ($mol.L^{-1}$) and the path-length l (cm), corresponding to the distance the light travels through the absorbing material:

$$A(\nu) = -log_{10}\frac{I}{I_0} = \epsilon(\nu)cl \tag{3.1}$$

Absorption spectra in this study were taken on a solution of concentration 10^{-4} M using a UV-Visible spectrometer in a 1 mm path-length cell. The spectrometer had a deuterium lamp as the UV source and a hollow-cathode lamp as the visible source.

Fluorescence is the light emitted by a sample as it relaxes from an excited-state to the ground-state. Fluorescence spectra of the samples in this study were obtained by exciting the samples at 400 nm with a frequency-doubled titanium sapphire femtosecond laser and the fluorescence was collected using a 3" diameter lens and focussed onto a spectrometer with a Peltier-cooled CCD detector, as shown in figure 3.2.

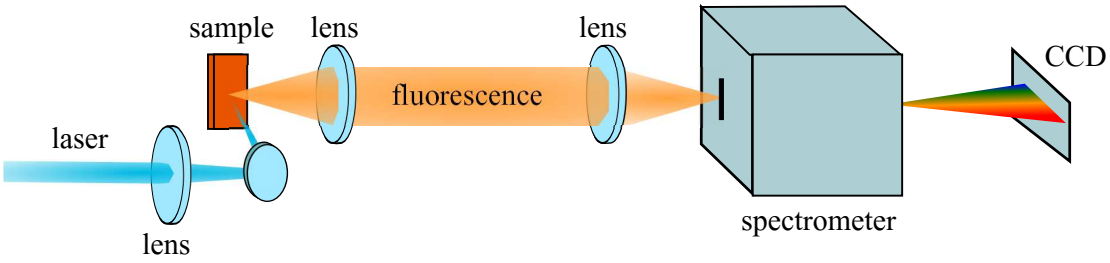

Figure 3.2: *Laser pumped steady-state fluorescence experiment. A laser is tuned to a wavelength within the molecule's absorption spectrum. The excited-state molecules decay via fluorescence and other processes. The emitted fluorescence is collected with a lens and focussed into a spectrometer. A CCD detector reads out the intensity at each wavelength and thus a spectrum is generated.*

The steady-state fluorescence spectrum is usually shifted to a lower energy

with respect to the absorption spectrum (Stokes shift) due to internal processes such as vibrational relaxation and solvation. It includes contributions from all intervening emissive states integrated over the collection time. Thus short-lived states do not contribute much to the spectrum.

3.2 Time-resolved spectroscopy

The steady-state techniques give an average over time of the absorption and fluorescence spectra. If the excited-state dynamics are very fast, as is the case with DCM, short-lived states can be washed out in the time-integrated average. Time-resolved spectroscopy can be used to observe these short-lived states as they are populated and depopulated, and to measure their dynamics [70]. This allows the experimentalist to study the relaxation pathways and the mechanisms that give rise to the features seen.

For relatively long-lived states a time-resolved experiment can be as simple as placing a mechanical shutter in between the excitation source and the sample, and synchronising detection with a fast detector. However, many molecular photochemical processes of interest, particularly intramolecular relaxation, occur on much faster timescales than this technique will measure. For this reason this study has gained great benefit from the development of femtosecond pulsed lasers.

3.2.1 The laser system

The laser system used in this work consisted of a mode-locked Ti:Sapphire oscillator (Tsunami, Spectra-Physics), amplified by a regenerative amplifier (Spitfire, Spectra-Physics) with two independently tunable optical parametric amplifiers. Each of these components will be described in the following section.

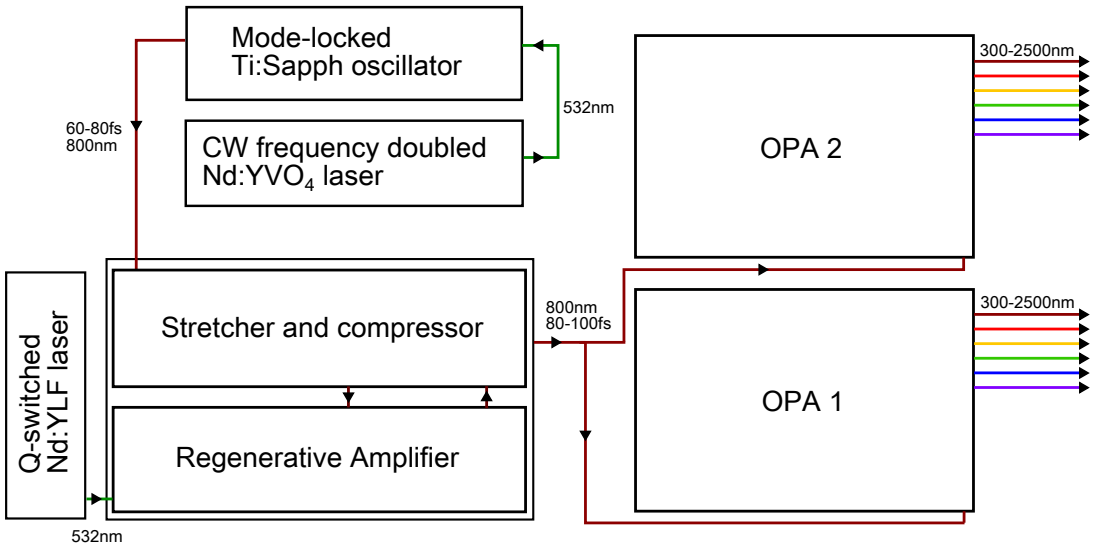

Figure 3.3: *Ultrafast laser system with OPAs for nonlinear spectroscopy. Pulses are generated by a mode-locked titanium sapphire oscillator and then amplified by a regenerative amplifier. 100 fs pulses with a central wavelength of 800 nm are converted to a range of UV, visible and IR wavelengths in a pair of optical parametric amplifiers (OPAs).*

3.2.1.1 Ultrafast laser

Lasers are known for their ability to produce highly intense, highly directed beams of light, often with a very well defined colour or wavelength. While these properties are attractive as a light source for spectroscopy experiments, they are not the properties most exploited in this study. Further explanation requires some background about the basics of what a laser is and how they work.

A laser, in simple terms, is a light amplifier with feedback. The amplification happens within a so-called gain medium, whose properties are chosen such that incoming photons passing through the medium produce more photons, in a process known as **stimulated emission**. The feedback comes from the fact that the gain medium is placed within a resonant optical cavity composed of a pair of highly reflective parallel mirrors. Photons travelling in the correct direction will find themselves confined to the cavity as they make successive passes, reflecting off the mirrors back and forth and passing through the gain medium each time.

In this way, the number of photons increases very rapidly. At a certain point, the gain medium becomes saturated and each successive pass produces no more photons on average than the number coming in. One of the cavity mirrors allows a small fraction of the photons within the cavity to escape as a laser beam.

But the cavity produces more effects than just allowing the light intensity to increase. **Interference** of the light waves within the cavity means that only certain light frequencies are allowed to propagate, while others cannot due to destructive interference. These allowed light frequencies are known as cavity modes.

In so-called multi-mode operation of a laser, many cavity modes are allowed to propagate within the cavity. The frequency separation of cavity modes $\Delta\nu$ is given by:

$$\Delta\nu = 2d/c \tag{3.2}$$

where d is the separation of the cavity mirrors and c is the speed of light.

Lasers can be designed such that a component or process in the cavity favours modes with a fixed phase relationship - referred to as **mode-locking** [71, 72, 73]. Under this condition, constructive interference occurs at regular intervals, creating a periodic train of intense laser pulses as shown in figure 3.4. This process can allow lasers to produce pulses of less than 100 femtoseconds ($< 10^{-13}$ seconds)!

The minimum width of the laser pulses in a mode-locked laser is determined by the so-called Fourier-limit. The more phase-locked modes that can be added together, the shorter the pulse-width can be. One major limiting factor for the Fourier-limit is the gain bandwidth of the laser crystal. Gain media have a range of photon energies (or light frequencies) that they can amplify; thus the spectrum of the laser output is determined by the shape of the gain curve, which in turn determines the range of cavity modes that are amplified and thus able to

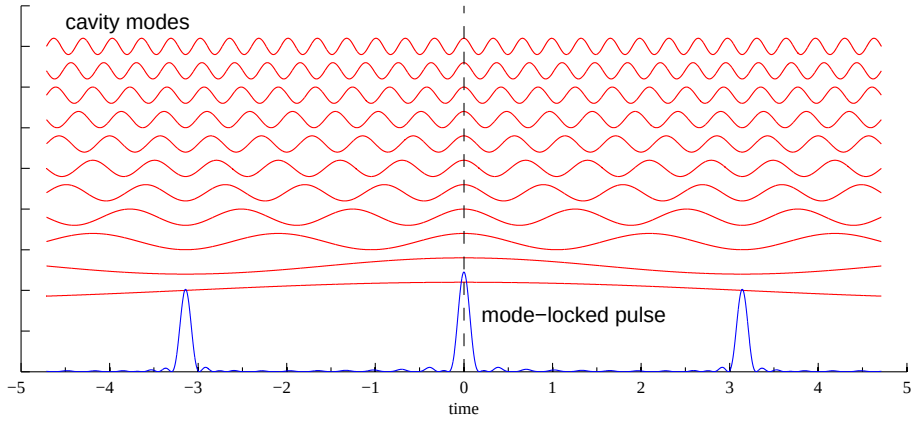

Figure 3.4: *Phase-locked cavity modes interfere constructively at regular intervals to produce a train of short pulses.*

contribute to the mode-locked pulses. Figure 3.5 shows the cavity modes in the frequency domain and how the gain medium bandwidth amplifies only a selected range.

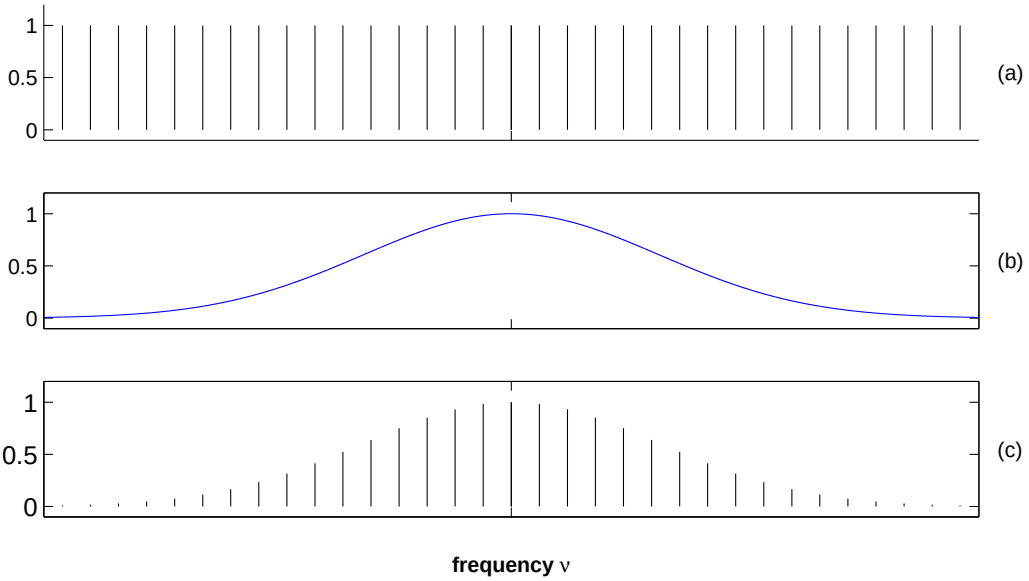

Figure 3.5: *The allowed cavity modes with frequencies given by $\Delta\nu = 2d/c$ are shown in (a). The gain profile of the laser medium gives the frequency range over which amplification of the incoming radiation will occur (b). The amplified modes are thus given by the overlap of the cavity modes with the gain profile (c).*

Kerr lens mode-locking (KLM)[74, 75, 76] is a mode-locking scheme that

relies on the optical Kerr effect, which is a nonlinear optical process that gives rise to an intensity dependent refractive index (Equation 3.3):

$$n(\omega, I) = n_0(\omega) + n_2(\omega)I \tag{3.3}$$

The intensity cross section (or beam profile) of the beam within the cavity is approximately Gaussian, meaning it is brightest in the centre and tails off radially. If the intensity of the beam within the gain medium is high enough, the nonlinear component of the refractive index will also have a Gaussian profile. This spatially dependent refractive index acts as a lens which focuses high-intensity parts of the beam most strongly in an effect known as **self-focussing** [77]. A circular aperture placed in the cavity can then be used to spatially truncate the low-intensity, and therefore less focussed, parts of the beam. As the temporal profile of the pulse is also Gaussian, the high-intensity regions correspond to the middle of the pulse and the low-intensity regions correspond to the leading and trailing edges of the pulse. The aperture spatially removes the lower intensity edges of the pulse to produce a shorter truncated pulse. Newer generation KLM schemes do not require an aperture and achieve an equivalent effect by exploiting the spatial variation of the gain in the laser medium (as determined by the volume of the focussed pump-beam within the gain medium) to favour the high-intensity part of the pulse.

The laser used in this study uses this method with a titanium sapphire gain medium to generate pulses of approximately 80 fs in duration with a pulse repetition rate of 82 MHz. The pulse energies are of the order of 1nJ per pulse.

3.2.1.2 Regenerative amplifier

While very useful for ultrafast experiments, the pulsed output of the titanium-sapphire femtosecond oscillator described above can only be used to probe molecules that have transitions within the efficient lasing range of the system, determined by the gain profile of the titanium-sapphire gain medium - around 800 nm (or 400 nm if the light is frequency-doubled). In order to extend the range of energies available for probing the excited-state transitions of DCM, a device known as an optical parametric amplifier (OPA) [78, 76] was used in combination with frequency mixing techniques to create a tunable source able to probe transitions in the UV, through the visible to the IR regime. This device requires high pulse energies to operate efficiently; so first, the mode-locked output was amplified in a **regenerative amplifier**.

The regenerative amplifier uses a technique known as **chirped pulse amplification (CPA)** [79, 80] to increase the peak pulse power to the terawatt regime. The output of the mode-locked laser, or 'seed' beam, is amplified in this device by passing it through the active gain medium - another titanium-sapphire crystal. However, the high peak power of the ultrafast pulses can cause the gain to saturate by de-populating the medium before appreciable amplification can be obtained, causing unwanted nonlinear effects and even damage to the optics.

To overcome these problems, temporal dispersion, or *chirp*, is first introduced in the seed beam by an arrangement of diffraction gratings (stretching) whereby different frequency components in the pulse are made to follow different optical path-lengths, as shown in figure 3.6. As the pulse duration is now much longer than the original pulse, the peak power is greatly diminished, thus allowing further amplification without saturating the gain medium.

A single stretched pulse from the 82 MHz pulse-train is then switched into the cavity by a Pockel's cell, which is an electric-field induced $\lambda/4$ plate. The

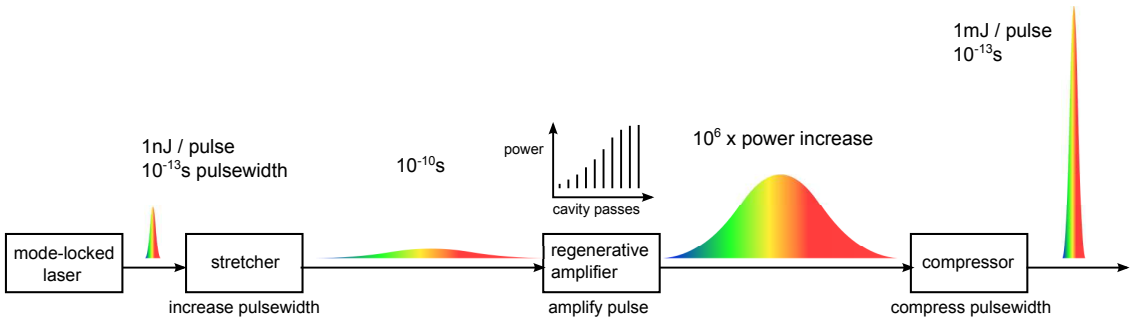

Figure 3.6: *Schematic of chirped pulse amplification in regenerative amplifier. Pulses from a mode-locked laser are temporally stretched and amplified by multiple passes within a regenerative amplifier cavity and then compressed giving a power increase of six orders of magnitude.*

incoming light beam is polarised in such a way that it reflects from the surface of the titanium-sapphire gain medium and out of the cavity. When a suitably timed voltage is applied to the Pockel's cell, it acts to rotate the polarisation of the incoming beam such that a single pulse propagates through the gain medium rather than being reflected. The pulse is allowed to travel through approximately 10 round trips of the amplifier cavity, increasing in intensity with each pass. After this a 2nd Pockel's cell rotates the polarisation of the intra-cavity pulse, switching it out of the cavity.

The amplified pulse is then sent through the reverse of the stretching optics where the dispersed components are allowed to "catch up" thereby producing a short, highly amplified pulse. The pulse energy at the output of the amplifier is 1 mJ with a pulse duration of 100 fs, corresponding to a 10^6-fold energy increase.

3.2.1.3 Optical parametric amplifier

The extremely high electric fields associated with amplified ultrashort pulses allows access to the nonlinear optical regime. The optical parametric amplifier (OPA) takes advantage of these processes to tune the pulsed laser output through the UV, visible and infrared regimes. The key component of an OPA is the

nonlinear crystal. Nonlinear crystals are **birefringent** materials that have a high nonlinear response to intense radiation.

Optical parametric amplification specifically refers to the process of stimulated down-conversion in a nonlinear crystal where a high energy 'pump' photon is split into two lower energy photons (designated as the signal and idler) - satisfying conservation of energy

$$\omega_{pump} = \omega_{signal} + \omega_{idler} \tag{3.4}$$

where ω is the optical frequency (proportional to photon energy), and conservation of momentum otherwise known as the phase-matching condition:

$$\mathbf{k}_{pump} = \mathbf{k}_{signal} + \mathbf{k}_{idler} \tag{3.5}$$

where **k** refers to the wave vectors of the pump, signal and idler beams.

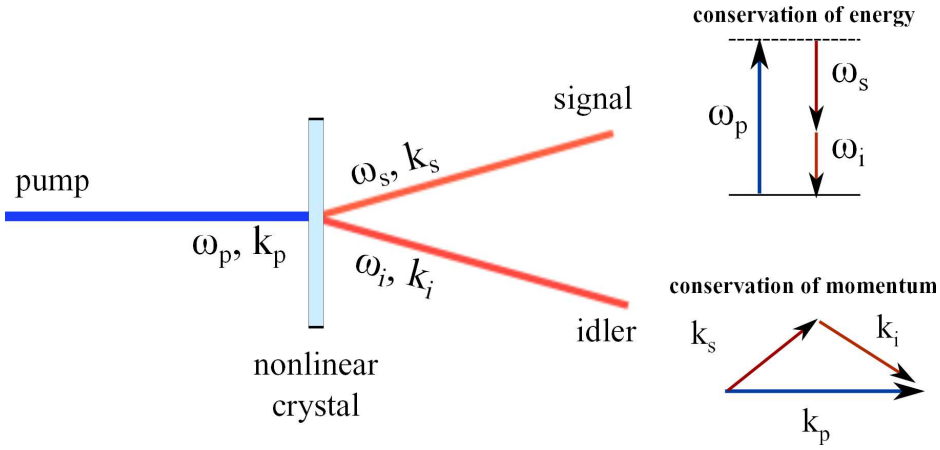

Figure 3.7: *Parametric down-conversion in which a pump photon is split into two photons whose frequencies add to the original pump frequency, thus satisfying conservation of energy. Phase-matching ensures conservation of momentum.*

In the optical parametric amplifier (OPA), stimulated down-conversion was induced by overlapping the 800 nm pump beam from the regenerative amplifier with a white light continuum (see section 3.4.1) beam. This broad bandwidth

seed beam contained photons within the frequency range of the generated signal and idler photons; thus down-conversion was **stimulated**. As stimulated down-conversion does not rely on random fluctuations (as in spontaneous down conversion) the stability and efficiency of the process is enhanced (see figure 3.8).

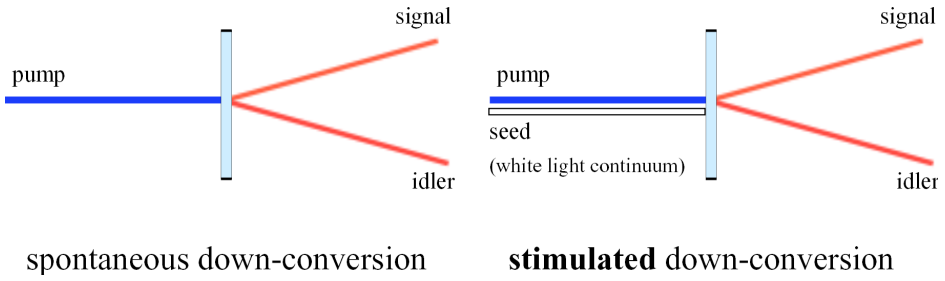

Figure 3.8: *Spontaneous parametric down-conversion is induced by random fluctuations, whereas stimulated down-conversion is seeded by photons from a white light continuum beam.*

It should be noted that the k-vector of the signal and idler does not need to be in a different direction to the pump as shown in figures 3.7 and 3.8 because the refractive index experienced by the three waves also depends on their frequency and polarisation with respect to the crystal axis. In fact down-conversion is more efficient when the beams are collinear as it increases overlap within the crystal. Figure 3.9 shows the momentum conservation for non-collinear and collinear phase-matching.

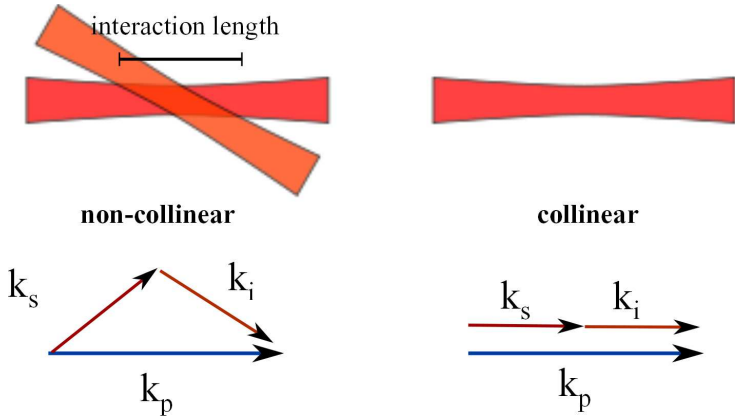

Figure 3.9: *Collinear phase-matching.*

By changing the angle of the crystal's optical axis with respect to the pump

beam, the phase-matching condition allows selection of which combination of ω_{signal} and ω_{idler} are able to propagate. Hence by choosing the appropriate phase-matching angle and delay between the seed and pump beams, the down-conversion can be tuned to preferentially choose the wavelengths of the signal and idler. The resulting signal and idler beam seeds a second "power stage" pass of the crystal, pumped by a higher intensity (than the pump in the first pass) 800 nm beam.

As the signal and idler photons produced in this process are lower in energy than the 800 nm fundamental, the output radiation is in the infrared region (~900-2500 nm). To extend the range of these tunable pulses back into the visible and UV region, a number of other nonlinear processes can be used.

The signal or idler can be frequency-doubled by the process of second-harmonic generation or SHG whereby two incoming pump photons can be converted into a single photon with twice the energy, again satisfying conservation of energy:

$$\omega = 2\omega_{pump} \tag{3.6}$$

and momentum with the phase-matching condition:

$$k(2\omega) = 2k(\omega) \tag{3.7}$$

The SHG output (ω_i) from the previous step can be extended further still into the blue and UV regime by frequency mixing with the residual 800 nm pump beam (ω_j) (figure 3.10), generating the sum-frequency signal:

$$\omega = \omega_i + \omega_j \tag{3.8}$$

The processes are all summarised in Figure 3.11.

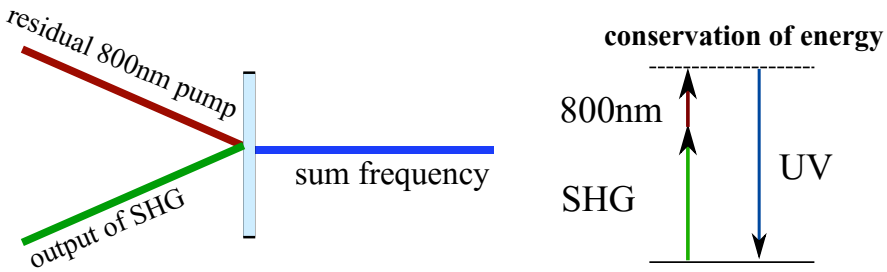

Figure 3.10: *Sum-frequency mixing of second harmonic output with residual 800 nm gives output into the ultraviolet.*

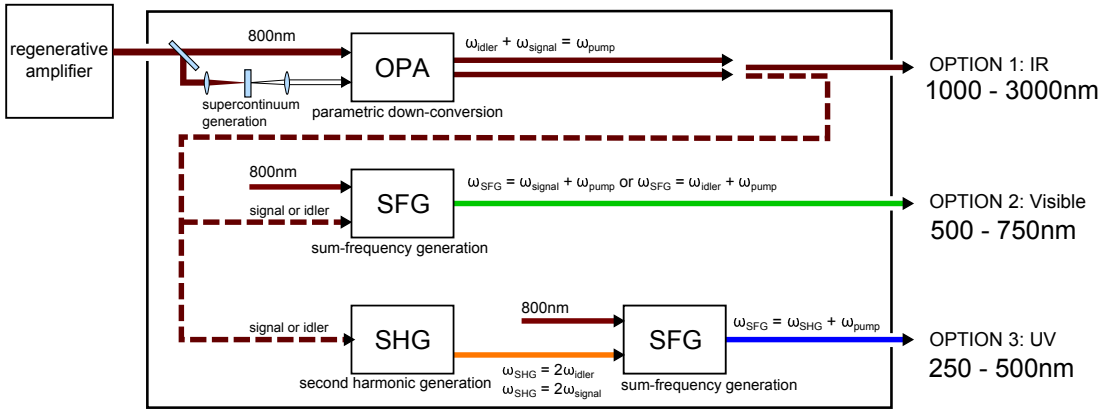

Figure 3.11: *Schematic showing 3 main options for wavelength tuning of optical parametric amplifier output: 1. Signal or idler, 2. frequency mixing signal or idler with 800 nm or 3. second harmonic of signal or idler and mixing with 800 nm*

3.3 Streak camera

A picosecond streak camera (shown in Figure 3.12) was used to investigate the time-dependent fluorescence of DCM and DCJ in a number of solvents.

A spectrometer was used to select the wavelength range of interest and the streak camera then resolved the time-dependent behaviour. In the streak camera [81, 82, 83], fluorescence is collected by the lens and focussed onto a photocathode, producing a burst of electrons where the number of electrons, $N_e(t)$, is proportional to the intensity $I(t)$. The electron pulse is then passed between a pair of deflection plates onto which a linear ramping voltage is applied.

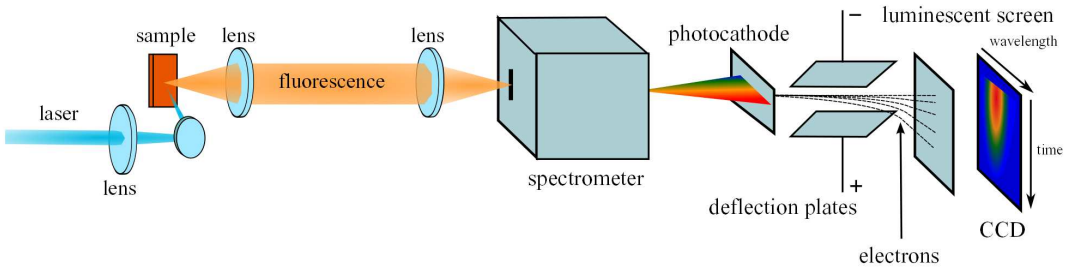

Figure 3.12: *Schematic of time-resolved fluorescence setup using a streak camera. A spectrometer separates the spectral components, which are imaged onto the x-axis of the CCD. A photocathode converts the time-dependent intensity to a time-dependent pulse of electrons which are deflected by ramping the voltage on a pair of deflection plates. The spatial profile (in the y-axis) can then be correlated to the original time profile. Figure 3.13 describes this further.*

Electrons at different points in time experience a higher voltage and are thus deflected by different amounts. In this way the temporal information is converted to spatial information as shown in figure 3.13. The electron positions were recorded by a luminescent screen which is imaged by a 2D CCD.

3.3.1 Fluorescence anisotropy

The anisotropy (section 2.2.3.2) of the time-resolved fluorescence can be determined by detecting the signals that are parallel and perpendicularly polarised with respect to the laser polarisation. When taking such measurements, it is important to take into account differences in the detection sensitivity of the two polarised components by calculating a so-called "G-factor" given by

$$G = \frac{I_{HV}}{I_{VH}} \tag{3.9}$$

This perpendicular signal is multiplied by the G-factor giving a modified equation for the anisotropy function

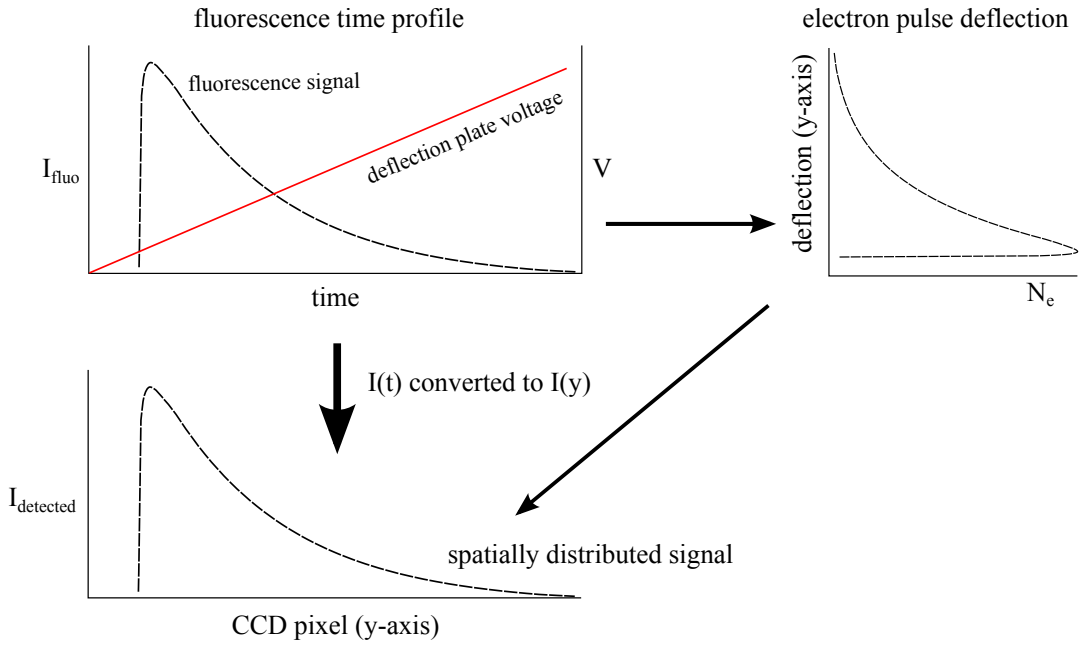

Figure 3.13: *In a streak camera, the time-dependent fluorescence $I(t)$ is converted to a time-dependent pulse of electrons $N_e(t)$. A linear voltage ramp is applied to deflection plates such that different temporal components of the electron pulse experience increased vertical deflection. The spatial distribution of electrons is focussed onto a luminescent screen which is then imaged onto a CCD. The spatial distribution can then be calibrated to re-construct the temporal profile.*

$$r = \frac{I_{\parallel} - GI_{\perp}}{I_{\parallel} + 2GI_{\perp}} \tag{3.10}$$

This ensures that the anisotropy is measured correctly.

3.3.2 Experimental issues with the streak camera technique

The streak camera resolution is limited by the speed or ramp of the voltage sweep as this determines the ability of the camera to appreciably deflect the temporal components of the signal such that they can be resolved on the CCD. In the case of this experiment, the streak camera has a resolution of approximately 1 picosecond. Any dynamics shorter than this will either not be seen at all or temporally smeared or smoothed.

The particular streak camera used in this study has an anomalous region that is less sensitive than the rest of the detector. This can be seen in the spectra as a decreased intensity as shown in figure 3.14. This feature is seen in all streak camera data presented in this thesis and and in all analyses it has been assumed to be an experimental artefact and not due to sample dynamics.

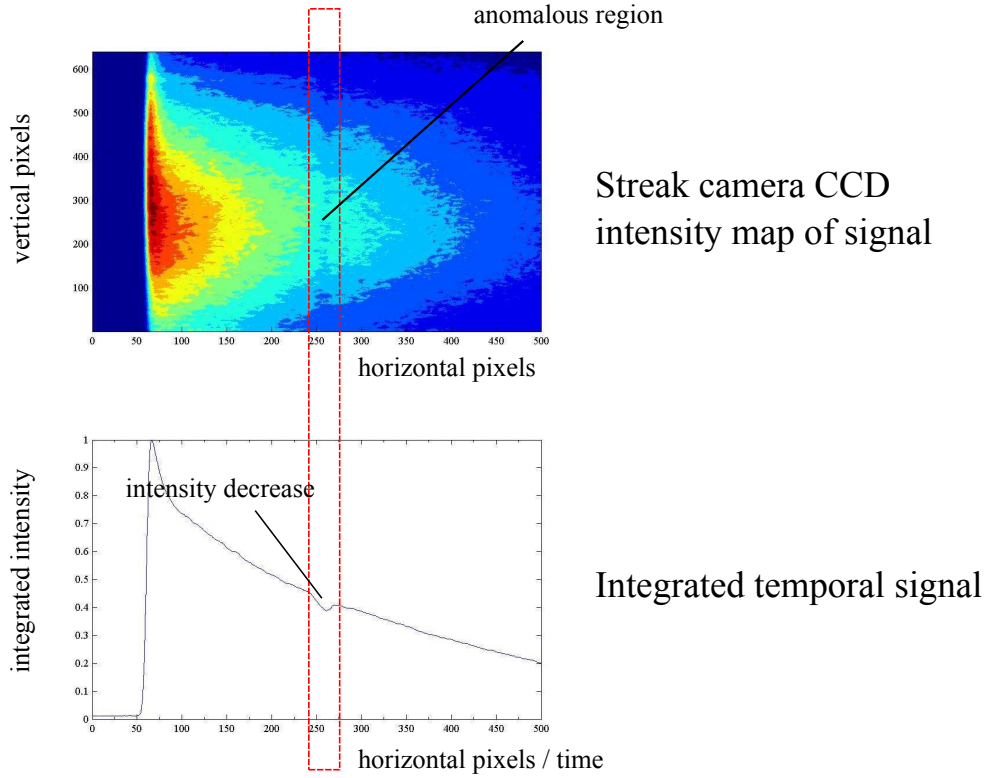

Figure 3.14: *A lower sensitivity region of the streak camera detector CCD in the vertical direction causes an intensity dip in time resolved fluorescence signals.*

3.4 Pump-probe spectroscopy

A limitation of fluorescence based measurements is that the molecule being studied is required to relax radiatively, which is not always the case. There may also be processes prior to fluorescence that are non-radiative. So, an experiment

is needed that can examine the dynamic molecular processes independent of the presence of fluorescence.

An experiment that accomplishes this feat is time-resolved pump-probe spectroscopy [84, 85]. This technique is used to study transient changes in the excited-states of the molecule. As with fluorescence spectroscopy, a high-intensity pump laser creates a population of molecules in the excited-state. Instead of measuring the spontaneously emitted fluorescence signal, a probe beam is overlapped with the pump beam. The time-resolved evolution of the excited-state(s) is then monitored by observing the transient gain or attenuation of the transmitted probe beam.

The difference between this and time-resolved fluorescence is that the probe can be tuned to any optical transition from the ground or excited-state of the molecule, including intermediate and short-lived states.

A custom pump-probe experimental setup was built for this study with the purpose of measurements with higher temporal resolution dynamics than possible with the picosecond streak camera experiment described above. The requirements for the experiment were high time resolution (pulse-width limited to 100 femtoseconds), high spectral bandwidth (400-800 nm) with white-light continuum probe discussed in section 3.4.1 and polarisation resolved.

A typical setup of pump-probe spectroscopy is shown in figure 3.15, where the pump and probe beams are overlapped in a common focal region within the sample. The probe beam was focussed to a smaller spot size at the centre of the excited-state volume so that diffusion of ground-state molecules from outside the pump region did not influence the signal. An optical delay line consisting of a pair of movable retro-reflecting mirrors was used to control the time separation between the pump and probe pulses and a photo-detector was used to measure the changes in probe intensity. Note that the figure shows the optical delay line

is on the pump beam rather than the probe beam. This was done for practical reasons. Thus, the probe delay was increased by advancing the pump-beam i.e. decreasing the path-length of the pump with respect to that of the probe.

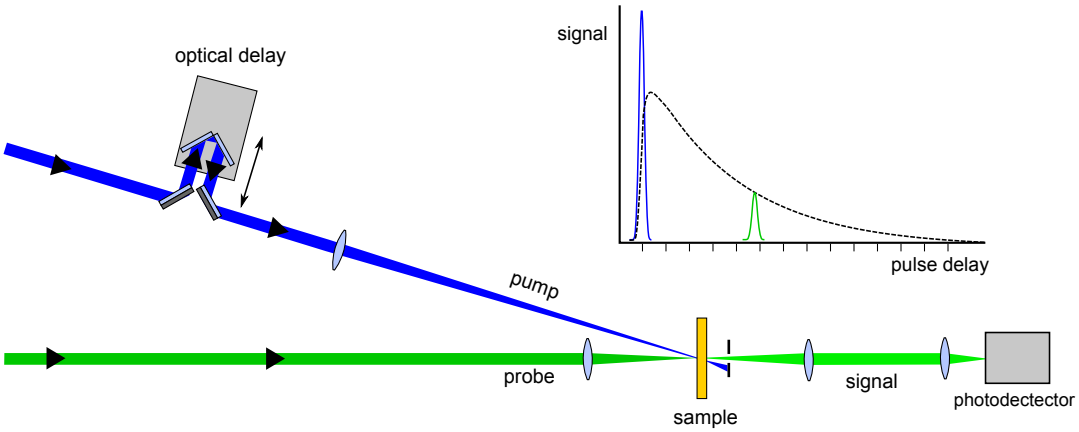

Figure 3.15: *Schematic diagram of a pump probe experiment. The pump beam puts the molecule in an excited state. The probe intensity is measured at increasing pulse-delay times with respect to the pump-pulse. The probe intensity can increase or decrease compared with the pre-pump intensity due to absorption or stimulated-emission transitions from the excited state.*

Increases in probe transmission intensity ($\Delta T > 0$) may be due to either stimulated emission by probe photons or ground-state bleaching (where a depletion of population in the ground-state causes a "spectral hole" in the ground-state absorption region). Negative signals ($\Delta T < 0$) originate from excited-state absorption in which transitions from excited-states to higher excited-states can occur. These processes are summarised in figure 3.16.

By measuring the transient rise and decay of these effects we can examine the relaxation dynamics of the sample of interest, in particular the formation of highly polar species due to charge transfer and other configurational changes such as isomerisation.

The optical delay line consisted of a retro-reflecting mirror arrangement on a linear translation stage controlled by computer. The linear actuators could be moved in steps as small as d=0.1 μm, which corresponds to a delay time of 0.67

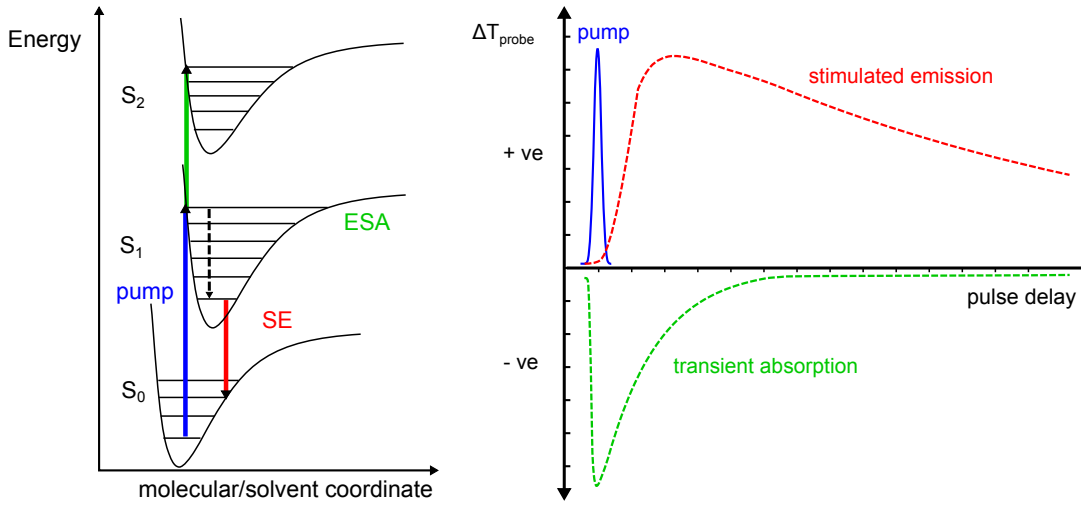

Figure 3.16: *Energy diagrams and pump-probe signals illustrating the origin of stimulated emission (SE) without inversion and excited-state absorption (ESA) signals.*

fs calculated using:

$$delay = \frac{2d}{c} = \frac{2 \times 10^{-7} m}{3 \times 10^{8} m/s} = 6.7 \times 10^{-16} s = 0.67 fs \tag{3.11}$$

Thus the limit to time resolution is the pulse-width (~100 femtoseconds at FWHM).

The pump pulses used to excite the molecules in this study were generated by wavelength tuning of one of the laser system's two optical parametric amplifiers.

3.4.1 White-light continuum probe

A simple pump-probe spectroscopy setup uses a probe that is tuned to a single excited-state transition, thus only a simple photo-detector is required. However excited-state relaxation often involves numerous states with different contributions to the overall signal. A technique known as supercontinuum generation [86] can be used to produce a broad bandwidth white-light probe source that can retain the short pulse-width of the laser used to generate it.

A supercontinuum probe source can thus be used to simultaneously probe an excited-state spectrum [20, 87] which includes absorption and stimulated emission contributions. This type of setup is very widely used in the ultrafast spectroscopy community due to the rapid overall picture of the dynamics of excited-state transitions that can be obtained [88, 89, 90].

Focussing an intense femtosecond beam into a transparent medium can generate a pulsed supercontinuum beam as shown in Figure 3.17.

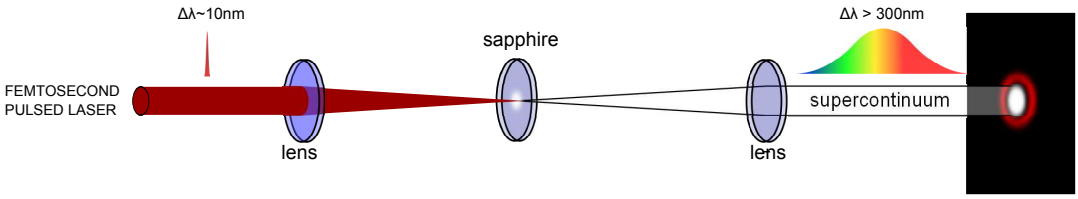

Figure 3.17: *Supercontinuum generation.*

The process of continuum generation makes use of the intensity dependent component of the nonlinear refractive index $n_2(\mathrm{I})$. Assuming the pulse envelope is Gaussian, the material will see a time-dependent intensity as the pulse propagates through it. Thus different parts of the pulse experience a different refractive index.

This condition gives rise to a time-dependent phase shift, $d\phi/dt$; a process known as *self phase modulation*. Equation 3.12 describes the optical frequency shift ω relative to the input frequency ω_0 (as shown in figure 3.18).

$$\omega = \frac{d\phi}{dt} = \omega_0 - A\frac{dI}{dt} \tag{3.12}$$

As the optical frequency from the above equation is proportional to dI/dt, the frequency decreases at the front edge of the pulse and increases at the trailing edge. Thus the pulse spectrum is broadened as shown in 3.18.

Some investigation was undertaken on the most suitable material for con-

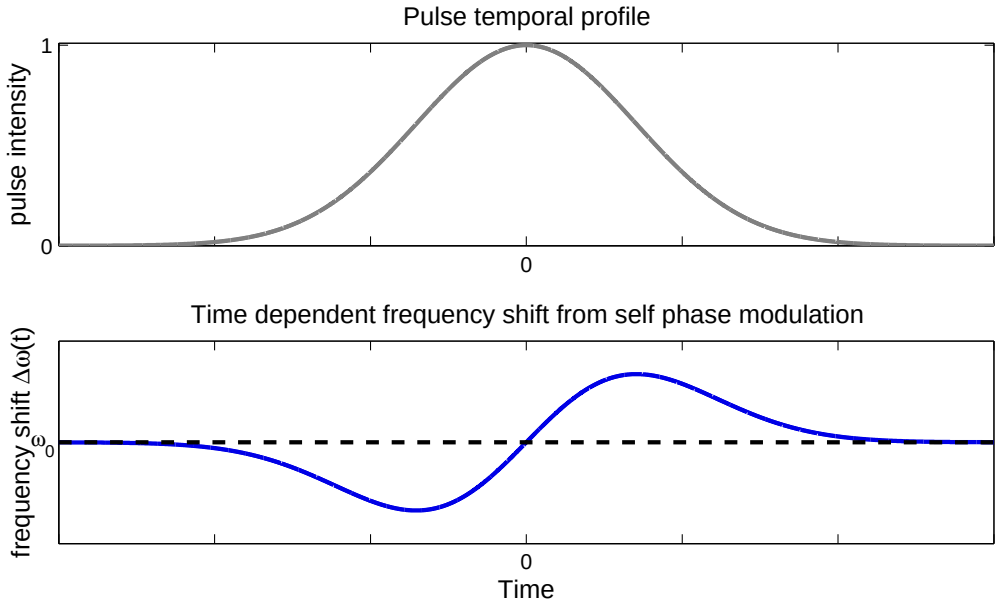

Figure 3.18: *Temporal profile of femtosecond pulse and frequency shift caused by the intensity dependent nonlinear refractive index $n_2(I)$ as given by equation 3.12.*

tinuum generation. Calcium fluoride, sapphire, silicon glass and a number of liquids - acetone, water, heavy water, methanol and ethanol - were looked at and it was concluded that intensity stability and quality of the continuum was best in a solid glass. Sapphire was used for the pump-probe experiments in this study as it gives a broad continuum with good intensity stability.

The spectrum of the continuum spans the range from approximately 450-1200 nm as shown in Figure 3.19 in which an 800 nm beam of 1 mJ pulses was focussed into a 2mm thick sapphire window.

The continuum generation process is complicated by the other possible nonlinear processes that occur in conjunction to the self phase modulation such as four wave mixing, stimulated Raman scattering, up-conversion, down-conversion and harmonic generation. This produces a more complicated spectral characteristic of the continuum than that predicted by self phase modulation alone. However, a reference beam is picked off from the probe beam before

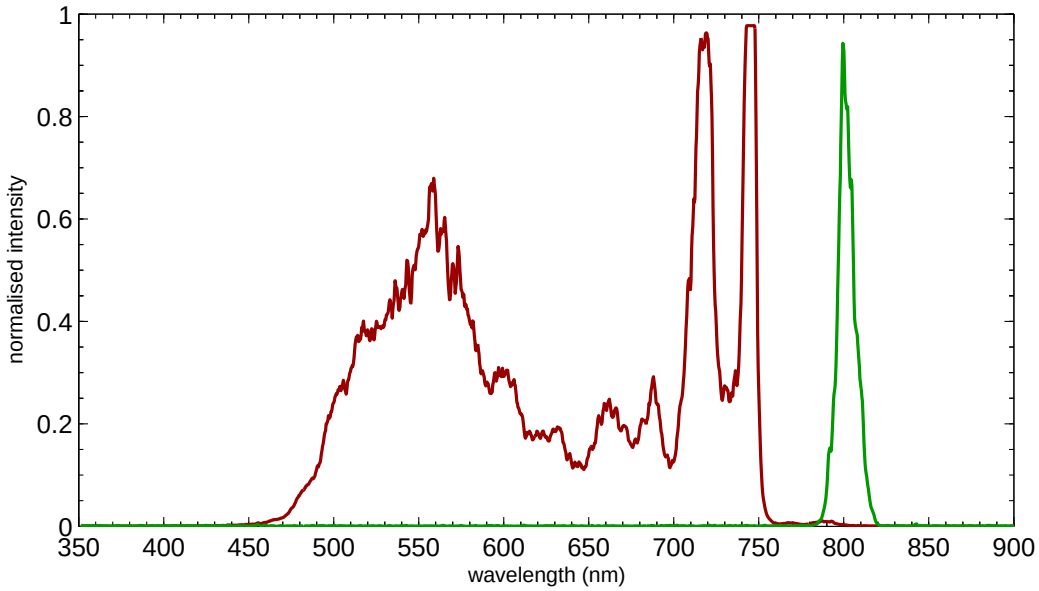

Figure 3.19: *Increase in spectral bandwidth upon generation of white light continuum by focussed 800 nm pulse into 2 mm thick sapphire window. * Continuum spectrum attenuated by bandpass filter at $\lambda > 750$ nm to remove residual fundamental laser*

traversing the sample and detected simultaneously with the signal channel (as shown in Figure 3.22). This provides a reference spectrum to allow the actual transmission/absorption spectrum to be calculated.

3.4.2 Time zero and measurement of temporal chirp

Time zero in a pump-probe experiment is defined as the condition when the pump and probe pulses arrive at the sample simultaneously. This can be found approximately by eye by monitoring the probe brightness on a card while moving the retro-reflecting delay stage. On the negative side of time zero there is a characteristic jump in the transmission of the probe. This effect is seen because the pump pulse changes the state of the molecules from which the probe transitions occur, and at time zero the population of molecules in this state is at a maximum, whereas just before time-zero there is zero (or negligible) population in the excited-state. The probe intensity at a given wavelength is proportional

to the population of molecules in the state at which a transition occurs. The probe signal (intensity change) can be either negative, such as in excited-state absorption, or positive from a ground-state bleach or stimulated emission signal.

To more effectively find the time zero point position of the delay stage, a BBO (beta-barium borate) nonlinear crystal was placed at the overlap point of the pump and probe beams. At the time-zero position, a cross-correlation second harmonic signal is generated between the pump and the probe. By monitoring the intensity of the cross-correlation signal versus the fine position of the delay stage, the pulse overlap maximum was determined.

In the white light continuum probe version of this experiment there is an added complication - temporal chirp. Temporal chirp refers to the spreading out of the pulse in time as a function of wavelength due to the dispersion properties of the material (supercontinuum generating medium, lenses) through which it propagates before reaching the overlap with the pump pulse [91]. This effectively means that time zero is not a single position for every wavelength within the probe spectrum. In order to characterise this temporal chirp and correct for it in the experiments, a technique called optical Kerr gating [92, 76] was used.

The Kerr effect encompasses a range of optical phenomena that occur when materials through which light propagates are subject to high electric fields. The electric field causes distortion of the electrons within the material such that the refractive index changes in the direction of the applied field. The DC Kerr effect, such as when the optical material is placed between two electrodes with a voltage between them, causes the material to be birefringent, where the refractive index depends on the orientation of the incoming light with respect to the electric field of the electrodes.

The AC Kerr or optical Kerr effect is the equivalent effect caused by an alternating electric field such as an intense light beam. This effect accounts

for the intensity dependent refractive index required for the Kerr-lens mode-locking scheme described earlier in the chapter. Essentially, an intense light beam (pump) with its fast-varying AC electric field can modulate the refractive index of a transparent material in the direction of its polarisation, such that a second light beam passing through this overlap point will experience a shift in its polarisation direction due to the material's induced birefringence. If the two beams are pulsed, this effect will only occur if the two pulses are overlapped spatially and temporally.

By placing crossed polarising filters in the second (probe) beam on either side of the overlap point and a detector after the second polarising film, a probe intensity signal will only be detected when the AC Kerr effect occurs. The polarisation shift causes the probe to have polarisation components that are orthogonal to the extinguishing polarisation direction of the filter, allowing transmission to the detector.

The chirp can be measured using the frequency resolved optical gating (FROG) technique the optical setup of which is shown in figure 3.20. The basis of the FROG measurement is conceptually a simple one. A pump pulse causes the optical properties of an active material to change within the pulse duration such that the coincident component of the probe pulse (in this case the polarisation) is altered during this time period.

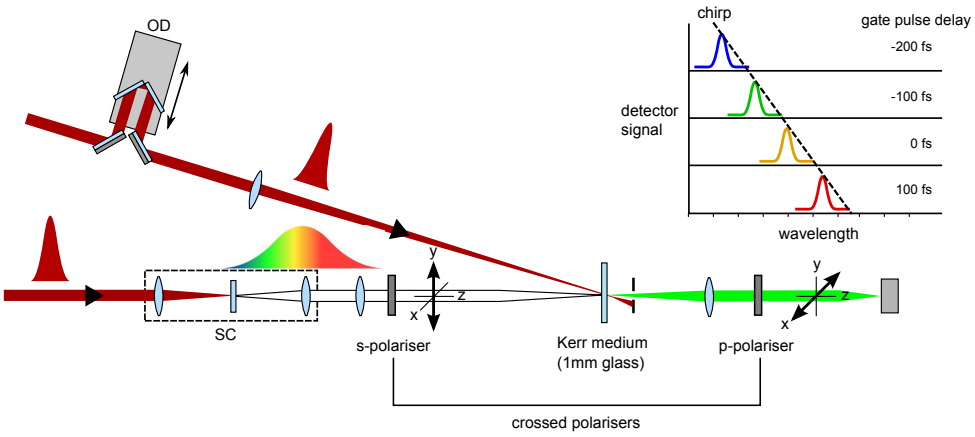

Figure 3.20: *Kerr gate method for Frequency Resolved Optical Gating (FROG) chirp characterisation of white light continuum.*

In this case we rely upon the AC electric Kerr effect in transparent dielectric media. The high electric field ($\sim 10^{14}$ V.pulse^{-1}cm^{-2}) of the pump pulse can induce an oscillating dipole in the solid material creating birefringence. This causes the polarisation of the continuum beam (the beam of interest) to be rotated.

By placing polarising filters before and after the Kerr medium in the crossed configuration, the Kerr effect acts as a temporal **gate** allowing light through the polariser only when the polarisation is rotated. Thus, in conjunction with a spectrometer, the wavelength dependent shift of the time overlap between the gate and the chirped supercontinuum pulse can be determined. This gives a picture of the temporal and spectral profile of the white light pulse.

In principle this experiment can also be used to determine the phase of a pulse for complete pulse characterisation, but for our purposes we are only interested in the intensity information as this is sufficient to characterise the temporal dispersion of the pulse.

A measurement of the chirp from a 2mm sapphire window is shown in figure 3.21, in which the red side of the pulse is delayed in time with respect to the blue

side. The chirp t(λ) was fit satisfactorily with a cubic function and corrected by subtracting this function from the measured spectrum - corresponding to a shift of the measured delay time at each wavelength.

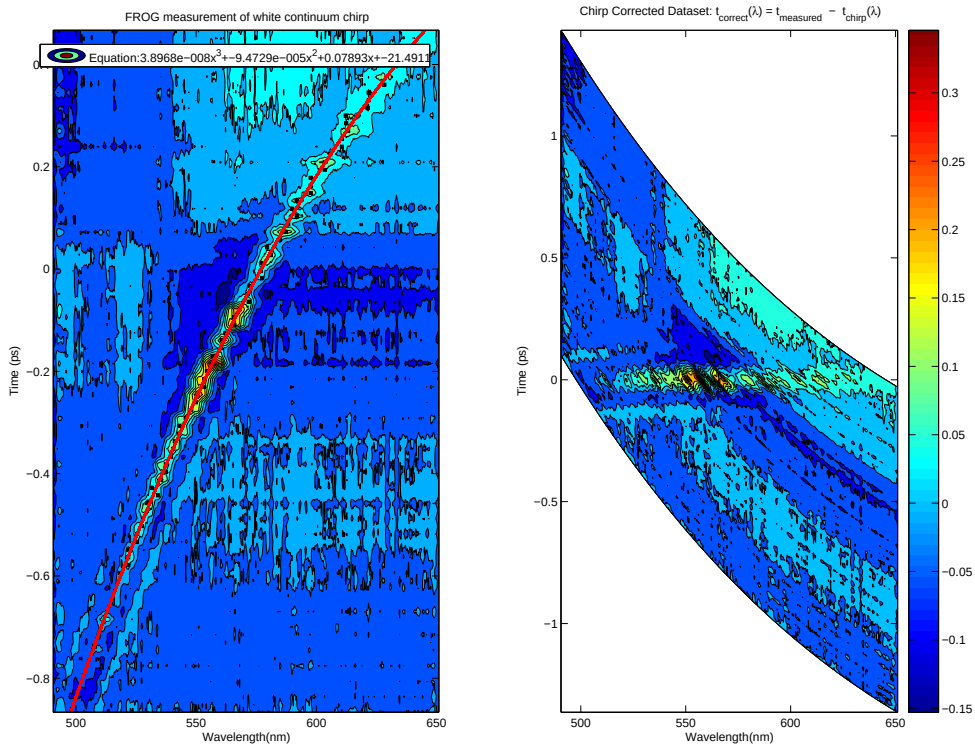

Figure 3.21: *Optical Kerr gate measurement of chirp of white light supercontinuum generated from 2 mm sapphire window (left) and corrected data (right)*

This information was used to post-process the data to minimise artifacts due to the temporal chirp of the white light supercontinuum probe.

3.4.3 Pump-probe anisotropy

The time-dependent anisotropy can also be measured in a pump-probe experiment. This involves rotating the polarisation of the probe beam 45° relative to that of the pump such that the vector components of the polarisation that

are parallel and perpendicular to the pump polarisation are equal in magnitude. After transmission through the sample, the two components are then split into separate beams as the s and p polarised reflections from a polarising beam-splitter cube.

These components and a pre-sample probe reference spectrum of the probe (to calculate absorption and to account for change in the spectrum over time) are detected simultaneously via a 3 channel multi-fibre coupled Triax 350 spectrometer with a 2D 1024 x 256 pixel CCD array.

The layout of the optics for the pump-probe experiment (including anisotropy measurement) is shown in figure 3.22.

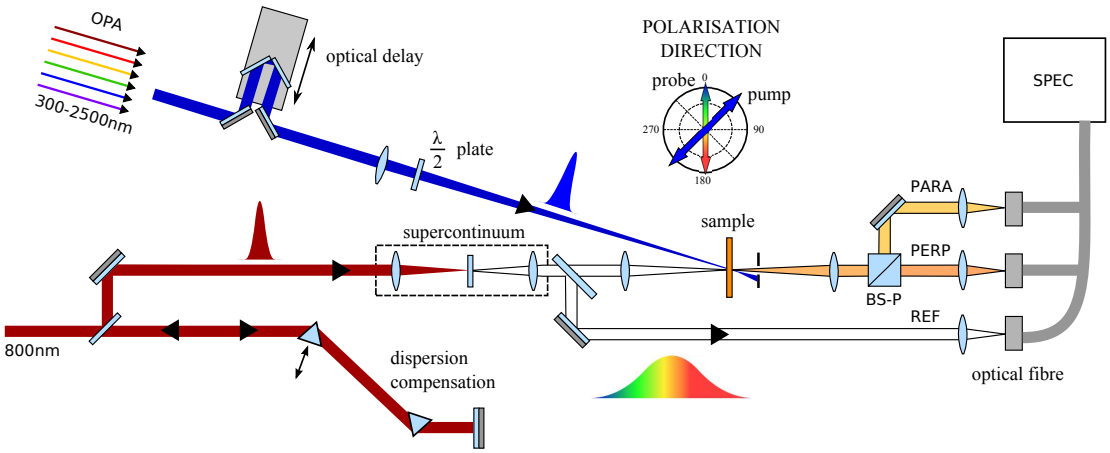

Figure 3.22: *Pump-supercontinuum-probe time-resolved polarisation anisotropy experiment.*

3.4.4 Calculations for pump-probe parameters

Rather than being a raw transmittance or intensity measurement, the white light pump-probe experiment has been calculated as a differential transmittance ΔT. This parameter is a measure of the gain or loss in the wavelength dependent transmission through the sample solution at times during and after the molecule is excited by the pump-pulse. It is calculated by subtraction of the pre-pump,

$T(t < 0)$, signal response from $T(t)$. Thus, $\Delta T(t < 0)$ is zero before the pump-pulse, an increase in transmission caused by ground-state bleach or stimulated emission gives $\Delta T > 0$ and a decrease caused by excited-state absorption gives a negative differential transmission of $\Delta T < 0$. In this study, the positive stimulated emission signal was chosen as it measures the stimulated emission from the proposed intramolecular charge transfer state but with a higher resolution than the streak camera fluorescence measurement.

Table 3.1 summarises the data collected from the experiment described in the previous section.

Variable	Description
$\mathrm{I}_{steady}(\lambda)$	Transmitted probe intensity in the steady-state - before pump pulse
$\mathrm{I}(\lambda, t)$	Transmitted probe intensity after pump
$\mathrm{I}_{ref}(\lambda)$	Supercontinuum reference spectrum versus time*

Table 3.1: *Raw measured signals from pump-probe experiment described in figure 3.22.*

From this raw data, a number of parameters were calculated.

The difference in optical response of the parallel and perpendicular channels were corrected by the following method:

1. A **correction factor** (equation 3.13) was calculated by taking the ratio of the parallel and perpendicular channels at times much less than zero i.e. before the pump creates an anisotropic population distribution. The assumption is that at this point in time, all transition dipoles are randomly aligned and thus the actual responses for $I_{\parallel}$ and $I_{\perp}$ should be equal.

$$c(\lambda) = \frac{I_{\parallel}(\lambda, t \ll 0)}{I_{\perp}(\lambda, t \ll 0)} \tag{3.13}$$

2. A corrected perpendicular channel was calculated by multiplying the uncorrected channel by the correction factor to account for differences in detection

efficiency.

$$I'_{\perp}(\lambda, t) = I_{\perp}(\lambda, t).c(\lambda) \tag{3.14}$$

3. The transmission in the absence of the pump T_0 (equation 3.15) and the transmission after the pump T_1 (equation 3.16) were calculated by dividing each raw spectral intensity value by the reference beam.

$$T_0 = \frac{I_{signal}}{I_{ref}} \tag{3.15}$$

$$T_1 = \frac{I_{signal}(t)}{I_{ref}(t)} \tag{3.16}$$

The differential transmission or the change in transmission (positive or negative) caused by the influence of the pump beam was calculated using equation 3.17.

$$T = \frac{T_1 - T_0}{T_0} \tag{3.17}$$

As with the fluorescence anisotropy, the pump-probe anisotropy parameters can be calculated:

Magic angle:

$$\Delta T_{MA} = \Delta T_{\parallel} + 2\Delta T_{\perp} \tag{3.18}$$

and anisotropy:

$$r = \frac{\Delta T_{\parallel} - \Delta T_{\perp}}{\Delta T_{\parallel} + 2\Delta T_{\perp}} \tag{3.19}$$

3.5 Samples

3.5.1 Laser dyes

The laser dyes DCM and DCJ were obtained from Lambda Physik and were used without further purification.

3.5.2 Solvent properties

A solvent's role in the photophysics of molecules in solution is not just to provide a convenient means of containing the sample molecules and allowing them to move. Rather, the solvent itself, both as a bulk material and in the local environment surrounding the dissolved solute, must be considered as a part of the overall system. The solvent and its interactions with the solute play an integral part in the excited-state energies available to the molecule and the dynamics of those states. As discussed in chapter 2, there are a number of important solvent parameters that play a major role in the dynamics of donor-acceptors in solution. The dipole moment, dielectric constant, refractive index, absorption spectrum and viscosity are all expected to have an effect. In order to isolate the contributions of each of these parameters to the features seen in the steady-state and time-resolved spectroscopic measurements, the experiments were performed and are presented in the results section in a specific order.

In order to establish a baseline of spectroscopic features to investigate in this study, a solvent was chosen that has well understood properties and has a precedent for use in similar studies of charge transfer states and solvation. Methanol is commonly used in many spectroscopic studies of DCM and other donor-acceptor compounds in the literature [19, 20, 21, 16, 17, 18]. It is a polar solvent, has a simple structure and its properties are reasonably well

characterised and understood. For this reason, methanol was chosen as the solvent for these initial investigations of DCM.

As seen in chapter 2, the time-dependent behaviour of excited-states can depend on the ability (or inability) of the solvent and solute to diffuse. The solvent viscosity can thus effect the dynamics of excited-states by changing the diffusion rates and thereby changing the rates of decay processes that require diffusion to operate such as solvation and intermolecular charge transfer. In order to determine which features seen for DCM in methanol are dependent on diffusion, a series of solvents with different viscosities were chosen. Methanol, ethanol and n-pentanol (1-pentanol) are all straight chain hydrocarbon based solvents with polar hydroxyl-groups at one end. They have very similar dipole moments and viscosities that are related to their size/molecular weight.

The ability of solvents to solvate highly polar charge-transfer excited-states depends on the ability of solvent dipoles to align to the electric (reaction) field induced by the change in dipole moment of the solute. A solvent with a permanent dipole moment can rotate and translate within the solvent cage to accomplish this, whereas a non-polar solvent cannot. In order to then investigate the effect of dipole moment and dielectric constant on the excited-state energetics and dynamics of the excited-state of DCM, it was investigated in a non-polar solvent, toluene, and a more polar solvent than methanol, acetone.

Methanol, ethanol, n-pentanol, acetone, toluene and ethylene glycol for solvent dependence studies were spectroscopic grade from Sigma-Aldrich.

Some relevant physical parameters are given in table 3.2, which will be referred to in the results section

Solvent	Dipole Moment μ (D)	Dielectric Constant ϵ @ 20°C	Refractive Index n_D @ 20°C	Viscosity η mPa.s @ 25°C
Methanol	1.7	33	1.3265	0.539
Ethanol	1.69	25.3	1.3594	1.057
n-Pentanol	1.7	17.84	1.4080	3.425
Acetone	2.88	21	1.3560	0.308
Ethylene Glycol	2.31	41.4	1.4306	17.65
Toluene	0.36	2.385	1.4941	0.548

Table 3.2: Solvent properties - μ, ϵ sourced from [93] and n_D, η from [94]

3.5.3 Photo-bleaching

Prolonged exposure to the pump laser can cause irreversible photo-bleaching or photo-degradation of the sample molecules by processes such as photo-oxidation, photo-dissociation, photo-induced free-radical reactions and isomerisation. In order to minimise these effects during experimental measurements, a custom built apparatus for circulating the solution through the focal region was built.

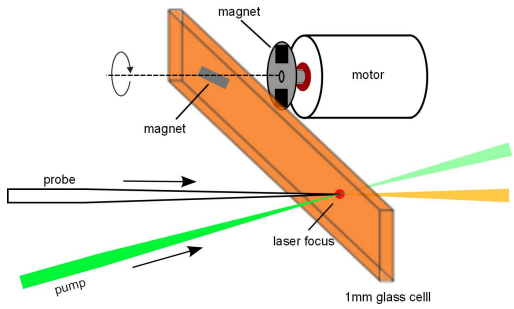

Figure 3.23: *Custom built magnetic stirrer circulates the sample through the laser focus point to minimise photo-bleaching.*

Figure 3.23 shows a diagram of the stirrer, which consists of a motor with a wheel on the shaft, to which is attached a pair of permanent magnets. A small permanent magnet placed in the cuvette then rotates as the wheel rotates, circulating the solvent and target molecules through the focus volume of the laser.

3.5.4 Streak camera versus pump-probe: Advantages and advantages

As discussed in section 3.3.2, the streak camera has a resolution of a a few picoseconds and as will be seen in the results chapters, this timescale is sufficient to observe dynamics in the population and anisotropy data. Thus, for these processes the streak camera data is presented. As the entire 3D time-resolved fluorescence spectrum is captured almost simultaneously in a streak camera, the influence of changes in the pump laser intensity during measurements is minimised. Variation in the pump intensity with time causes variation in the population of excited molecules produced with each pump-pulse, which in turn causes the signal intensity to vary with time and is therefore a source of noise. While still susceptible to rapid intensity variations of the excitation beam, the fluorescence streak camera technique is less sensitive to relatively slow intensity variations due to the simultaneous way in which spectral and temporal information is gathered on the CCD. Noise due to rapid fluctuations can be reduced by averaging many time-resolved spectra.

The pump-probe experiment used in this study, however, relies upon the mechanical motion of the retro-reflecting mirrors in the delay stage to measure the temporal dependence of the spectral signal and therefore is susceptible to variations in the pump-intensity (though there have been novel experimental designs built to overcome this problem [95]). It is of course possible to get intensity variations of the probe, but the reference channel (shown in figure 3.22) is measured to account for this.

A significant advantage of the pump-probe experiment for this study is its smaller temporal resolution compared with the streak camera. As the resolution is determined by the pulse-width of the pump and probe beams which are of the order of 100 femtoseconds, there is a 10-20 times improvement in temporal

resolution. The solvation of DCM occurs in the range from 10-150 picoseconds depending on the solvent. In chapter 4, both pump-probe and streak camera techniques are compared to determine which timescales, and therefore which experiment, is appropriate to study the photodynamics of DCM.

In general, the streak camera experiment is useful for dynamics that occur on the 100 picoseconds to several nanoseconds time-scale. The pump-probe is useful to study processes that occur from 100 femtoseconds to 100 picoseconds.

Chapter 4

DCM in methanol

4.1 Introduction

Studying DCM and other donor-acceptor molecules in solution allows investigation of the effect of solvent parameters on the energetics and dynamics of the excited-state. To establish a point of comparison, this chapter presents steady-state and time-resolved spectra of DCM in methanol, as it is a common solvent with well defined parameters [96, 97, 98, 99]. As a polar solvent, methanol is expected to stabilise the polar excited-state of DCM by solvation (section 2.2.2).

The steady-state absorption and fluorescence spectra and the signals from time-resolved fluorescence and pump-probe spectroscopy were measured to analyse the formation and relaxation of the excited-state. Further information was then obtained by analysing the randomisation of the anisotropic population created by the excitation light.

4.2 Steady-state

The steady-state absorption and fluorescence spectra, in which the energy of ground to excited-state transitions and excited-state radiative decay transitions are measured, are an important starting point for time-resolved spectroscopy. The measurements show what excitation energy/frequency to use, what energy to expect emission to be detected at but, more importantly, how much energy is lost before fluorescence occurs. This energy difference is the Stokes shift mentioned in chapter 2 2.1.

DCM was dissolved in methanol at a concentration of 10^{-4} M and the steady-state absorption spectrum was measured with a Shimadzu UV-visible spectrometer. The fluorescence spectrum was measured by excitation with a pulsed 400 nm laser (1 nJ pulses with a duration of 100 fs and repetition rate of 80 MHz - corresponding to an average power of 80 mW) and the emitted fluorescence was focussed into a scanning monochromator and detected with a photomultiplier. The spectra are shown below in figure 4.1.

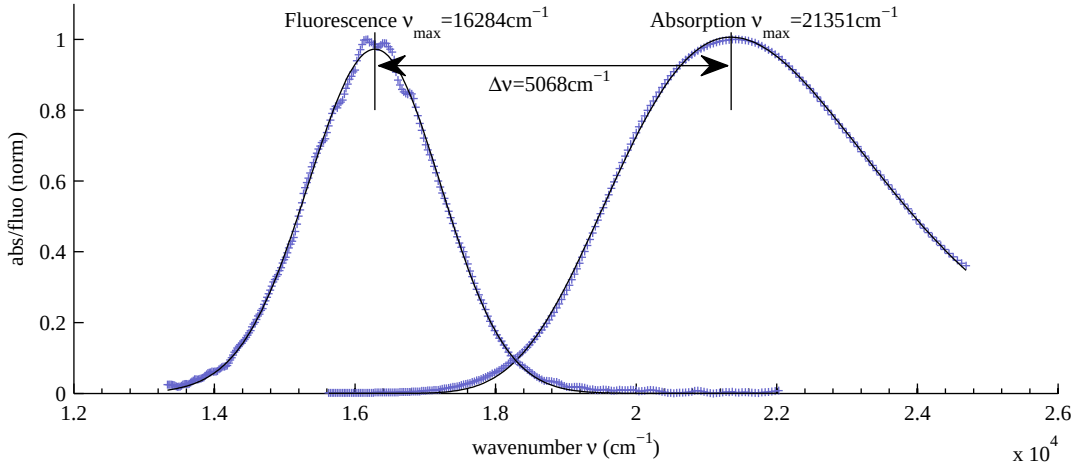

Figure 4.1: *Normalised absorption and fluorescence spectra of DCM in methanol*

4.2.1 Band-shape and general features

The visible absorption and fluorescence spectra of DCM in methanol are broad and exhibit very little structure. This is expected for a molecule in solution due to the large number of solvent environments altering the energy of each absorbing and emitting species.

4.2.2 Spectral fitting - Log-normal function

In order to quantify the parameters of the absorption and emission bands, the measured spectra were fit with a log-normal function of the following form as, unlike the more typically used Gaussian function, it allows for asymmetric band-shapes for complex molecular spectra [100],

$$g(\nu) = \left\{ \begin{array}{ll} g_0 exp\left(-ln(2)(\frac{ln[1+2b(\nu-\nu_0)/\Delta]}{b})^2\right) & \text{if } 2b(\nu-\nu_0)/\Delta > -1; \\ 0 & \text{if } 2b(\nu-\nu_0)/\Delta \leq -1. \end{array} \right\}.$$

where g_0 is the amplitude, ν_0 is the frequency of the fluorescence maximum, Δ is the bandwidth and b is an asymmetry parameter describing the deviation from a Gaussian line-shape. The fit parameters are shown in table 4.1.

$\nu_0 abs$ (cm^{-1})	Δabs (cm^{-1})	$\nu_0 fluo$ (cm^{-1})	$\Delta fluo$ (cm^{-1})	$\nu_{abs} - \nu_{fluo}$ (cm^{-1})
21352	4387	16284	2218	5069

Table 4.1: Central frequency, bandwidth of absorption and fluorescence spectra, and Stokes shift for DCM in methanol

The difference in energy between the central fluorescence and absorption band (the Stokes shift) is 5069 cm^{-1} consistent with previous studies [15]. This large shift indicates a significant loss of internal energy in the excited-state before emission occurs. This shift is likely to be the result of a combination of

a number of processes - vibrational relaxation from the initially excited Franck-Condon state, relaxation to a higher vibrational state in the ground electronic state, solvation to accommodate an increased dipole moment, energy transfer to adjacent DCM molecules and other internal processes.

4.2.3 Bandwidth

The absorption spectrum has almost double the band-width of the fluorescence spectrum. If the fluorescent state of DCM is highly polar and undergoes solvation, we might expect the fluorescence to be broader due to different solvent configurations surrounding molecules within the excitation volume of the laser excitation source. We have seen in chapter 2 that the energy of a polar excited-state is highly dependent on the structure of the solvent cage surrounding it; thus a range of solvent environments would mean that individual molecules emit at different energies, giving a broader spectrum.

It is therefore particularly interesting that the less polar. It is clear that there is something else going on.

4.3 Picosecond resolved fluorescence

The fluorescent state of DCM in methanol is known to decay within 1.3-1.4 ns [19, 42]; thus measurement of the time dependent spectral dynamics must be able to resolve timescales shorter than this. The picosecond streak camera setup described in chapter 3 is an ideal experiment for such measurements as it has a resolution of a few picoseconds. The spectrally resolved fluorescence decay measured by the streak camera reveals much about the long time dynamics of the fluorescence state of DCM. The time dependent fluorescence spectra were measured at a parallel and perpendicular polarisation (with respect to

the excitation source) and intensity matched as discussed in chapter 2. The detection scheme is shown diagrammatically in figure 4.2. The total (polarisation independent) time-resolved fluorescence was calculated, as well as the time dependent anisotropy.

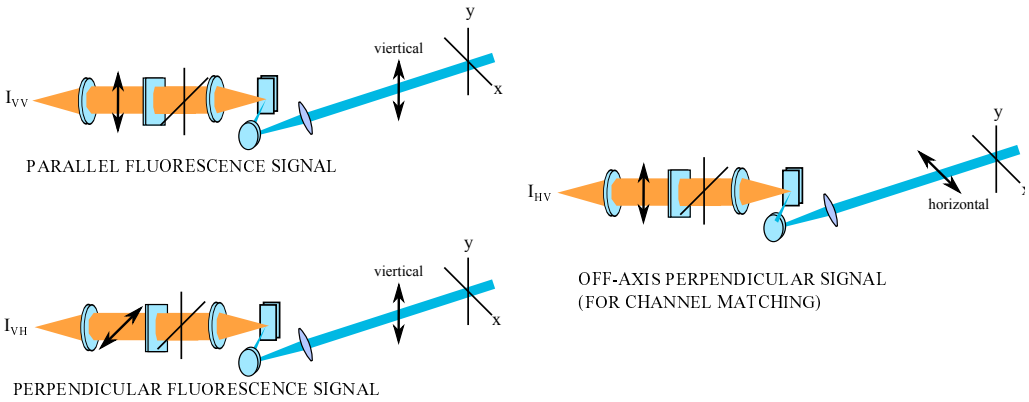

Figure 4.2: *Streak camera measurement of the polarisation dependent fluorescence for calculation of time-resolved anisotropy*

The contour plot in figure 4.3 shows the results of this experiment. The emission intensity is plotted as a function of the emission energy (expressed in frequency as wavenumbers) and time. The lifetime of the fluorescent state was characterised by spectrally integrating the decay of the magic angle signal from the streak camera. A bi-exponential fit of this decay trace shows a short-lived component with a time constant of τ=100ps and a longer lifetime of τ=1.3ns, which corresponds to the excited-state lifetime in the literature for DCM in methanol [42, 19].

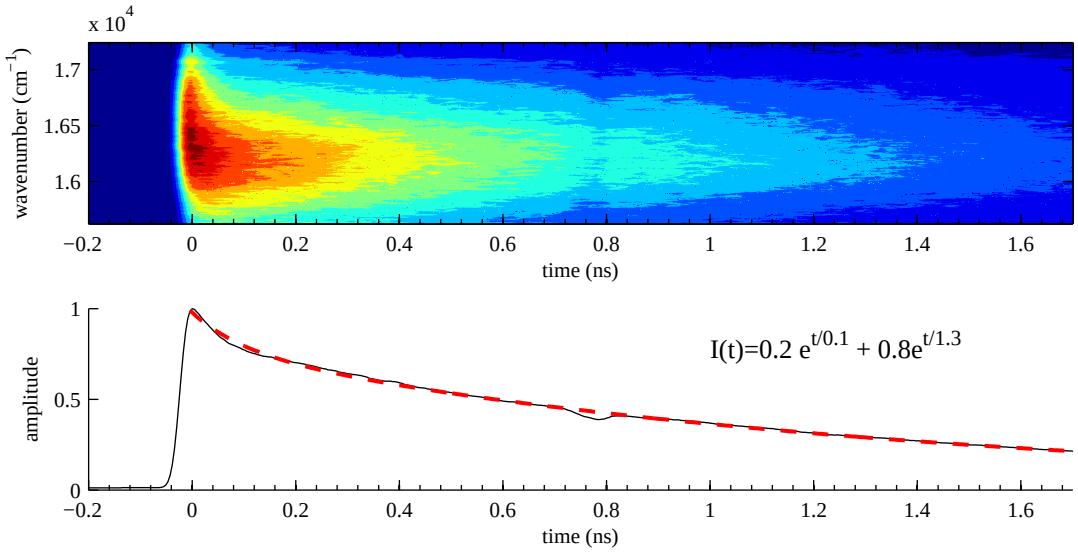

Figure 4.3: *Integrated fluorescence decay of DCM in methanol showing lifetime*

The data reveals changes in the shape, centre and width of the fluorescence band during the measured time period. The peak clearly shifts to the red in the early times which is an indicator of solvation [16].

This shift from high to low energy states can be seen in figure 4.4 in which slices of the time-dependent fluorescence at given emission energies show a gradual increase in the rise and decay times from the high to low energy regions of the band. The high-energy short-lived decay times correspond to the rate at which energy is funneled from the non-equilibrium solvent orientation to the lower energy states. The decay time at the red limit of the shift should correspond to the excited-state lifetime.

The red-shift of the emission band with time is consistent with the solvation of a polar excited-state, where the non-equilibrium solvent geometry responds to the reaction field induced by the change in dipole moment by relaxing to a more stable solvated state. The shift with time corresponds to the energy of the solvent-solute system as the solvent configuration changes. The driving force for the solvation process is electrostatic, as the solvent dipoles feel a force from the

electric field induced by the increased dipole moment of the excited-state.

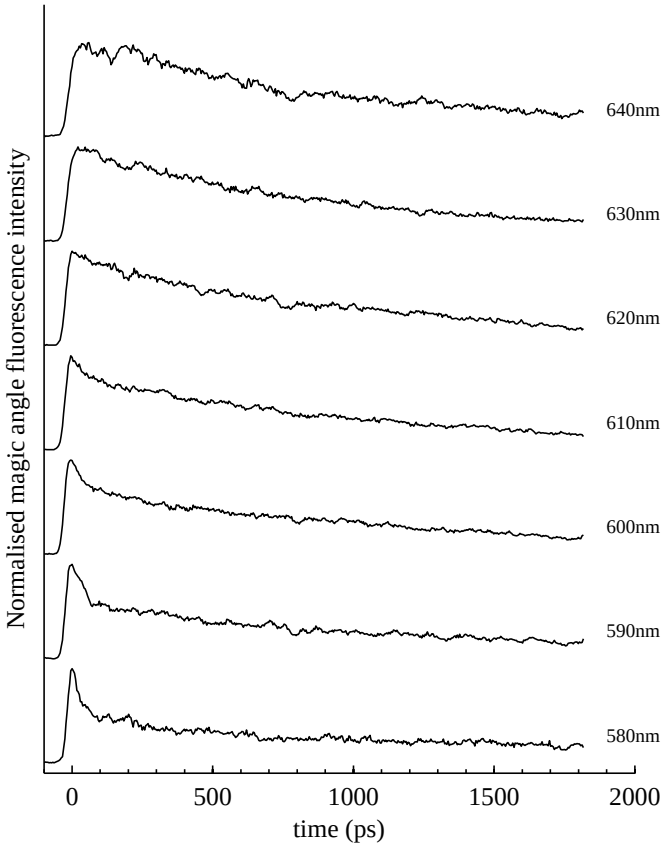

Figure 4.4: *Wavelength (energy) slices of the time-resolved fluorescence of DCM in methanol showing the gradual red shift of the fluorescence maximum as time progresses*

In order to quantify the features seen in the contour and time slices, the log-normal function used for the steady-state data was used to fit the emission spectra at each point in time. In this case, the fit parameters g_0, ν_0, Δ and b were calculated as a function of time and plotted. The results of this analysis are shown in figure 4.5. The figure shows the amplitude, peak maximum, bandwidth and shape parameter plotted as a function of time and the reconstructed 3D contour of the fluorescence decay.

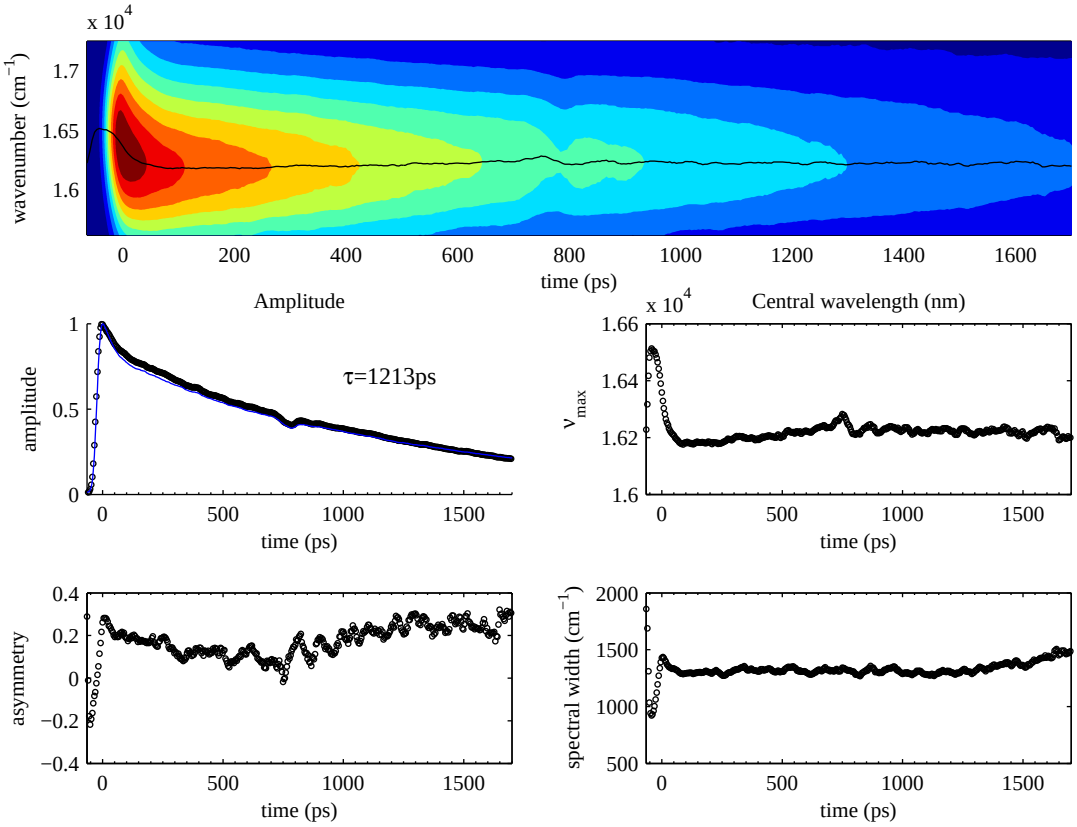

Figure 4.5: *Spectral decay parameters of DCM fluorescence in methanol from log normal fitting of picosecond streak camera data*

The time-dependent amplitude from this analysis is proportional to the excited-state population, and shows a decay consistent with the integrated plot but independent of shifts in the peak frequency. The asymmetry and bandwidth parameters show initial rise times within the amplitude rise time and then tend to drift around a mean value. This would suggest that there is not a significant change in the shape and width of the emitting band in long timescales after excitation.

The time-dependence of the ν_0 parameter, which defines the central frequency of the emission band, is a convenient means of quantifying the early-time spectral shift. The normalised solvation correlation function (equation 4.1) is often used in the literature [101, 14, 53, 17] to characterise time-resolved

spectral red shifts caused by solvation. This function decays from one (the initial excited-state energy) to zero (the equilibrium or steady-state energy). Fitting this function then allows a time constant(s) to be determined for the relaxation process.

$$C(t) = \frac{\nu_s(t) - \nu_s(\infty)}{\nu_s(0) - \nu_s(\infty)} \tag{4.1}$$

Figure 4.6 shows the early-time solvation correlation function as calculated from ν_0. The shift fits well to a single exponential with a decay constant of 26 ps. This is longer than the 5 picosecond component of the solvation measured by Meulen et al [102] which he attributed to rotational diffusion. Meulen also found a faster solvation component with a time constant of 0.7 picoseconds which does not appear to be resolved in the streak camera data. The solvation seen here is thus attributed to rotational diffusion of the surrounding solvent cage [103] whereas the unresolved components are attributed to "inertial free streaming" [102] or small angle motion of solvent molecules after photoexcitation of the sample molecule [104].

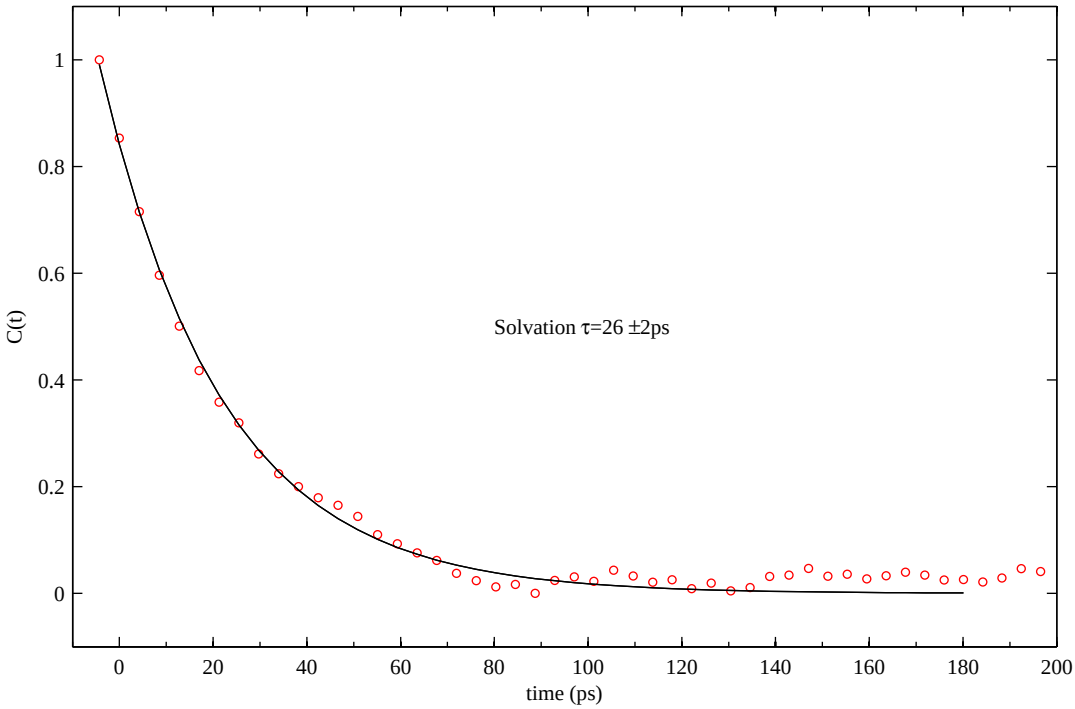

Figure 4.6: *Solvation decay of polar excited-state of DCM in methanol*

4.3.1 Fluorescence anisotropy

The time and wavelength dependent anisotropy dynamics were calculated from the parallel and perpendicular fluorescence signals with the anisotropy equation 4.2 discussed in chapter 3.

$$r = \frac{I_{\parallel} - GI_{\perp}}{I_{\parallel} + 2GI_{\perp}} \tag{4.2}$$

Figure 4.7 shows the spectrally integrated decays of the parallel and perpendicularly polarised detection channels. The data clearly shows the fast initial rise of the photo-selected parallel (blue) component of the fluorescence and its subsequent decay into the perpendicular (red) channel. The magic angle (black) signal is also shown. It was calculated on the 3-dimensional time, frequency

and intensity data sets of the parallel and perpendicular channels using the "G-factor" measured during the experiment.

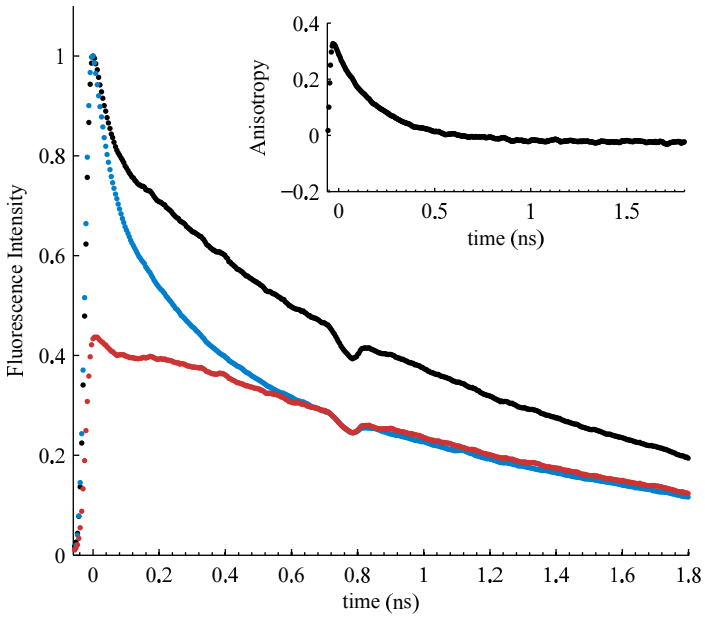

Figure 4.7: *Integrated parallel (blue), perpendicular (red) and magic angle fluorescence (black) signals. Inset: Anisotropy decay.*

The anisotropy data shown in the subset of the figure clearly shows the photoselection of a population of molecules aligned with the excitation laser polarisation. A larger version of this graph is shown in figure 4.8 and highlights the decay to zero of the anisotropy. A decay to zero is generally an indication of the rotational diffusion time of DCM; however a shift of the transition dipole direction of the excited molecules (or energy transfer to a nearby molecule) can also account for a time dependent change of this parameter. Here the anisotropy decays with a spectrally averaged time of 236 picoseconds.

The viscosity dependence of this decay time will be explored in chapter 5 to determine the origin of the decay. A linear dependence of the decay rate on viscosity would suggest that the decay is due to the rotational diffusion of the excited-state molecules.

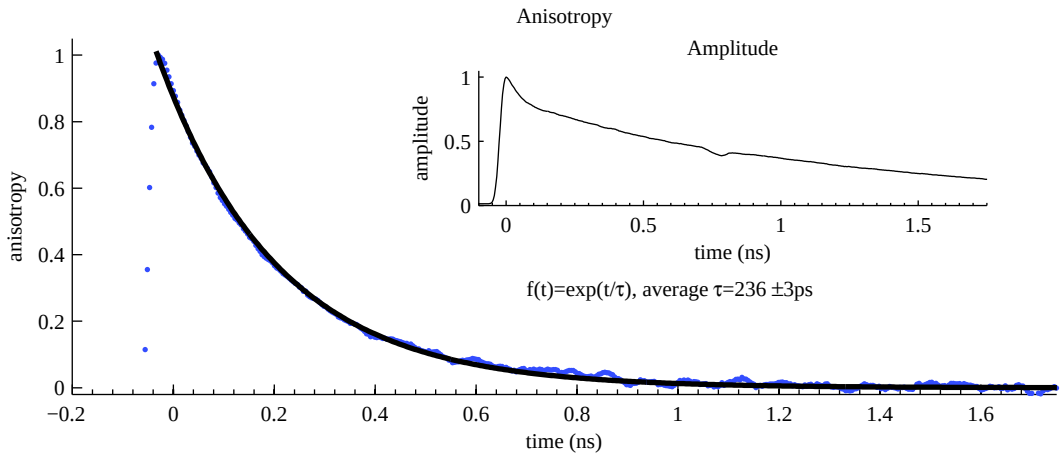

Figure 4.8: *Decay of the time dependent anisotropy for DCM in methanol with a decay time of 166 ps. The inset shows the rotationally independent (magic-angle) amplitude decay from the same data set.*

Anisotropy should not display a significant spectral dependence unless there is a difference in the transition dipole orientation of different emission states. Figure 4.9 shows a 3D of the wavelength dependence of the anisotropy and there does appear to be some dependence of the absolute anisotropy on the wavelength. This effect is possibly due to the unequal response of the parallel and perpendicular channels with wavelength. For the purposes of this study, the wavelength dependence of the anisotropy is treated as an experimental artifact and only the dynamics of the averaged anisotropy are used for comparisons of the solvent dependence of DCM and DCJ.

4.3.2 Summary of time-resolved fluorescence in methanol

A comparison of the lifetimes measured from the fluorescence decay of DCM in methanol (figure 4.10) shows that the amplitude, anisotropy and solvation decays occur on a number of time scales. Up until now, we have only considered the contribution of solvent motion upon the energy shift with solvation. But solvation relaxation only requires the distribution of solvent molecules to change

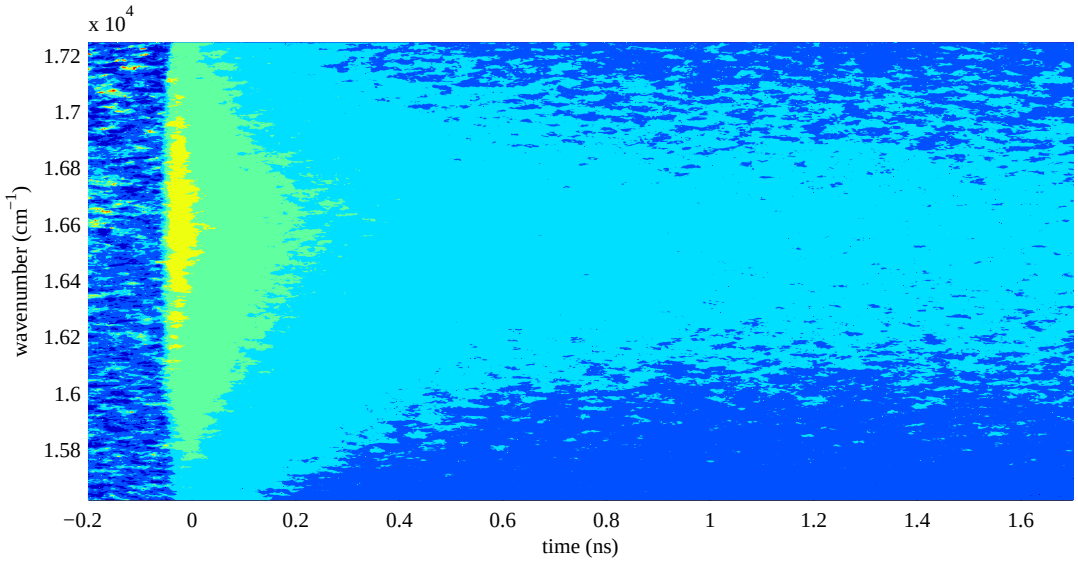

Figure 4.9: *3D contour of the anisotropy decay of DCM in methanol showing a clear difference in the absolute anisotropy across the measured fluorescence band. This is contrary to the expectation for an anisotropy experiment.*

with respect to a reference frame of the solute. Therefore, the translational and rotational motion of DCM itself will have a contribution to the solvation as well [64]. In this case, the measured solvation rate is about six times faster than the anisotropy decay rate, so the contributions of solute diffusion to the solvation are likely to be small.

The solvation occurs in 26 picoseconds and it is assumed that subsequent decay occurs radiatively from the equilibrium solvated charge transfer state. This is longer than previously reported solvation times of less than 10 picoseconds for DCM in methanol [53]. This discrepancy is probably due to the time-resolution of the pump-probe experiment as the comparison between the lower resolution streak camera fluorescence and pump-probe solvation times yielded a similar discrepancy. It is useful to discuss the anisotropy decay of DCM with respect to the effect of solvent parameters on this parameter and this will be the focus of the following chapters.

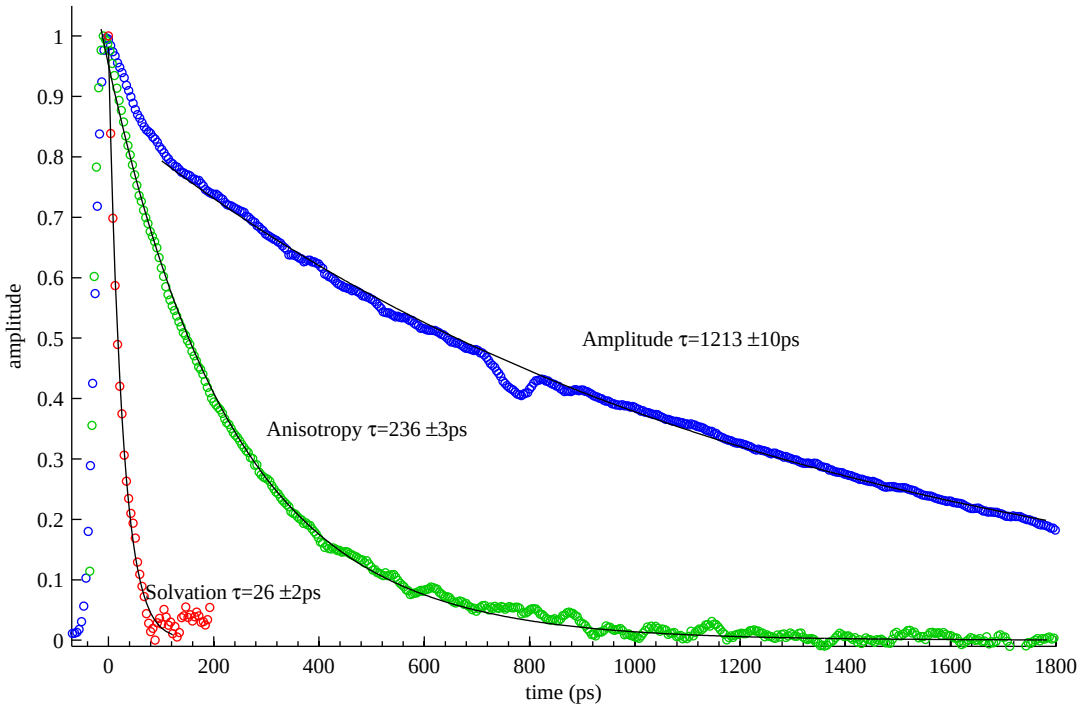

Figure 4.10: *Comparison of amplitude, anisotropy and solvation decays from streak camera fluorescence decay of DCM in methanol*

4.4 Pump-probe

The pump-probe experiment, with a higher resolution, highlights the early changes that occur after photo-excitation of DCM in methanol.

The pump-probe measurements of DCM were undertaken using the pump-supercontinuum-probe setup described in chapter 3. A 10^{-4} M solution of DCM in methanol was placed in a 2mm path-length cuvette and excited at the absorption maximum (473 nm or 21142 cm^{-1}) with pulsed light from an optical parametric amplifier. The transmitted probe intensity is detected in two separate channels that are parallel and perpendicularly polarised with respect to the pump-beam polarisation. This allows the rotationally-independent (magic-angle) signal and the anisotropy to be calculated.

Figure 4.11 shows the contour of the magic-angle signal calculated from par-

allel and perpendicularly polarised channels along with the spectrally integrated magic-angle, parallel and perpendicular signals. Over this shorter time-scale, the buildup of the emission intensity with time is evident.

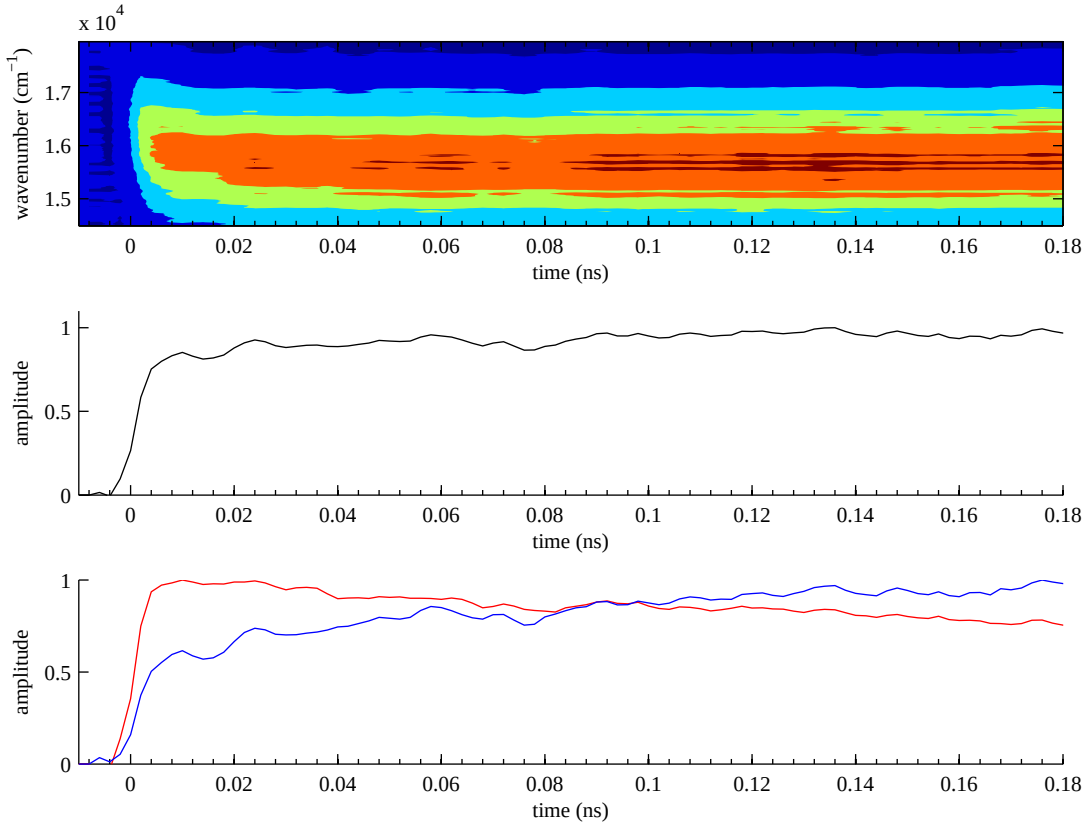

Figure 4.11: *The positive component of the pump-probe signal of DCM in methanol, corresponding to stimulated emission from the excited-state. The spectrally integrated magic-angle signal is shown in black integrated parallel (red) and perpendicular (blue) channels to highlight the anisotropic response from which the time-dependent anisotropy, r, can be calculated.*

As with the time-resolved fluorescence, a more quantitative analysis can be assisted by fitting the time-resolved spectra to a log-normal function. In this case the positive component of the time and frequency-resolved pump-probe signal was analysed with a log-normal spectral shape. The results of this analysis are shown in figure 4.12.

The log-normal fit parameters in this experiment all show features of interest.

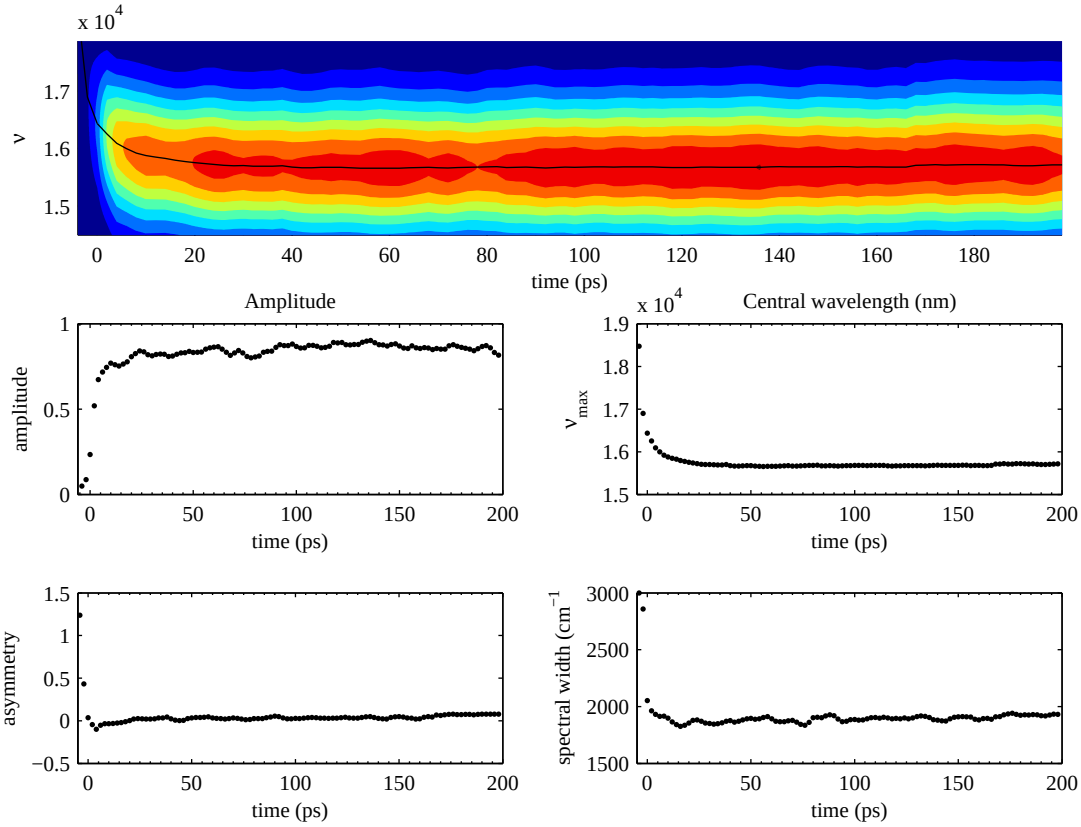

Figure 4.12: *Spectral decay parameters of DCM fluorescence in methanol from log normal fitting of white light pump-probe data*

The time-dependent amplitude is consistent with the integrated signal from figure 4.11. Of more interest are the early time asymmetry, band-width and band-shift parameters. Each of which show a sharp decrease during the amplitude build up.

Figure 4.13 compares the anisotropy and solvation signals from the pump-probe experiment. The solvation correlation and anisotropy decay times are in both cases measured to be more than twice as fast in the pump-probe experiment compared to the Streak camera fluorescence. The most likely a consequence of the difference in resolution between the two techniques causing blurring of short-time features and insufficient points for a reliable fit of the streak camera solvation data. Thus the higher resolution pump-probe experiment will be

trusted for more reliable early time (less than 50 picoseconds) decay parameters. As the anisotropy parameter in the pump-probe measurements does not decay to zero within the measurement window of the experiment, the anisotropy parameter decay time from the streak camera experiment is considered to be more accurate.

The pump-probe solvation decay time of 12 picoseconds is closer to that reported by Meulen [102] when compared to the decay rate from the streak camera measurements in figure 4.6 though still larger by a factor of two. Assuming the presence of a shorter lifetime inertial diffusion component of the solvation, a bi-exponential fit of this data may give a τ_2 decay time that more closely corresponds to this previous work. However, for simplicity the single exponential decay will be used to compare the solvation behaviour of DCM in methanol and other solvents in the following results chapters.

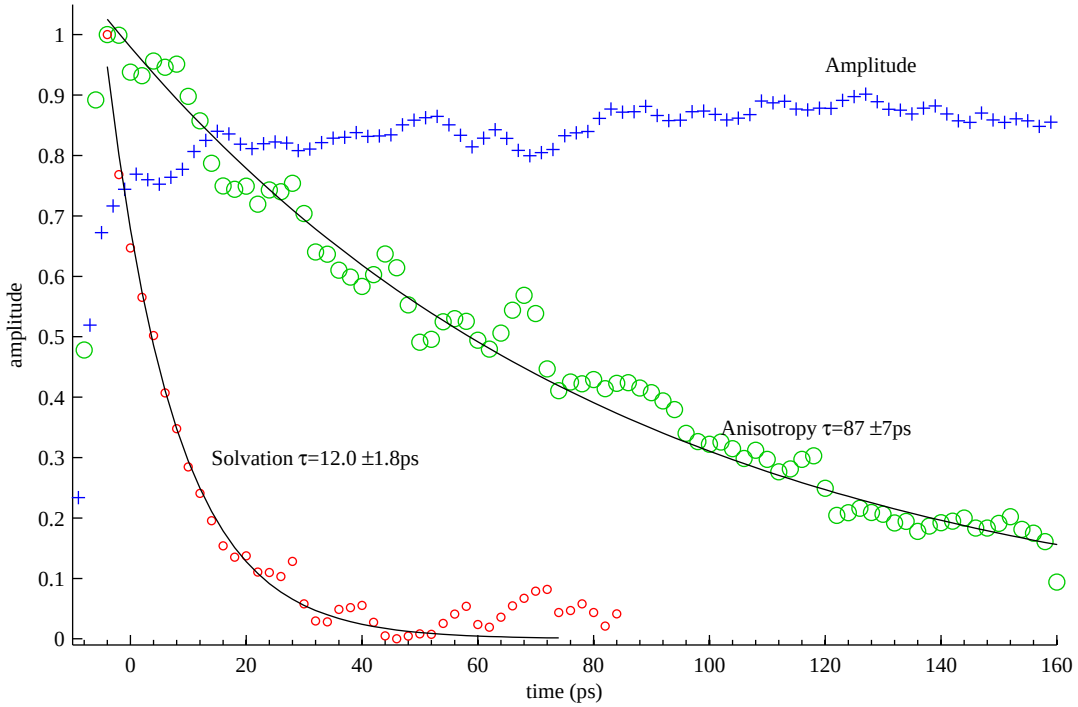

Figure 4.13: *Comparison of amplitude, anisotropy and solvation decays of pump-probe signal*

4.4.1 Summary of pump-probe dynamics in methanol

To summarise the results for DCM in methanol, conclusions from each experimental method will be drawn.

There is a significant Stokes shift from the steady-state data which suggests the existence of a non-radiative decay mechanism. This could include vibrational relaxation and solvation processes.

The time-resolved fluorescence scan shows that over short timescales, the fluorescence band shifts to the red with a decay time for the shift of 26 picoseconds. This can be attributed to solvation of a polar ICT state. Previous studied have suggested that the ICT state of DCM in methanol is formed within the first 300 fs [53], therefore solvation would be expected to occur at this time due to the shift in the dipole moment of the excited state relative to the locally excited state. The solvation mechanism explanation will be tested in chapter 5 where the dependence of the shifting dynamics on the solvent viscosity will be determined. As the rotational component of the solvation is dependent on the diffusion rate of the solvent molecules, a dependence of the time-dependent Stokes shift on viscosity indicates that the observed dynamics are due to solvation.

The anisotropy of the photo-selected population of DCM molecules in methanol, as measured by time-resolved fluorescence, decays in approximately 236 picoseconds. Over these timescales it is expected that this decay rate corresponds to the rotational diffusion time or the time it takes for the orientational distribution of the excited-state molecules to randomise. It is likely that this diffusion time depends on the shape and configuration of the excited-state molecule as well as local interactions between the solvent and solute. Importantly, as a diffusion process, the orientational diffusion time is dependent on the solvent viscosity. Again this will be examined in chapter 5.

Chapter 5

Viscosity dependence

The relaxation of DCM in solution relies on the ability of the solvent cage to re-orientate itself to a new equilibrium position and excited-state dynamics are heavily influenced by solvent diffusion rates [105]. The viscosity of a solvent affects the rates of diffusion of both the solute and the solvent molecules. One would thus expect the solvent relaxation times, measured by the time-dependent Stokes shift, and the rotational diffusion times of the solute, as measured by anisotropy, to be dependent upon the solvent viscosity.

A study by Wilhelm et al. [106] using a kinetic model concluded that fluorescence decay times would be proportional to the viscosity raised to a power α i.e. η^{α}. Where α is a parameter that is dependent on the fluorescent solute molecule. A later study by Drake [42], however, did not find this dependence, citing that solvent-solute interactions had not been taken into account. This thesis attempts to disentangle the viscosity from the solvent interactions treating them in separate chapters. The viscosity will be analysed first and the conclusions from this chapter will inform the analysis of the dependence of the measurements on the solvent dipole/dielectric properties.

Essentially, the viscosity is a measure of the resistance to flow that a solvent

has. At a molecular level therefore, the solvent molecules diffuse more slowly in a more viscous medium. Diffusive solvation that occurs after the initial, much faster, response of the electrons within the solvent, is dependent on the diffusion rate of solvent molecules as they reorient and translate to form a more stable cage surrounding the excited-state solute.

The Stokes-Debye-Einstein (SDE) diffusion relation described in chapter 2 and shown again below (equation 5.1), relates the rotational diffusion time of a probe-molecule, as measured by anisotropy experiments, to the solvent viscosity η. Study of the viscosity dependence of the excitation dynamics of DCM, therefore, allows identification of the processes mediated by solvent and solute diffusion.

$$\tau_{rot} = \frac{\eta V}{k_B T} \tag{5.1}$$

where η is the solvent viscosity, V is the volume of the rotating molecule, T is the temperature (Kelvin) and k_B is the Boltzmann constant.

A homologous series of linear alcohols provides a convenient way of altering the bulk viscosity of the DCM solution. As the number of carbons in the alcohol chain increases, so does the mass of the solvent and the viscosity. The dipole moment does not change significantly however, allowing isolation of the effect of diffusion from changes in the dynamics that are due to interactions between the solute and solvent electric fields and/or specific molecular bonding forces such as hydrogen bonding, van der Waals or aromatic π-π orbital interactions.

An increase in viscosity decreases the relative motion of solvent molecules, thus one would expect the solvation and orientational diffusion rates of the solvent to decrease.

This chapter presents the influence of the solvent viscosity on the steady-state absorption and fluorescence spectra, time dependent fluorescence (picosecond streak camera) and pump-probe response of DCM in methanol, ethanol and n-

pentanol. These solvent molecules differ only in hydrocarbon chain length - having 1, 2 and 5 saturated carbons respectively. The idea of a homologous series for this part of the study is to alter the viscosity without significantly altering the dipole moment (and ideally the dielectric constant).

The important solvent parameters for this chapter are shown in table 5.1.

Solvent	Dipole Moment μ (D)	Dielectric Constant ϵ @ 20°C	Refractive Index n_D @ 20°C	Viscosity η mPa.s @ 25°C
Methanol	1.70	33	1.3265	0.539
Ethanol	1.69	25.3	1.3594	1.057
n-Pentanol	1.70	17.84	1.4080	3.425

Table 5.1: Properties of homologous series of alcohols

5.0.2 Steady-state spectra

DCM was dissolved in methanol and n-pentanol at a concentration of 10^{-4} M for the steady-state absorption and fluorescence measurements. Both molecules were excited at 400 nm pulsed light from the frequency-doubled 82 MHz output of the titanium sapphire oscillator described in chapter 3. Figure 5.1 shows the measured spectra.

Table 5.2 summarises this data and shows that the band-shapes and band-widths of the absorption and fluorescence spectra of DCM in methanol and n-pentanol are very similar. However, the fluorescence peaks of show a decreasing Stokes shift from methanol to n-pentanol. Particularly for n-pentanol which is significantly larger than methanol and ethanol, it may be that the size of the n-pentanol molecule prevents an optimum solvent cage structure for the excited-state dipole moment when compared with the smaller methanol and ethanol molecules. Another possible explanation is that proposed in a recent paper from 2013 by Catalan et al [107] for another TICT compound, 9,9-bisanthracenyl.

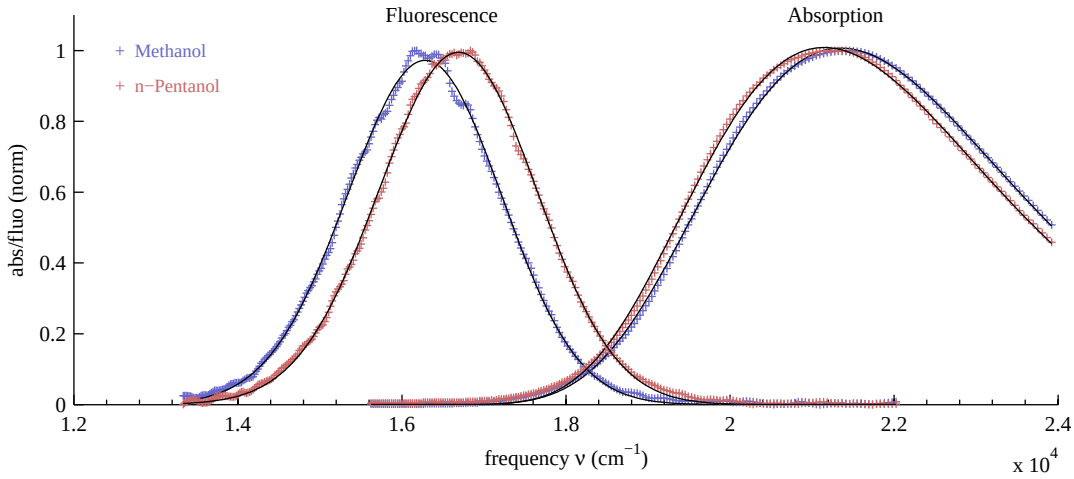

Figure 5.1: *The steady absorption and fluorescence spectra of DCM in solvents of low (methanol) and high (n-pentanol) viscosity*

Their study of the temperature dependence of the compound's steady-state fluorescence peak maximum and quantum yield in a series of binary solvent mixtures suggests that the viscosity increases the barrier to TICT formation in addition to the effect of the solvent dipole moment.

Solvent	$\nu_0 abs$ (cm^{-1})	Δabs (cm^{-1})	$\nu_0 fluo$ (cm^{-1})	$\Delta fluo$ (cm^{-1})	$\nu_{abs} - \nu_{fluo}$ (cm^{-1})
Methanol	21352	4387	16284	2218	5068
Ethanol*	21000	-	16390	-	4610
n-Pentanol	21147	4280	16690	2274	4457

Table 5.2: Central frequency and bandwidth of absorption and fluorescence spectra, and Stokes shift for DCM in methanol, ethanol and n-pentanol (* ethanol data from [52])

These preliminary features were studied in more detailed with time-resolved fluorescence and pump-probe.

5.0.3 Streak camera

In order to allow direct comparison of the solvent effect on the time-resolved fluorescence of DCM, measurements were made under the same experimental conditions on the same apparatus with the same setup and all three solutions were excited with a frequency-doubled pulsed laser source at 400 nm. As with the steady-state measurements, DCM was dissolved in methanol, ethanol and n-pentanol at a concentration of 10^{-4} M.

Figure 5.2 shows the raw time-resolved fluorescence data for DCM in the three alcohols.

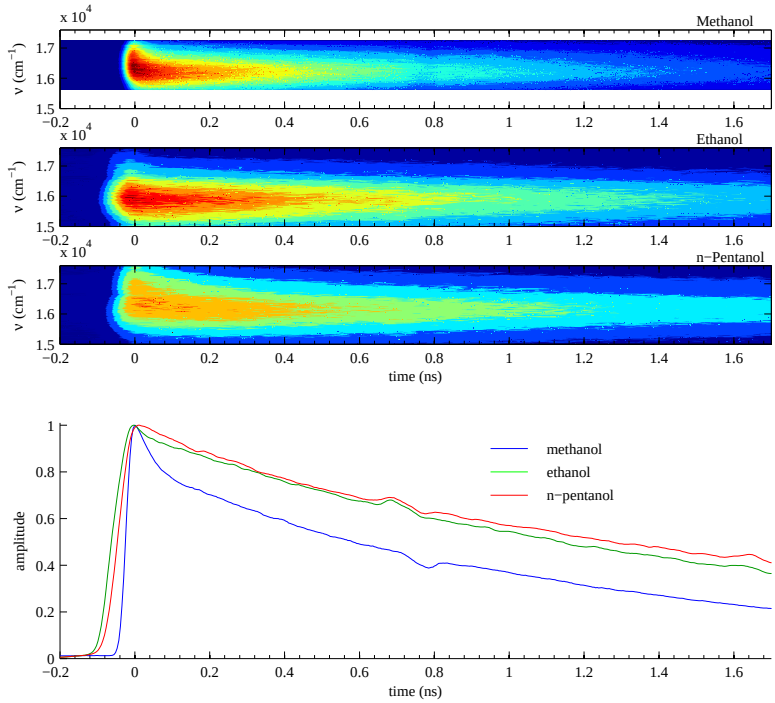

Figure 5.2: *Time-dependent fluorescence spectra of DCM in polar solvents of increasing viscosity*

The contour plots show an increase in the amplitude, anisotropy and solvation decay times with increasing solvent viscosity, suggesting that the rate of population decay, rotational diffusion of DCM and the solvation by diffusion of solvent

molecules are all diffusion dependent. The curves showing the time-dependence of the spectrally-integrated fluorescence intensity are also shown.

The log-normal function was applied to the streak-camera spectral data to allow a more quantitative comparison of these trends. Figure 5.3 shows the amplitude decay parameter from the log-normal fit. It highlights a trend of increasing excited-state lifetime with solvent viscosity.

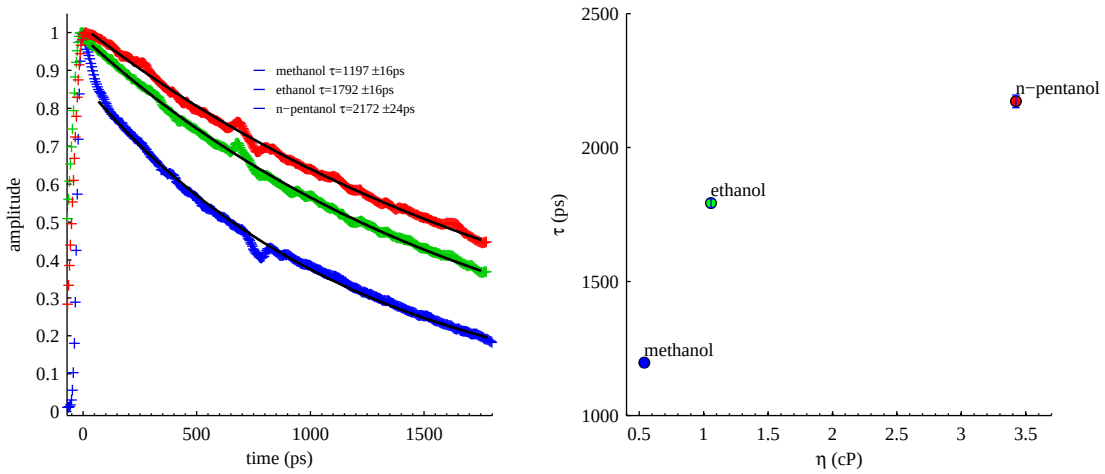

Figure 5.3: *Fluorescence amplitude of DCM in solvents of increasing viscosity with mono-exponential fit show an increase in lifetime with increasing solvent viscosity.*

The steady-state data suggests that DCM is not in its optimally relaxed solvation state in n-pentanol (compared with the smaller alcohols). This may explain why the fluorescence lifetime of DCM in n-pentanol does not significantly increase in comparison to ethanol, despite the solvent having three times the viscosity. If the formation of the proposed twisted charge transfer state is mediated by solvent diffusion, then the recombination is also likely to be affected, as the solvent must again re-orient to a new dipole moment in the ground-state.

A non-optimal solvent cage structure would change the energy surface of the charge transfer reaction by decreasing the range of solvent coordinates available to the system. This in turn would effect the extent to which charge transfer could occur as the energy minimum that stabilises the state would not be as low. If a

TICT state is valid, this would mean that the donor-acceptor bond twist angle is closer to the ground-state planar orientation, increasing overlap of the π acceptor orbital with the n donor orbital to make recombination easier and faster. If, however, the ICT state is not twisted, the donor and acceptor orbitals would remain relatively strongly coupled, allowing recombination.

The solvation times shown in figure 5.4, as measured by the frequency shift of the fluorescence maximum, follow a trend to increase with increasing viscosity.

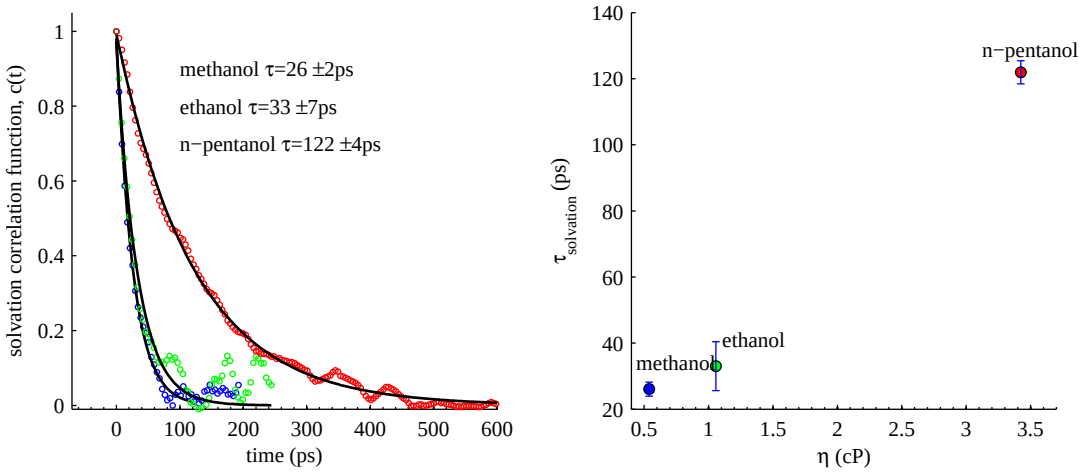

Figure 5.4: *Solvation times of DCM in solvents of increasing viscosity with mono-exponential fit increase with increasing solvent viscosity in keeping with slower motion of solvent molecules.*

This trend is consistent with the expected trend with viscosity. The solvation time of DCM in n-pentanol is faster than expected from the SDE equation with increasing viscosity. As the steady-state data suggests that the excited-state of DCM is not solvated to the same extent in n-pentanol, this trend could be explained by the aforementioned idea that the solvent cage surrounding DCM is not able to reach as stable a configuration due to relatively large size of the solvent molecule. As this inability to reach optimum solvation would decrease the range of configurations the solvent cage could be in, the solvation would be expected to reach equilibrium at a faster rate. The data shows that the solvation rate is slower than the less viscous ethanol but presumably ethanol can reach a

more optimum solvation cage structure.

The rotational decay time of the photo-selected DCM molecules, as measured by the time-resolved fluorescence anisotropy, are shown in figure 5.5.

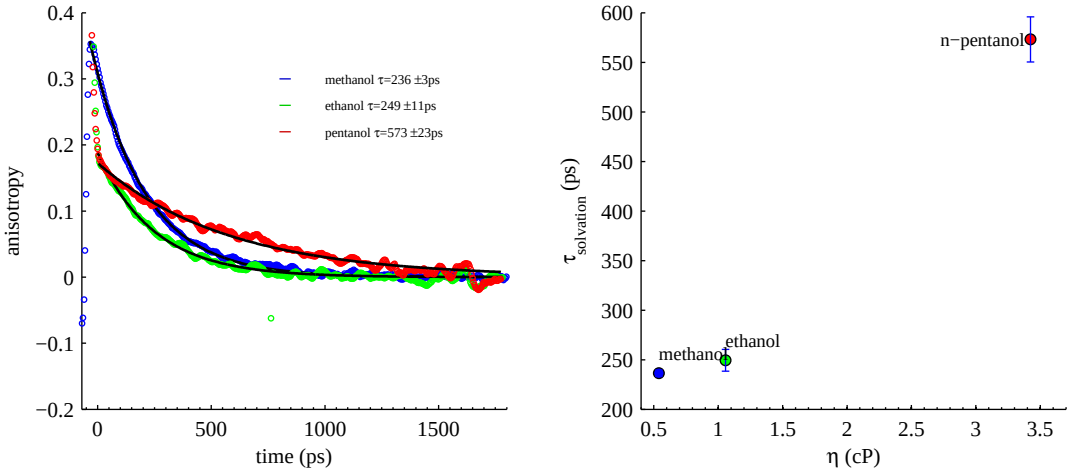

Figure 5.5: *Anisotropy decays of DCM in solvents of increasing viscosity show an increasing trend with solvent viscosity. Deviation from linearity suggests that there may be molecular interactions that dominate when solvent motion is slow i.e. for DCM n-pentanol*

Mono-exponential fits of these decays follow a trend that seems to be polynomial rather than linear. The reader will recall from section 2.2.3.4 in chapter 2, that the Stokes-Einstein-Debye equation predicts a linear relationship between diffusion rate and solvent viscosity. This deviation from linearity would suggest that the simple diffusion treatment for the anisotropy decay may not be a valid approach. In this instance, the relationship would hold only occur if the hydrodynamic volume (V) of the excited-state of DCM is the same in all the alcohols and that either no specific interactions occur between the solute and solvent molecules or that the interactions are independent of the solvent.

$$\tau_{rot} = \frac{\eta V F}{kTS} \tag{5.2}$$

thus

$$\frac{d\tau}{d\eta} = \frac{VF}{kTS} \tag{5.3}$$

A possible explanation for the non-linear behaviour could be molecular interactions between DCM and the solvent molecules which begin to dominate when viscosity is large and solvent motion is slow, further decreasing the diffusional motion of the solute.

This behaviour was investigated further in shorter timescales with the higher resolution time-resolved pump-probe experiment.

5.0.4 Pump-probe

The pump-probe measurements for this chapter were undertaken in each solvent at a concentration of 10^{-4} M in a 2mm path-length cuvette and excited at close to their absorption maximum (470 nm) with pulsed light from an optical parametric amplifier. Probe measurements were taken in polarisation directions parallel and perpendicular to that of the pump.

The pump-probe results for DCM in methanol, ethanol and n-pentanol show similar behaviour to the time-dependent fluorescence. The 3D contours in figure 5.6 show the stimulated emission pump-probe signal from 15000 to 19000cm^{-1}).

The time-dependent Stokes shift over the first few hundred picoseconds can clearly be seen. The energy shift in the high viscosity n-pentanol solvent appears to begin at a higher energy. The high energy tail of this band at early times is close to the 0-0 frequency given by the overlap of the absorption and fluorescence bands in n-pentanol. This suggests that the emissive state occurs directly from the lowest vibrational level of the S1 excited-state (after fast vibrational relaxation). The fluorescence of DCM in n-pentanol, thus presumably resolves the solvation from vibrational relaxation and longitudinal solvation, caused by electronic polarisation with the solvent molecules rather than diffusion. These processes are expected to occur on faster time scales in methanol [102, 104], possibly less than 100 femtoseconds, which would not be resolved by this

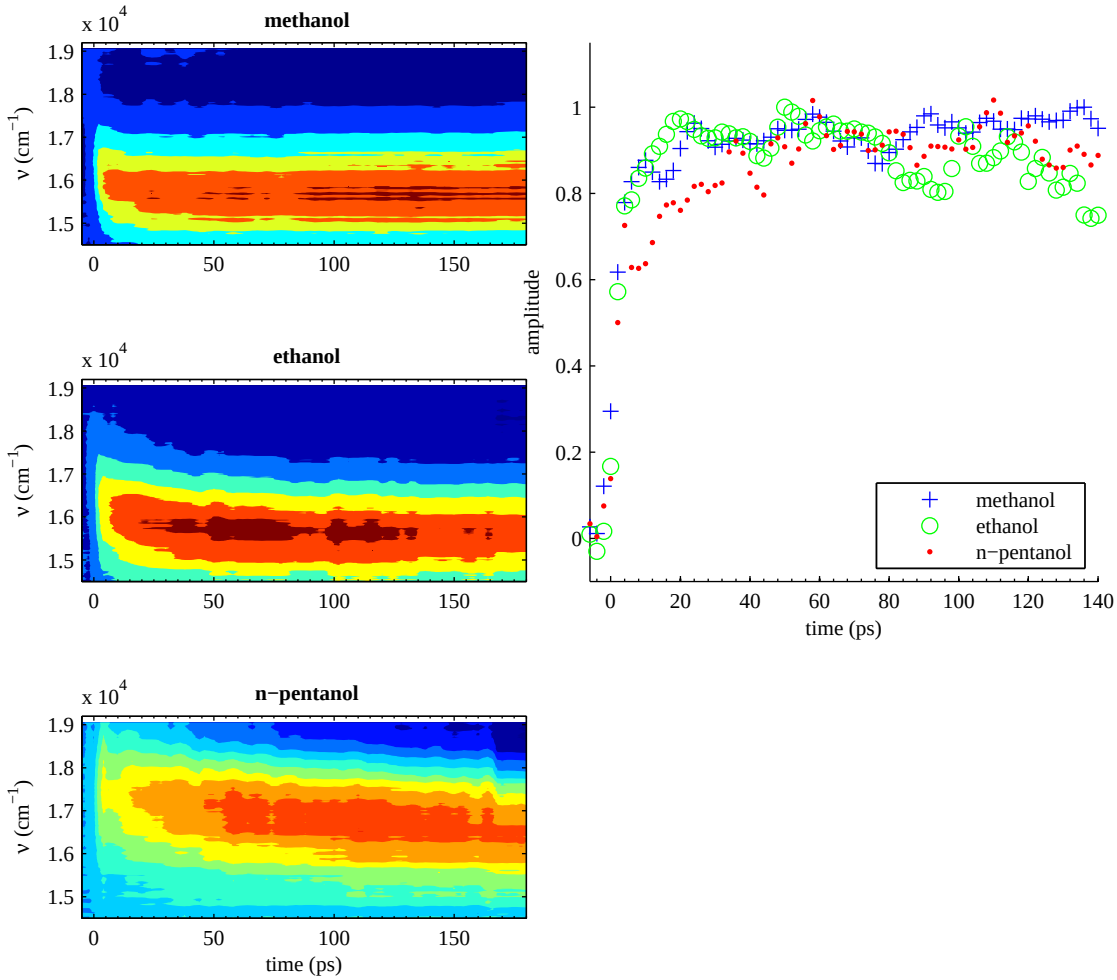

Figure 5.6: *Stimulated emission pump-probe signals of DCM in methanol, ethanol and n-pentanol. Normalised spectrally integrated plots (right) highlight the rise times that correspond to each solvent.*

experiment.

As in the streak camera data, the dynamics measured in the pump-probe experiment are strongly dependent on the solvent viscosity.

The log-normal fit amplitude of the stimulated-emission (positive) ΔT is shown in figure 5.7. The data shows the rise of the amplitude over the first 150 picoseconds and there appears to be a linear relationship between the rise time and solvent viscosity with values that are close to the solvation times

measured in the streak camera fluorescence data. This seems to indicate that the initial stimulated emission occurs from a different state with a magnitude of the transition dipole which then decays into the equilibrium emissive state.

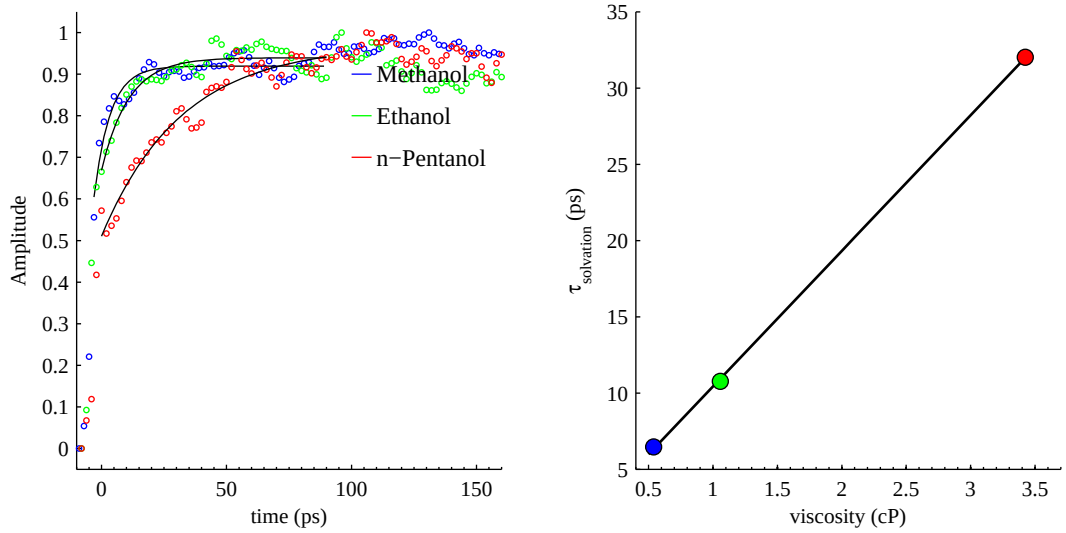

Figure 5.7: *Fit amplitude (population) rise time for pump-probe stimulated emission signal of DCM in a methanol, ethanol and n-pentanol to show the effect of solvent viscosity*

The time-dependent Stokes shift times shown in figure 5.8 have a strong linear dependence with viscosity. This suggests that solvation is the main relaxation mechanism from the initially excited Franck-Condon to the nanosecond timescale emissive state.

Again referring to figure 5.8, if we assume that the viscosity is the only variable that affects the long term solvation decay constant in the alcohol series, the derivative gives a constant. From the linear fit, the equation is:

$$\tau_{solvation} = 17\eta + 3.1 \tag{5.4}$$

A physical explanation of this empirical relation would include the other terms in the SDE equation. The origin of the offset term in the empirical fit is less clear but the relation will be used empirically to investigate the influence

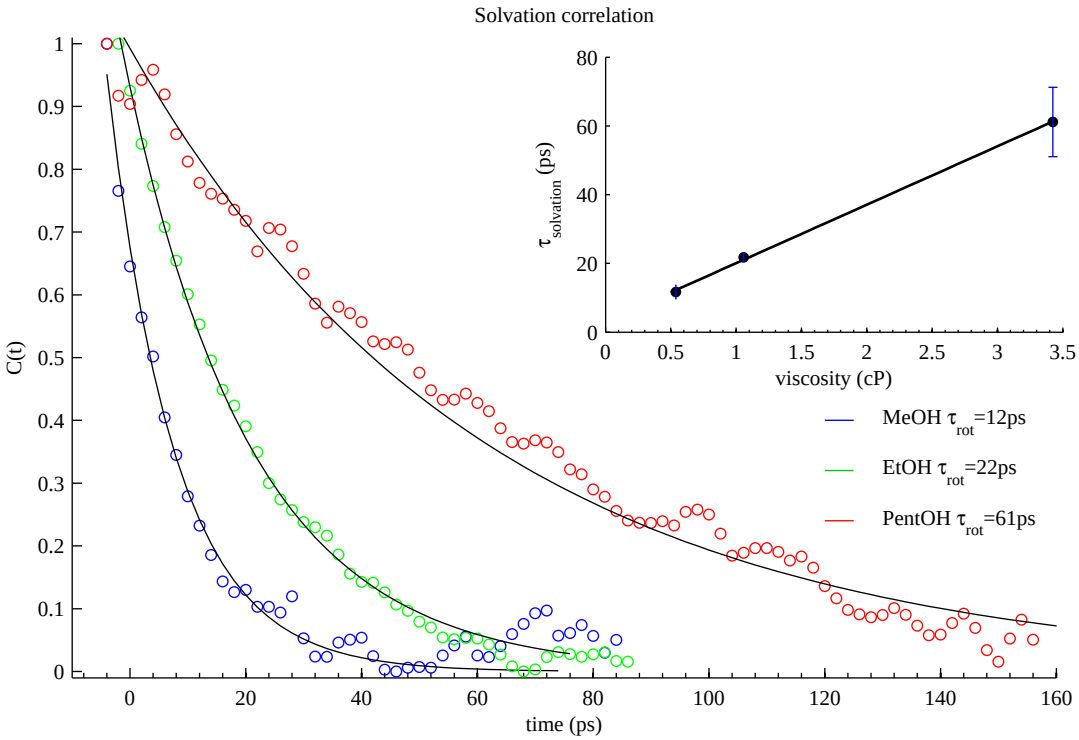

Figure 5.8: *Pump-probe solvation decays of DCM in methanol, ethanol and pentanol*

of solvent viscosity on the dipole moment dependence in chapter 6 in order to isolate the effect of dipole moment from the viscosity parameter.

To summarise the results for this chapter on viscosity dependence, the features and trends seen will be highlighted.

The steady-state Stokes shifts show a trend to decrease as the solvent viscosity increases. This could be due to the influence of the viscosity on the barrier to TICT formation as suggested by Catalan [107], or a consequence of a decreased ability of the solvent to be able to form an optimum solvated cage structure surrounding the polar excited state of DCM due to the increased size of the solvent.

The anisotropy decays of DCM in the homologous series of alcohols shows a linear trend with increasing viscosity. This agrees with the decay being attributed

to rotational diffusion rather than reorientation of the transition dipole-moment. However, this process cannot be ruled out as a contribution to the decay. The absolute value r at early times appears to be around 0.4 which is consistent with the absorption and emission transition-dipoles having similar orientations in the molecular frame.

With this information, the next chapter will investigate the effect of the solvent dielectric properties on the energetics and dynamics of the excited state independent of effects due to viscosity examined in this chapter.

Chapter 6

Solvent dipole moment and dielectric constant dependence

The dipole moment of the solvent molecules surrounding a sample compound have a substantial effect on the energy structure and relaxation dynamics. The creation of a highly polar excited-state in a solution is either suppressed or enhanced depending on the ability of the solvent molecules to solvate the excited molecule (thus lowering the energy of the system). The dielectric constant is a measure of the amount to which a dielectric medium can be polarised by an electric field. In a solvent medium, it includes the polarisability of the electrons within the solvent molecules and, more importantly in polar molecules, it includes the ability of the solvent to reorient and translate by diffusion within an electric field.

The reaction field in the theory of Onsager [108], which forms the basis of Lippert and Mataga's analysis of solvatochromatic Stokes shifts, is mediated by the response of the solvent to the electric field generated by the changed dipole moment of the solute in the excited state due to intramolecular charge transfer. As discussed in chapter 2 section 2.2.1, the parameter Δf describes the response

of the solvent to this change.

$$\Delta f = \frac{\epsilon - 1}{2\epsilon + 1} - \frac{n^2 - 1}{2n^2 + 1} \tag{6.1}$$

In this chapter, the steady-state and time-resolved spectra of DCM in methanol, toluene and acetone were studied. The properties of these solvents are shown in table 6.1. Note the difference in dipole moment (μ) and the related dielectric constant (ϵ). The Δf parameter has been calculated from these values.

Solvent	Dipole Moment μ (D)	Dielectric constant ϵ	Refractive Index n_D	Viscosity η mPa.s	Δf
Methanol	1.7	33	1.3265	0.539	0.3095
Acetone	2.88	21	1.3560	0.308	0.2858
Toluene	0.36	2.385	1.4941	0.548	0.0145

Table 6.1: Solvent properties (ϵ and n_D at 20°C and η at 25°C)

It is important to note that the viscosity of methanol and toluene are similar, whereas acetone has a smaller viscosity. Therefore one would expect diffusion dependent dynamics in methanol and toluene to highlight only specific interactions between the solvent and the solute or changes in the motion of solvent and solute molecules due to structural changes such as ICT or conformational changes (TICT or isomerisation).

6.1 Steady-state spectra

As for all previous chapters, DCM was dissolved in the solvents at a concentration of 10^{-4} M and the fluorescence was excited with a 400 nm pulsed laser source.

The steady-state spectra of DCM in methanol, acetone and toluene is shown below in figure 6.1). As can be seen, the fluorescence maximum in toluene has

a much smaller Stokes shift than the polar solvents, suggesting that there is a different state involved. This is not unexpected, as toluene has a very small dipole moment and dielectric constant. Solvation, therefore, would not significantly lower the energy of a highly polar excited-state. The fluorescence spectrum in toluene is thus attributed to a low-polarity non-charge transfer state. Possibly attributed to the locally-excited-state of Grabowski's theory, but also potentially involving the trans-cis isomerisation as this is expected to be more significant in non-polar solvents. This spectrum is similar to that of the early time pump-probe stimulated emission spectra before significant solvation occurs giving evidence for the existence of a transition from a locally excited-state to the charge transfer state.

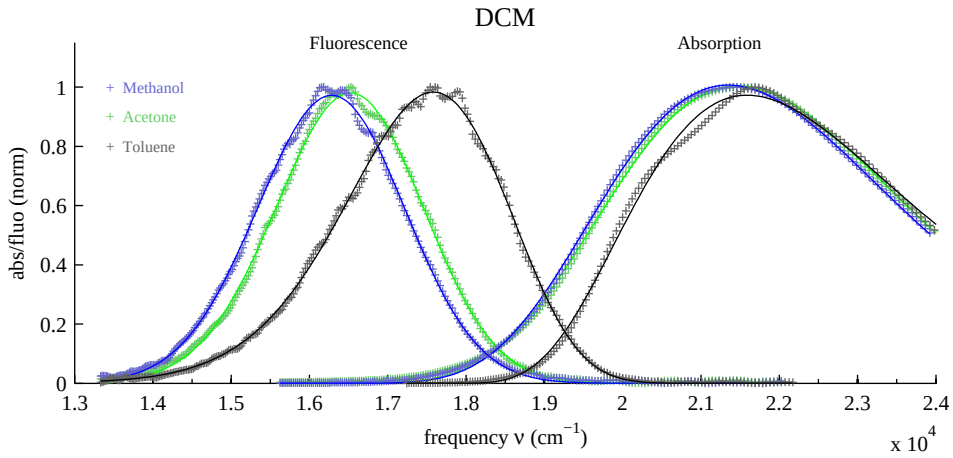

Figure 6.1: *Comparison of population (by amplitude of magic angle signal) and anisotropy decay from picosecond fluorescence*

The parameters obtained from a log-normal fit of the steady-state spectra are shown below in table 6.2.

Plotting the Stokes shift versus Δf (figure 6.2) showed a roughly linear trend for the methanol, n-pentanol and acetone.

Toluene does not fit in with this trend, which is consistent with the fluorescence occurring from a different state. The smaller Stoke's shift for n-

Solvent	Dipole Moment μ (D)	ν_{abs} (nm)	ν_{fluo} (nm)	$\nu_{abs} - \nu_{fluo}$ (cm^{-1})
Methanol	1.7	21352	16284	5069
Acetone	2.88	21471	16526	4945
Toluene	0.36	21590	17582	4008

Table 6.2: Steady-state absorption and fluorescence maxima for DCM in a range of solvents with different dipole moment

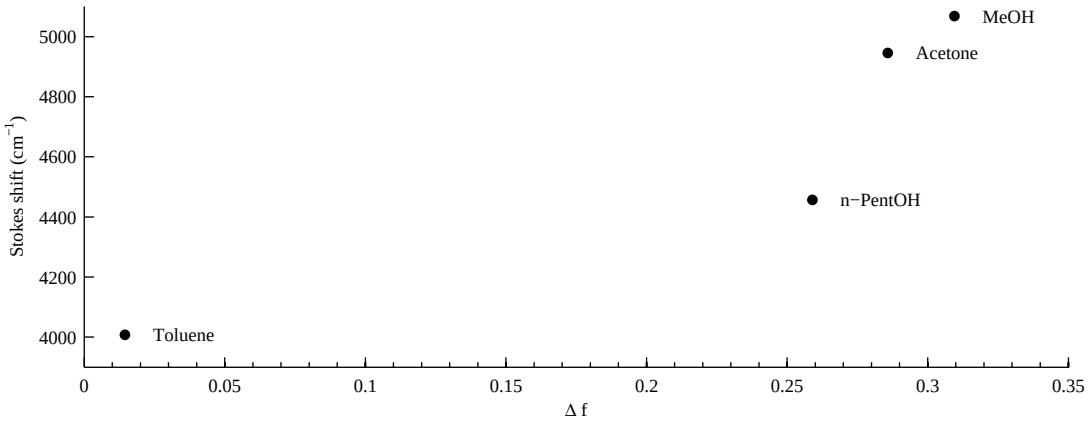

Figure 6.2: *Dependence of the Stokes shift (ν_a - ν_f)* of DCM on the reaction field parameter of the solvents studied Δf.

pentanol does appear to be consistent with the Lippert-Mataga theory based on its dielectric constant and refractive index. As the Δf parameter takes into account rotational motion of the solvent molecules, it has the viscosity (or at least solvent diffusion rates) built into it. Though the theory by treating the solvent as a continuum, does not take into account local interactions between solvent and solute, nor does it take into account restrictions in formation of an optimum solvent cage, which might still be significant.

The steady-state bandwidth of the absorption and fluorescence spectra were plotted against the reaction-field parameter in figure 6.3 and show a trend for increasing absorption bandwidth and decreasing fluorescence band-width with an increase in Δf. The increasing absorption bandwidth is likely due to the

increased number of solvent environments available to the sample in a polar-solvent, i.e., the number of states that a dipolar solvent can be in that significantly change the local electric field around the solute will be greater when the dipole moment is large. The decreasing fluorescence band-width with Δf is less obvious but is likely due to a narrow potential for the solvation minimum in more polar solvents, i.e., in a polar solvent there are a narrow range of solvation states that significantly minimise the energy of the DCM-solvent system and the minimum energy is lower (the Stokes shift is larger) creating a deeper well.

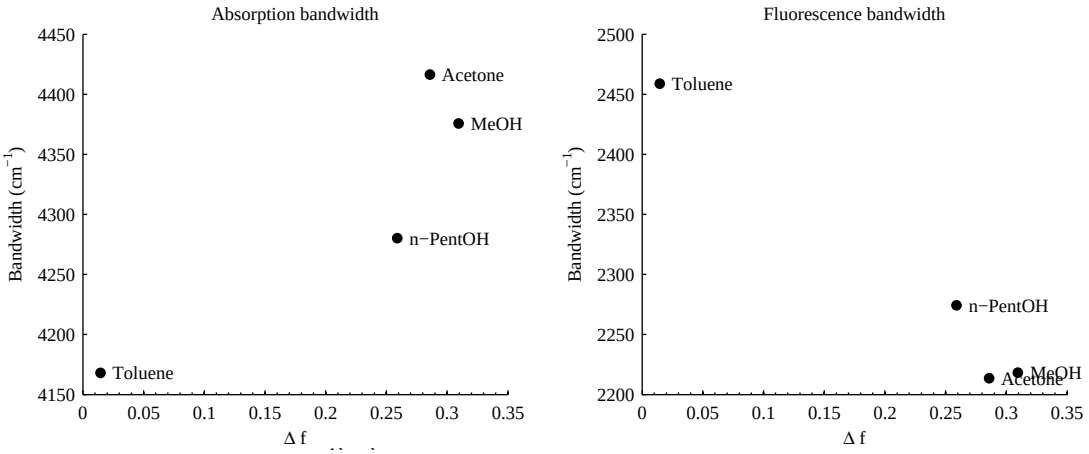

Figure 6.3: *Dependence of band-widths of the absorption and fluorescence spectra of DCM on the reaction field parameter Δf.*

6.2 Streak camera

Figure 6.4 shows the the time-dependent fluorescence of DCM in acetone, methanol and toluene at a concentration of 10^{-4} M

An important feature seen in this data is the lack of a significant shift of the peak fluorescence within the time resolution of the streak camera. This is a striking difference compared to the methanol (and indeed the ethanol and n-pentanol data from chapter 5) where there is a clearly visible red-shift in the early

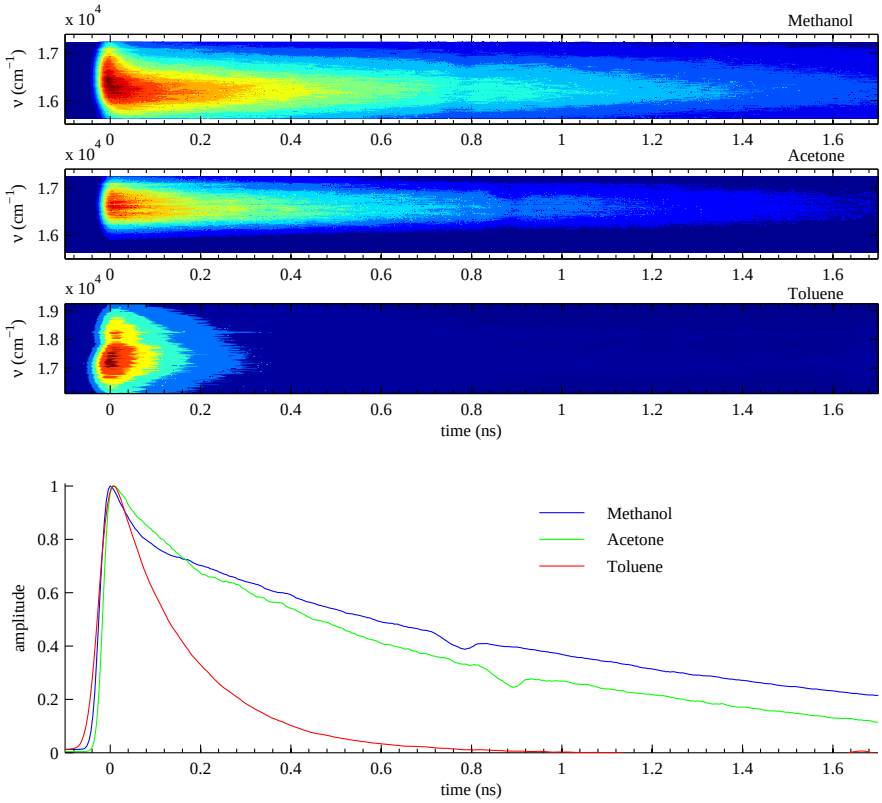

Figure 6.4: *Comparison of population (by amplitude of magic angle signal) and anisotropy decay from picosecond fluorescence*

times.

Acetone with a lower viscosity would be expected to solvate the DCM excited-state faster than methanol. Using the empirical linear fit of the dependence of solvation on viscosity from chapter 5,

$$\tau_{solvation} = 17\eta + 3.1 \tag{6.2}$$

we would expect DCM in acetone to have a solvation time of

$$\tau_{solvation} = 17 \times 0.308 + 3.1 = 8.3ps \tag{6.3}$$

Acetone's dielectric constant is less than methanol, it has a significantly larger

dipole moment (2.9 D) compared with methanol (1.7 D). Toluene, on the other hand, has a much smaller dielectric constant, a negligible dipole moment and thus very little ability to stabilise and lower the energy of a highly polar charge transfer state, such as a TICT state. Without this stabilisation, the charge transfer state has a higher energy than the less-polar locally excited-state. Thus, the emissive state of DCM in toluene is attributed to the locally excited-state. Coupled with the information about the way in which viscosity affects the population dynamics of the DCM excited-state, DCM in toluene will be considered as a model for the expected dynamics of a non-polar locally excited-state. This idea will be used in the next chapter to discuss the comparison of features in the time-dependent emission spectra of DCM and DCJ.

The log-normal fit of the time-resolved spectra are shown in figure 6.5. The difference in the fluorescence lifetime is clear in the amplitude parameter and a small but non-negligible time-dependent Stokes shift is clear in acetone. This feature seems to decay more slowly than the solvation of DCM in methanol, despite the viscosity of acetone being less than that for methanol. This suggests that the local solvent-solute dipole-dipole interactions are different for the two solvents. The hydroxyl group of methanol is able to undergo hydrogen bonding with the lone-pair and acetone does not have this capability, though the polar carbonyl group could interact with the lone-pair electrons in a similar way.

Figure 6.6 shows the dependence of the excited-state lifetime on the reaction field parameter Δf.

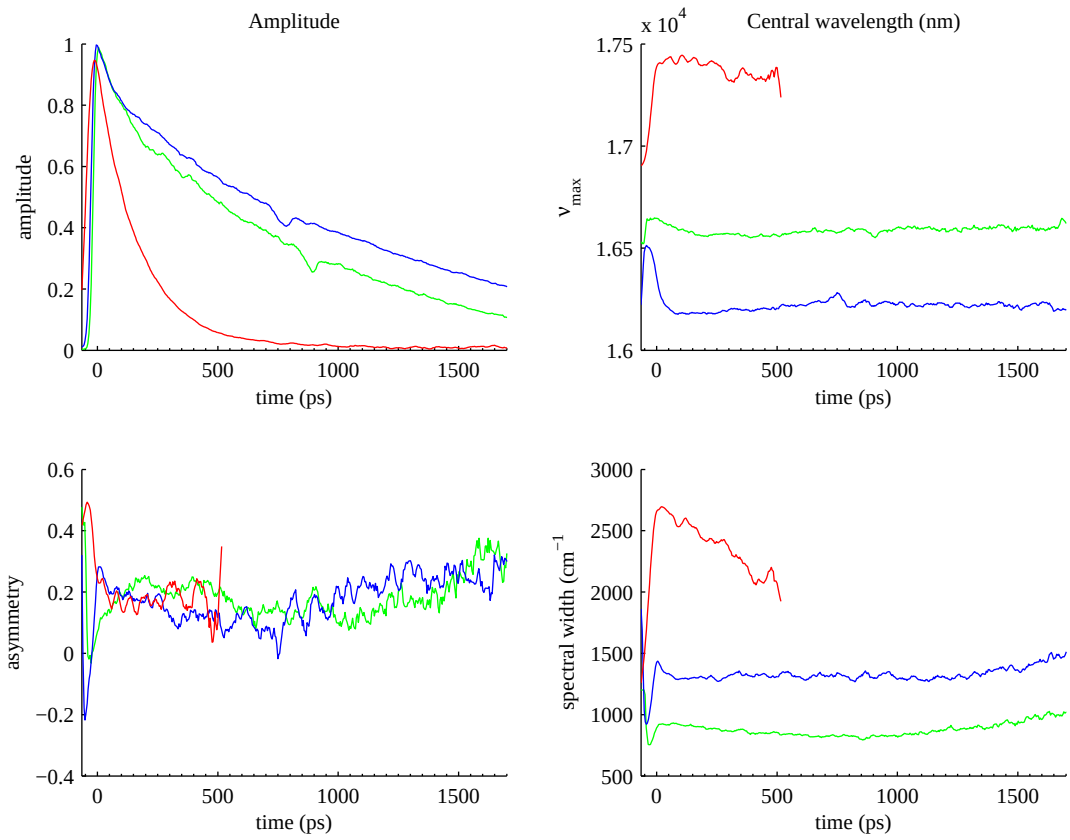

Figure 6.5: *Log-normal fit parameters for time-resolved fluorescence of DCM in methanol (blue), acetone (green) and toluene (red). Note: Toluene peak, asymmetry and spectral width parameters become noisy after 500 ps so the fit parameters for toluene are not plotted beyond this time.*

The reaction field parameter Δf is a measure of the ability of the solvent to solvate a polar excited-state. Figure 6.7 shows the fluorescence amplitude lifetime as a function of the reaction field parameter. The trend data suggests that the lifetime of the polar excited-state is much longer than the non-polar (locally-excited) state. One explanation for this could invoke the TICT model of Grabowski, as one would expect a low-polarity locally excited-state to have a short life-time due to the overlap of the donor and acceptor orbitals when DCM is in a planar configuration. Study of the lifetime of DCM solvents that have f-parameters in between toluene and methanol could yield more information to support this idea.

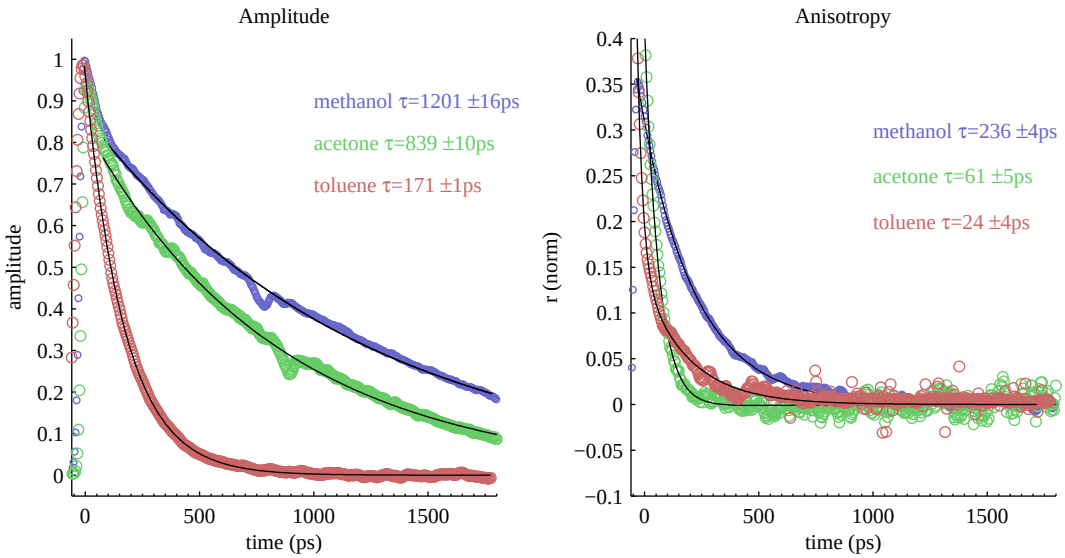

Figure 6.6: *Comparison of fluorescence lifetime and anisotropy decay of DCM in solvents with different reaction field parameter (Δf)*

A comparison of the viscosity and Δf dependence of the anisotropy of DCM in these solvents shown in figure 6.8 suggests that although viscosity does seem to play a role in the anisotropy decay rate, it is not the major reason for the shorter decay in toluene. This gives further evidence that DCM in toluene emits from a different excited-state that decays via a different mechanism.

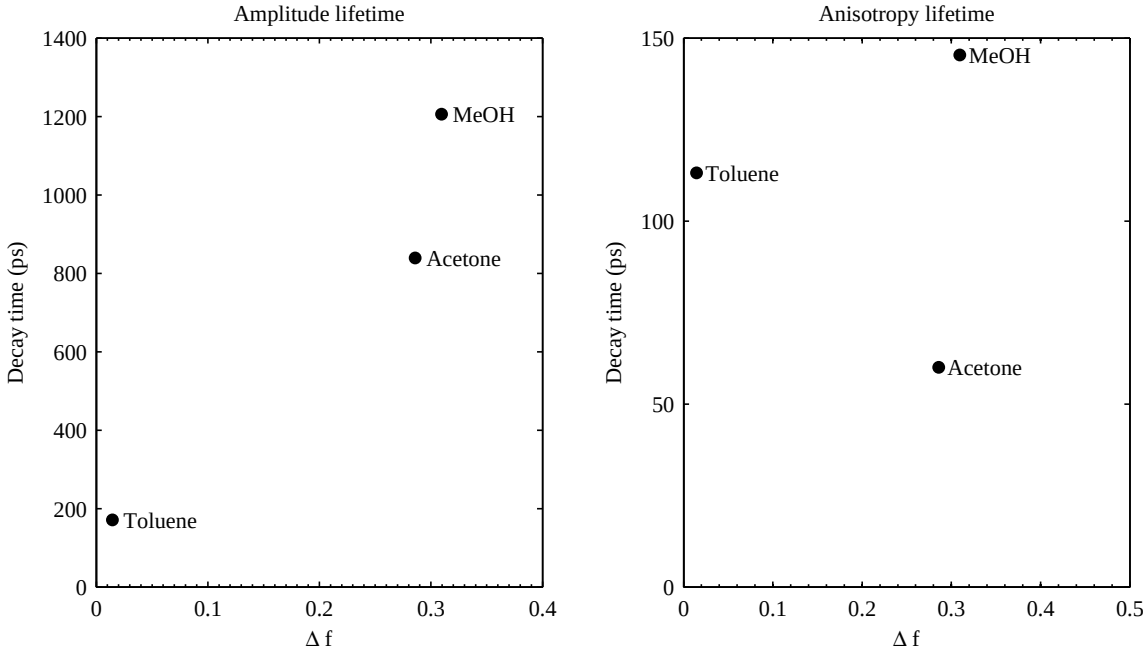

Figure 6.7: *Amplitude and anisotropy decay time as a function of the reaction field parameter* Δf.

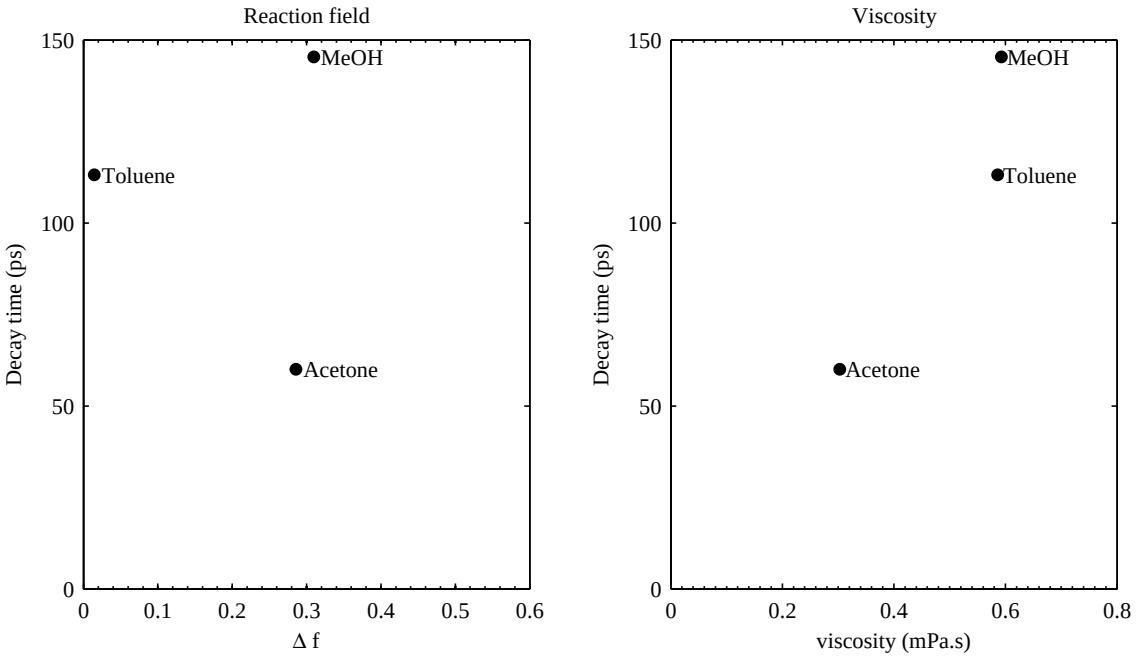

Figure 6.8: *Amplitude and anisotropy decay time as a function of the reaction field parameter* Δf.

Chapter 7

DCJ: An analogue of DCM that cannot twist

7.1 Introduction

The TICT state in DCM is proposed to occur via rotation of the dimethylamino bond upon excitation. The julolidine moiety in DCJ replaces the dimethylamino group in DCM, preventing rotation of the amine R_2N-Ph bond in the ground and excited-states as shown in figure 7.1. This chapter investigates differences in the dynamic spectral behaviour of DCJ compared with DCM, to provide evidence for the existence/non-existence of the twisted charge transfer state in DCM. The use of conformationally restricted analogues has been a useful approach to isolate twisted and non-twisted states in DMABN [109, 110, 111].

As mentioned in the background chapter, previous studies of restricted julolidine analogues of DCM in non-polar solvents [58] found an order of magnitude increase in the lifetime of the assigned S_1 state compared with unrestricted DCM. The TICT state in this study was assigned to the S_2 state from Marguet's study [13].

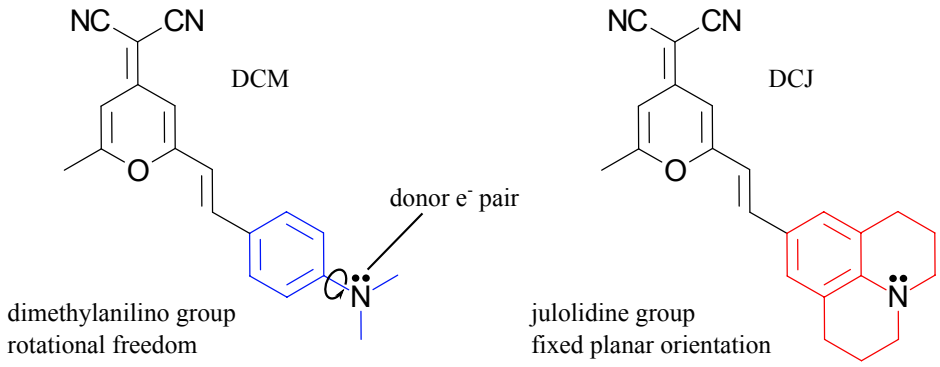

Figure 7.1: *Structure of DCM and DCJ*

As DCJ can be seen as a model compound for DCM with a constrained planar orientation of the dimethylamino group, one would expect that fluorescence should occur from a state analogous to the locally excited-state in DCM. However, it is important to note that the julolidine moiety is a stronger electron-donor than the dimethylanilino moiety as the constrained bond aligns the non-bonding n orbital with the π orbitals of the aromatic ring, increasing overlap and thus increasing the probability of electron transfer [35, 36, 37].

DCJ is not very soluble in the alcohols used in chapters 4 and 5. This fact in itself is important to note. There are two factors that might be at play here. Firstly the steric repulsion caused by the bulky julolidine moiety in DCJ likely minimises the ability of the amino nitrogen to form hydrogen bonds with the hydroxyl group of the alcohols. More importantly, as mentioned above, the restricted rotation of the julolidine moiety maintains planarity of the amino nitrogen with respect to the aromatic ring. This allows the lone-pair to contribute to the conjugation more readily, again decreasing the ability of the nitrogen to interact via hydrogen bonding by decreasing the availability of the lone-pair electrons for this purpose. This difference in the model compound's interaction with solvents compared with DCM and the fact that DCM dissolves more readily in alcohols is a factor in the interpretation of the data presented in this chapter.

7.2 Steady-state spectra

DCJ dissolved in all solvents used in this study to a sufficient extent to allow steady-state spectra to be measured due to the better signal-to-noise of these measurements. Due to the lower solubility of DCJ, all steady-state spectra were measured on solutions with concentrations of approximately 10^{-5} *M*.

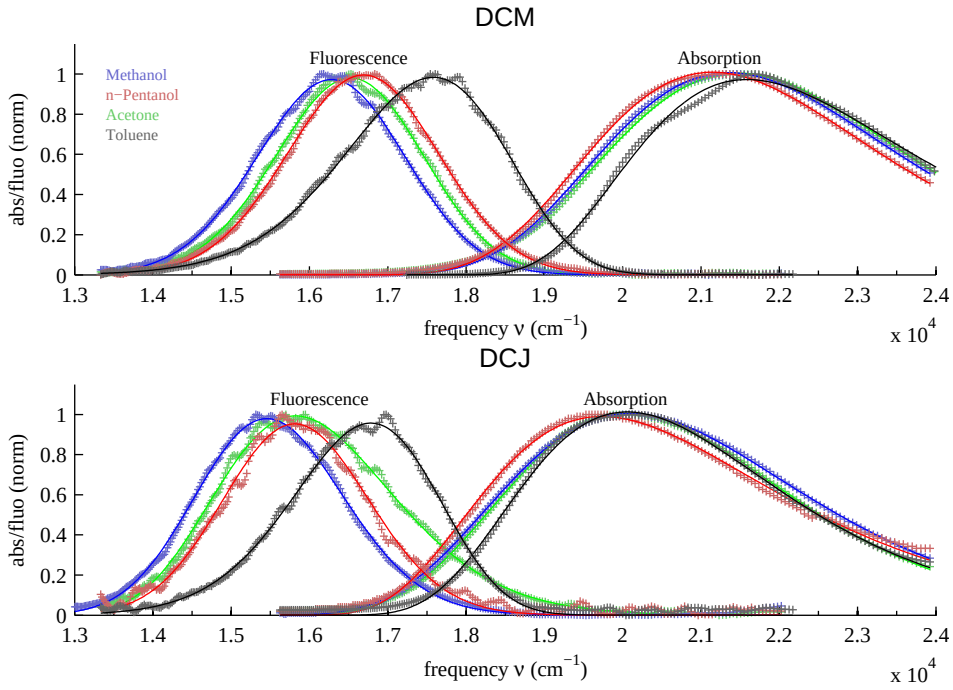

Figure 7.2: *Steady-state absorption and fluorescence spectra of (a) DCM and (b) DCJ*

The steady-state spectra of DCJ in figure 7.2 show a solvent dependent Stokes shift as with DCM. By far the most commonly proposed excited-state charge transfer structure of DCM involves twisting of the dimethylamino group. The spectra for DCJ then are counterintuitive, as the structure of the julolidine moiety prevents rotation of the amino nitrogen group with respect to the aromatic ring. DCJ is of course still a donor-acceptor and could form a planar charge transfer state but how can this result be reconciled with the much-cited simulations of Marguet [13] that suggest that in DCM only the twisted CT state has a significantly larger dipole-moment than the excited-state.

Looking at the fit parameters (table 4.1), it can be seen that although the absorption and emission spectra of DCJ are both red shifted with respect to those of DCM, the Stokes shifts are smaller. The shifts, however, are generally larger than those for DCM in toluene (which in chapter 6 we designated as a low-polarity locally excited-state) and they do increase with an increase in Δf of the solvent, suggesting that there is still some charge transfer character in the excited-state. DCJ in n-pentanol does have a Stokes shift that is less than DCM in toluene so the dipole moment of the DCJ emissive excited-state is likely to be less than that of DCM.

A likely explanation for the lower energy of the absorption and emission bands in DCJ in comparison to DCM is that the conjugation length is increased due to the restricted planarity of the donor and acceptor groups causing a stronger coupling of the non-bonding orbital of the julolidine nitrogen to the π-orbitals of the aromatic ring.

	DCM				DCJ			
Solvent	ν_{abs} (cm^{-1})	$\Delta\nu_{abs}$ (cm^{-1})	ν_{fluo} (cm^{-1})	$\Delta\nu_{fluo}$ (cm^{-1})	ν_{Abs} (cm^{-1})	$\Delta\nu_{abs}$ (cm^{-1})	ν_{fluo} (cm^{-1})	$\Delta\nu_{fluo}$ (cm^{-1})
Methanol	21352	4376	16284	2218	20093	4466	15456	2222
n-Pentanol	21148	4280	16691	2274	19732	4375	15812	2179
Acetone	21471	4416	16526	2214	20063	4187	15824	2659
Toluene	21590	4168	17582	2459	20056	3888	16784	2207

Table 7.1: Steady-state spectral parameters of DCM and DCJ in a range of solvents

Table 7.1 highlights that the difference in bandwidth of the fluorescence spectrum of DCJ in acetone compared with DCM is much larger than for the other three solvents. The origin of this difference is not yet clear.

Figure 7.3 shows the dependence of the absorption and fluorescence peak frequencies of DCM and DCJ versus the solvent reaction field parameter Δf. Except for the lower energy of the absorption and fluorescence bands for DCJ,

the trends are similar.

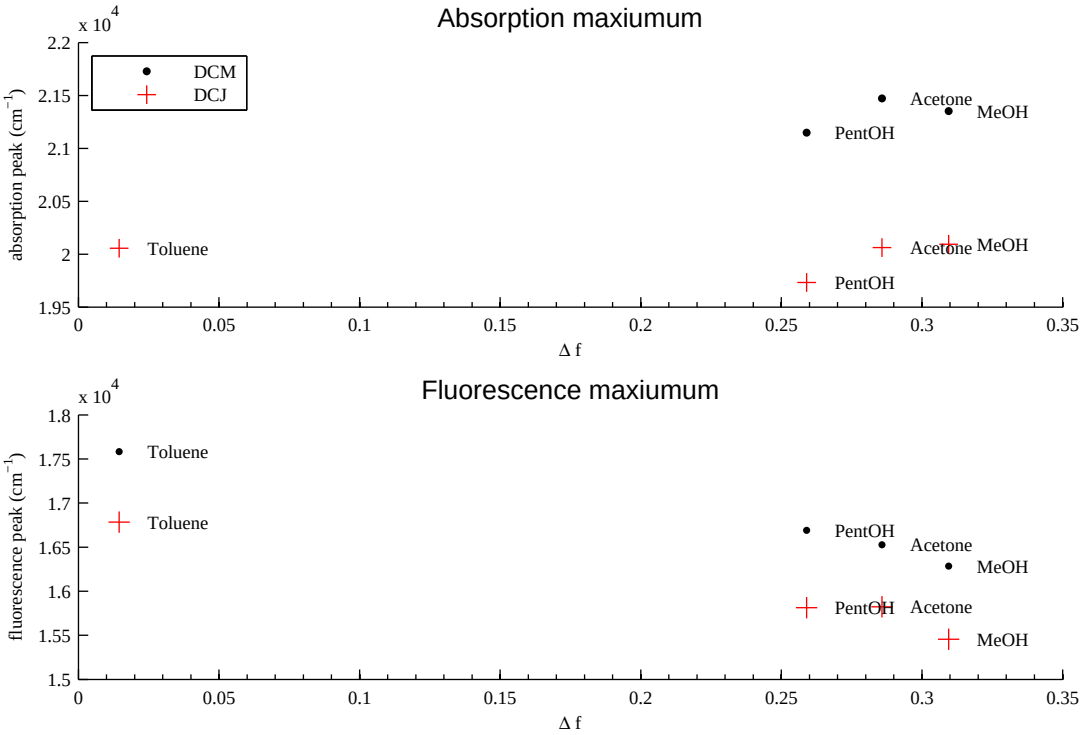

Figure 7.3: *Absorption and fluorescence peak frequency ($cm^{-}1$) as a function of the solvent reaction field parameter Δf*

The Stokes shift dependence on Δf also shows similar trends in figure 7.4, with the largest difference being in toluene.

Figure 7.5 shows the bandwidth parameter versus Δf. The most important feature here is the much larger bandwidth of DCJ in acetone (2659 cm^{-1}) versus that of DCM (2241 cm^{-1}). In comparison, the other solvents show a reasonably close bandwidth.

Clearly, the steady-state spectra of DCJ exhibit the hallmarks of a charge-transfer state - a large Stokes shift that is dependent on the solvent dipole moment. But is it the same state as that of DCM and if so, does this mean that the TICT model involving rotation of the dimethylamino bond is not valid for DCM? Time-dependent measurements were performed to investigate this question.

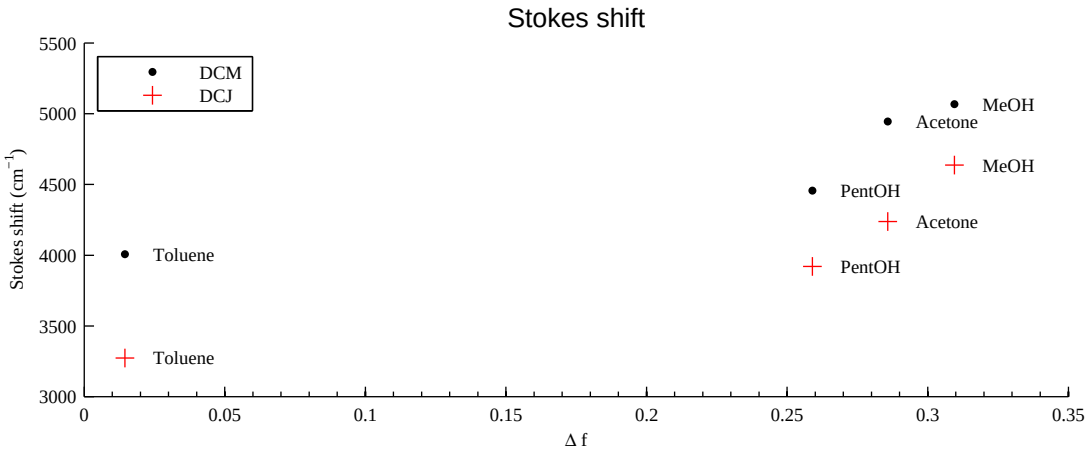

Figure 7.4: *Comparison between the Stokes shift of DCM and DCJ as a function of the solvent reaction field parameter* Δf

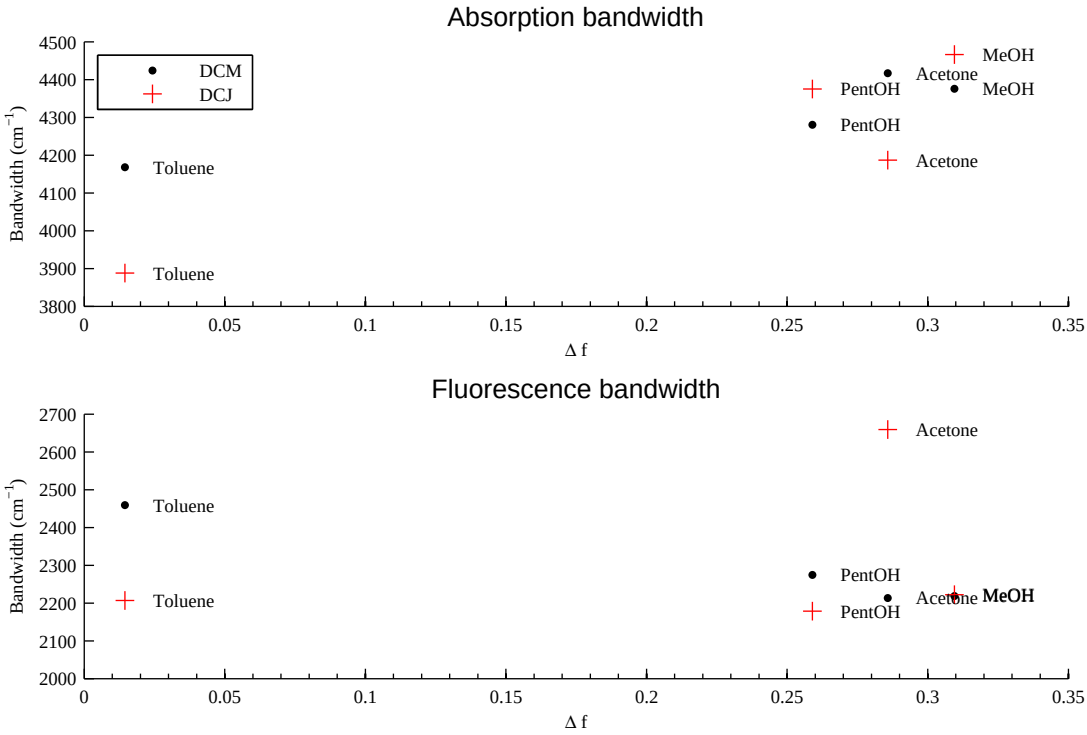

Figure 7.5: *The absorption and fluorescence spectral bandwidths of DCM and DCJ in solvents with different reaction field parameter* Δf

7.3 Streak camera

DCJ was found to dissolve readily in acetone, so due to the low solubility in the alcohol homologous series, this chapter presents data for DCM and DCJ dissolved in acetone. The influence of viscosity, dipole moment and local molecular interactions for the solvents have been characterised in the previous chapters so this chapter aims to present a comparison of DCM and DCJ that takes diffusion and solvation processes into account.

For all experiments presented in this chapter DCM and DCJ were dissolved in acetone at a concentration of 10^{-4} *M*.

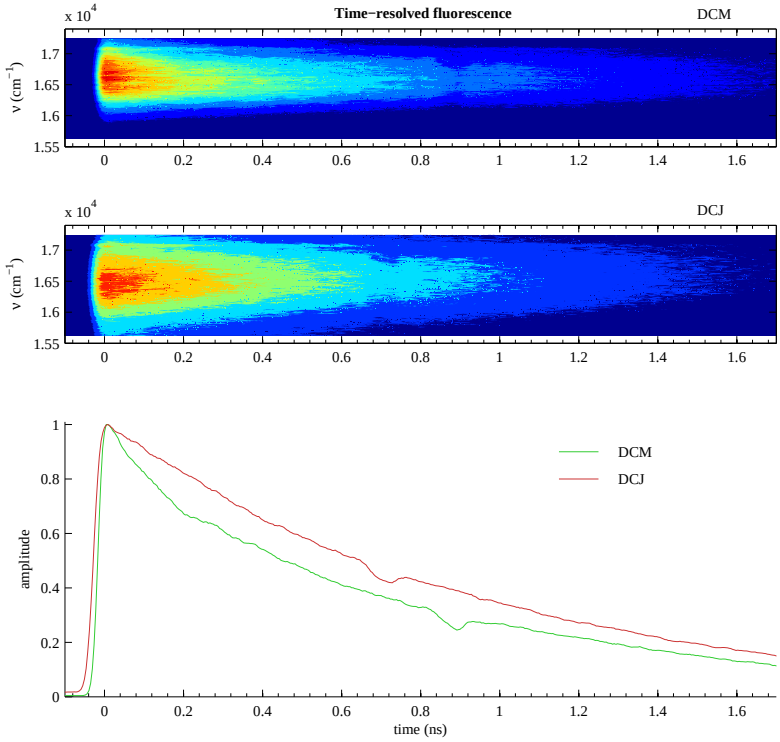

Figure 7.6: *Contour plots of the time-dependent fluorescence of DCM and DCJ in acetone*

The time-dependent fluorescence of DCM and DCJ in acetone excited on the high energy side of their absorption peaks at 400nm give more information about the nature of the DCJ excited-state. The contour plots in figure 7.6 show similar dynamics with little sign of a shift and closely matched lifetimes.

Figure 7.7 does show a small time-dependent Stokes shift for DCM in acetone. It is presumed that this feature is the tail-end of a fast and un-resolved solvation shift from a higher energy state.

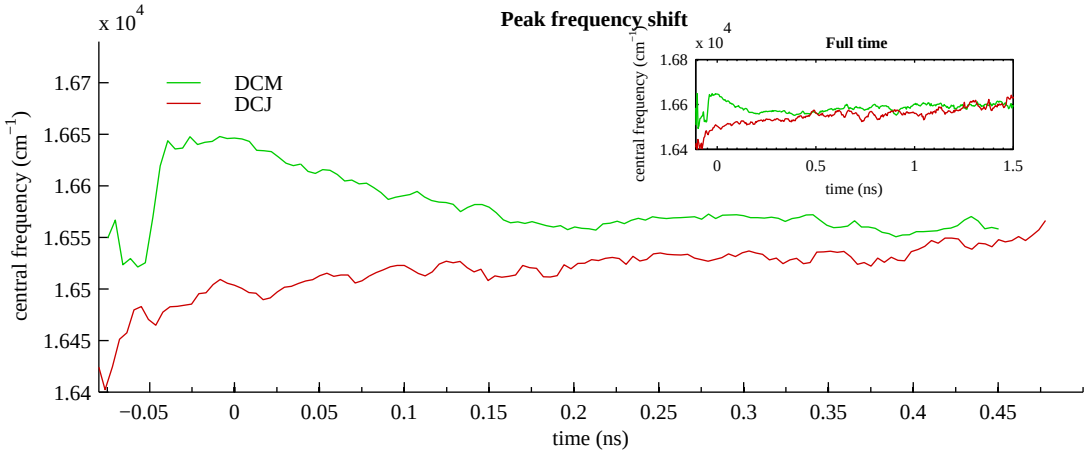

Figure 7.7: *The time-dependent fluorescence peak-shifts of DCM and DCJ in acetone. Inset shows the same data over a long time-period.*

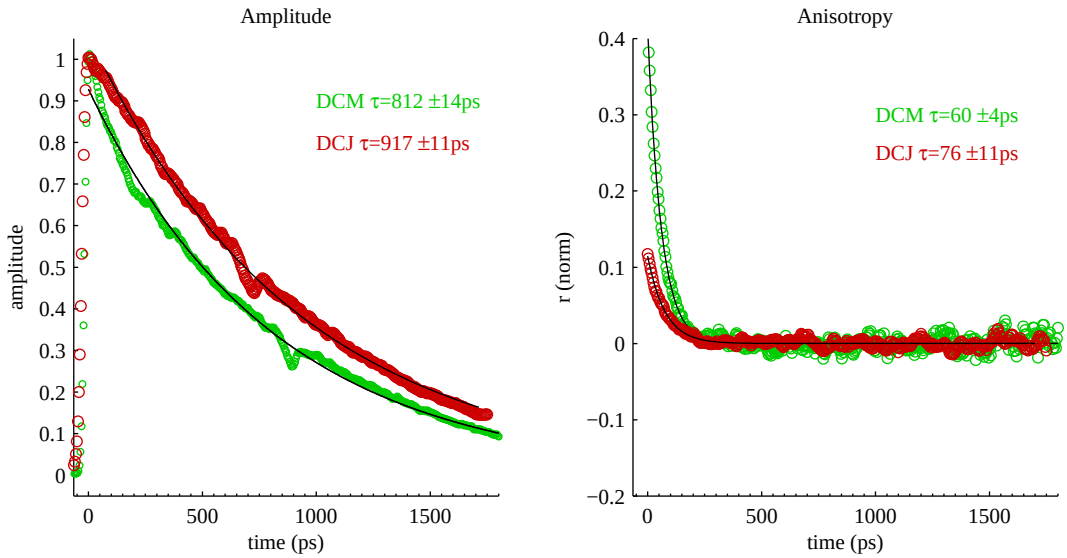

Figure 7.8: *The amplitude and anisotropy decay curves of DCM and DCJ in acetone. The similar decay rates suggest that the dynamics occur from equivalent excited-state conformations.*

As can be seen in figure 7.8 and table 7.2, the amplitude and anisotropy decays occur on similar timescales.

	DCM	DCJ
$\tau_{amplitude}\ (ps)$	812 ± 14	917 ± 11
$\tau_{anisotropy}\ (ps)$	60 ± 4	76 ± 11

Table 7.2: Fluorescence amplitude and anisotropy decay times for DCM and DCJ in acetone

Comparing the amplitude decay of DCM and DCJ in acetone to the lifetime of 170 ps for DCM in toluene, which we attribute to a non-polar locally excited-state, this data gives a strong indication that the DCJ emissive state in acetone is not an analogue of the locally excited-state in toluene as would be expected for a TICT mechanism involving the dimethylamino bond in DCM. The lifetime of the excited-state of DCJ suggests that it may be twisted or conformationally distorted like in DCM so that the donor and acceptor orbitals are de-coupled -

preventing re-combination of the charge separated state. However, considering the constrained nature of the dimethylamino bond in the rigid julolidine moiety of DCJ, the twist cannot occur here.

To explain this data, the presence of another twisted bond may be required. CASSCF calculations performed by Xu et al. [112] suggest that an excited-state structure where the dimethylanilino bond is twisted rather than the dimethylamino group in DCM is possible. This may explain the Stokes shift, as the stronger donor character of the constrained julolidine-aromatic group allows a fully twisted ICT state with a delocalised positive charge on the anilino moiety and a delocalised negative charge to be stabilised on the cyano-pyran group.

Another important observation to make is that the slower anisotropy decay of DCJ, attributed to rotational diffusion of the excited solute, makes sense. One would expect that the heavier molecule (355.43g.mol^{-1} versus 303.36g.mol^{-1} for DCM), and hence larger molecular volume, would rotate more slowly by an amount approximately proportional to the ratio of their weights. Though a different shape and different interactions between the solvent and solute molecules may mean that this direct proportionality does not hold.

There are a number of conclusions that can be drawn from this chapter's results when coupled with the results from the previous chapters. The first being that DCJ shows dynamics that are more similar to the dynamics of DCM than one would expect if the TICT mechanism on the dimethylamino bond explained the long lifetime of the charge transfer state of DCM. The large (though slightly smaller) Stokes shift suggests that the excited-state in DCJ is a charge transfer state however DCJ seems to have a lower solubility in the alcohols than DCJ. Therefore a direct comparison (by time-resolved Stokes shift) with the solvation dynamics of DCM in these solvents was not possible. One is led to the conclusion that the excited-states of DCM and DCJ are similar in terms of their energy and configuration.

These conclusions do not wholly rule out a TICT mechanism but they do indicate that the dimethylamino-phenyl bond may not be the one that twists. Chapter 8 will discuss these ideas further and will outline scope for experiments that would help to clear up the ambiguities.

Chapter 8

Summary and conclusions

8.1 Conclusions about the excited state of DCM

This thesis studied the steady-state and time-resolved spectral dynamics of the excited state of the donor-acceptor dye DCM with a view to clarifying the nature of the emissive state. As a point of comparison, DCM was first studied in a polar-solvent, methanol, to examine the features such as time-dependent Stokes shift that are indicative of a photo-excited intramolecular charge transfer state.

Time-resolved measurements were taken with a custom built optical setups. Laser excited fluorescence was measured with a picosecond streak camera setup and a pump-supercontinuum-probe experiment was built to measure the dynamics of the polarisation resolved stimulated emission signal with a higher resolution than the streak camera allows.

The viscosity and dielectric properties of the solvents were used to determine their effect on the excited state dynamics of DCM and their influence on the charge transfer character of the emissive state.

This study lends further evidence to the discussion on the nature of the

excited-states of DCM and the validity of the TICT model for this compound.

The large Stokes shift seen for DCM in the polar-solvents methanol, ethanol, n-pentanol and acetone is indicative of solvation of an intramolecular charge transfer state (ICT). This conclusion is reinforced by the viscosity and dielectric/dipole moment dependence experiments in chapter 5 and 6.

The viscosity dependence showed that the time-dependent Stokes shift is diffusion dependent as the solvation correlation time had an increasing trend with solvent viscosity. This finding is consistent with the diffusion of solvent molecules in response to the electric field induced by the change in dipole moment of DCM accompanying intramolecular charge transfer in the excited state.

The dielectric and orientational polarisability properties of the solvent as determined by the Δf parameter of Lippert and Mataga's theory were used in chapter 6 to investigate the effect on the solvation dynamics and stabilisation/destabilisation of the charge transfer state. It was seen that toluene, with a small dipole moment of 0.36 D, does not exhibit any significant time-dependent solvation (within the resolution of the streak camera fluorescence experiment) and the Stokes shift was much smaller than in the polar-solvents. This would suggest that the charge transfer state is unable to form in a non-polar solvent such as toluene and that the energy of the locally excited state is likely to be lower than a CT state in this solvent. Toluene exhibited a significantly smaller fluorescence lifetime than seen in the polar-solvents. This was attributed to the lifetime of the locally excited state.

Interestingly, DCM in acetone did not show a significant time-dependent shift either within the resolution of the streak camera. However, it did show a large Stokes shift similar to than of methanol and consistent with its large Δf value. This state was thus attributed to the same charge transfer state as seen for DCM

in methanol. The shift was presumed to be too fast to be resolved in acetone due to its lower viscosity than methanol.

The comparison of DCM and DCJ in acetone yielded interesting results. The restricted rotation of the dimethylamino donor group prevents formation of the twist deemed necessary by Marguet [13] et al. to form a twisted intramolecular charge transfer state; thus for the validity of the dimethylamino bond rotation hypothesis for TICT in DCM, one would expect significant differences in the spectral and decay dynamics of the excited state in DCJ.

The steady state spectra showed lower energies of the ground and excited state for DCJ compared with DCM in the range of solvents studied. Interestingly, DCJ in acetone showed a significantly larger fluorescence bandwidth compared to that of DCM in acetone. Despite this difference - which was also evident in the time-resolved fluorescence - the time-dependent measurements showed the fluorescent state lifetime and anisotropy decays to be very similar. One would expect that if the only ICT mechanism available to DCM was TICT about the dimethylamino bond, that DCJ should have a lifetime indicative of the locally excited state attributed to the fluorescent state of DCM in toluene. If DCM's excited state was a TICT state and DCJ's was planar, one would expect the lifetimes to be significantly different and indeed smaller in DCJ as the decoupling of the donor and acceptor orbitals is not possible by rotation of the dimethylamino group.

The alternative to ruling out a TICT state altogether for DCM and DCJ is that they both twist about the dimethylanilino bond between the carbon para to the donor group and the central double bond. Though possible, a twist at this bond would be expected to change the conjugation length of the molecules in the excited state which should be evident in the Stokes shift. A twist at that bond would also have a larger effect on the orientation of the transition dipole moment measured by the anisotropy.

With such a complex system that is strongly influenced by solvent effects, it is difficult to directly determine the dynamic structure associated with the excited-state for DCM.

The aim of this PhD thesis is to shed further light on the discussion about TICT states and their relevance to donor-acceptor stilbenoid compounds like DCM. Controversies have arisen about this molecule because it is very difficult to isolate all the variables that cause the spectral features and dynamics seen, and it is therefore also difficult to attribute them to well-defined states or conformations. Some work has been done in the past with model compounds [58] and more rigourous theories about solvation of donor-acceptor systems [96, 113, 114, 115] but it may be that the controversy will not be resolved once and for all until more direct measurements can be made.

8.2 Future directions

There are a number of techniques that could be used to further elucidate the excited-state of DCM and similar molecules:

* Time-resolved x-ray crystallography [116, 117] is a particularly promising technique as it allows a more direct observation of the conformation of the relaxed emissive excited-state however this technique requires the sample to be isolated and independent of a solvent environment.

* Similarly gas phase and cooled spectroscopic studies of DCM [118, 112] neglect the role that solvent plays in the dynamics of DCM.

* Molecular modelling, simulations and quantum chemical calculations have been used extensively [13, 114, 119, 112] to study the proposed excited-state structures of DCM with varying amounts of success. The difficulty is in determining which states are valid in a complex system such as DCM in a solvent

with many degrees of freedom.

* Many studies have looked at the influence of solvents on the excited-state spectra of DCM [19, 45, 55, 112], however large scale studies of DCM in many solvents has typically been restricted to steady-state rather than time-resolved spectra. As was seen in this thesis, solvent parameters can generally not be altered individually without affecting other parameters as well. And there are always local interactions between solvent and solute that can only be neglected when comparing parameters from a large number of solvents.

The ultrafast dynamics of DCM in a larger number of solvents would be difficult to analyse but it would allow the trends from parameters such as the viscosity and dielectric constant - as well as more local parameters such as the strength of hydrogen bonding - to be analysed.

* Other rotationally hindered model analogues, for example where the dimethylanilino group is blocked, could be used to rule out the presence of excited-state conformational candidates for a TICT state in DCM. This approach has been used to study the TICT state in DMABN [109, 110, 111]

It is likely that a combination of computer simulations, models and targeted experiments to check predictions of the models will need to be developed to correctly account for all the features seen in the spectra of complicated donor-acceptor systems like DCM where the parameter space is large and it is difficult to isolate the individual variables. The difficulty with many of these types of studies are that the surrounding solvent is a necessary part of the process of intramolecular charge transfer and thus the molecule can not be studied in isolation.

The author of this thesis looks forward to seeing the continuation of enquiry into TICT states in donor-acceptor systems and a hopeful resolution of the controversy surrounding this model in DCM and similar systems.

Bibliography

[1] W. Rettig. TICT states and beyond - reaction dimensionality and application to photosynthesis. *Proceedings of the Indian Academy of Sciences - Chemical Sciences*, 104(2):89–104, 1992.

[2] D. H. Hwang, J. D. Lee, M. J. Lee, and C. Lee. Organic light-emitting diode using a new dcm derivative as an efficient orange-red doping molecule. *Current Applied Physics*, 5(3):244–248, 2005.

[3] D. Berner, H. Houili, W. Leo, and L. Zuppiroli. Insights into OLED functioning through coordinated experimental measurements and numerical model simulations - review article. *Physica Status Solidi A - Applied Research*, 202(1):9–36, 2005.

[4] S. K. Lee, B. J. Jung, T. Ahn, Y. K. Jung, J. I. Lee, I. N. Kang, J. Lee, J. H. Park, and H. K. Shim. White electroluminescence from a single polyfluorene containing bis-DCM units. *Journal of Polymer Science Part A - Polymer Chemistry*, 45(15):3380–3390, 2007.

[5] A. M. Taleb, B. T. Chiad, and Z. S. Sadik. Spectroscopic study of DCM as an active medium for luminescent solar concentrators. *Renewable Energy*, 30(3):393–398, 2005.

[6] G. Kwak, S. Wang, M. S. Choi, H. Kim, K. H. Choi, Y. S. Han, Y. Hur, and S. H. Kim. 2d-pi-a type pyran-based dye derivatives: Photophysical properties related to intramolecular charge transfer and their electroluminescence application. *Dyes and Pigments*, 78(1):25–33, 2008.

[7] Kobayashi group home page. http://femto.pc.uec.ac.jp/. Accessed: 2013-07-18.

[8] Z. G. Zhang and J. Wang. Structures and properties of conjugated donor-dcceptor copolymers for solar cell applications. *Journal of Materials Chemistry*, 22:4178–4187, 2012.

[9] F. Webster and W. McGolgin. Arylidene dye lasers, US patent 3,852,683, 1974.

[10] K. Rotkiewicz, K.H. Grellmann, and Z. R. Grabowski. Reinterpretation of the anomalous fluorescense of p-n,n-dimethylamino-benzonitrile. *Chemical Physics Letters*, 19:315–318, 1973.

[11] W. Rettig and W. Majenz. Competing adiabatic photoreaction in stilbene derivatives. *Chemical Physics Letters*, 65:3610–3616, 1989.

[12] Z. R. Grabowski, K. Rotkiewicz, and W. Rettig. Structural changes accompanying intramolecular electron transfer: Focus on twisted intramolecular charge-transfer states and structures. *Chemical Reviews*, 103(10):3899–4031, 2003.

[13] S. Marguet, J.C. Mialocq, and P. Millie. Intramolecular charge transfer and trans-cis isomerization of the DCM styrene dye in polar solvents. a CS INDO MRCI study. *Journal of Physical Chemistry*, 160:265–279, 1992.

[14] D. Easter and A. Baronovski. Ultrafast relaxation in the fluorescent state of the laser dye DCM. *Chemical Physics Letters*, 201:153–158, 1993.

[15] S. Pommeret, T. Gustavsson, R. Naskrecki, G. Baldacchino, and J.C. Mialocq. Femtosecond absorption and emission spectroscopy of the DCM laser dye. *Journal of Molecular Liquids*, 64:101–112, 1995.

[16] D. Bingemann and N. P. Ernsting. Femtosecond solvation dynamics determining the band shape of stimulated-emission from a polar styryl dye. *Journal of Chemical Physics*, 102(7):2691–2700, 1995.

[17] T. Gustavsson, G. Baldacchino, J.C. Mialocq, and S. Pommeret. A femtosecond fluorescence up-conversion study of the dynamic stokes shift of the DCM dye molecule in polar and non-polar solvents. *Chemical Physics Letters*, 236:587–594, 1995.

[18] J. C. Gumy, O. Nicolet, and E. Vauthey. Investigation of the solvation dynamics of an organic dye in polar solvents using the femtosecond transient grating technique. *Journal of Physical Chemistry A*, 103(50):10737–10743, 1999.

[19] M. Meyer and J. Mialocq. Fluorescence lifetime measurements of the two isomers of the laser dye DCM. *Chemical Physics Letters*, 150:484–490, 1988.

[20] S. Kovalenko, N. Ernsting, J. Ruthmann. Femtosecond hole-burning spectroscopy of the dye DCM in solution: the transiton from the locally excited-state to a charge-transfer state. *Chemical Physics Letters*, 258:445–454, 1996.

[21] S. Lee, K. Jung, Sung J.H., K. Hong, and C.H. Nam. Adaptive quantum control of DCM fluorescence in the liquid phase. *Journal of Chemical Physics*, 117:9858–9861, 2002.

[22] D. McDonald, C. Hall, P. Hannaford, and L.V. Dao. Poster: Investigation of photoinduced structural dynamics in DCM by femtosecond time and spectrally resolved anisotropy. *Femtochemistry and Femtobiology (Femto8): Conference*, 2007.

[23] L.V. Dao, D. McDonald, and P. Hannaford. Multidimensional anisotropic spectroscopy for the study of intramolecular charge transfer. *15th International Conference on Ultrafast Phenomena, OSA Technical Digest Series (CD)*, page paper TuG25, 2006.

[24] P. Hammond. Laser dye DCM, its spectral properties, synthesis and

comparison with other dyes in the red. *Optics Communications*, 29:331–333, 1979.

[25] E. G. Marason. Laser dye DCM: CW, synchronously pumped, cavity pumped and single-frequency performance. *Optics Communications*, 37(1):56–58, 1981.

[26] E. Hückel. *Zeitschrift für Physik*, 83:632, 1933.

[27] C.A. Coulson, B. O'Leary, and R.B. Mallion. *Hückel Theory for Organic Chemists*. Academic Press, New York, 1978.

[28] Y. Volatron (tranlated by Jeremy Burdett). *An Introduction To Molecular Oribtals*. Oxford University Press, Oxford UK, 1993.

[29] K. Ruedenberg and C. W. Scherr. Free-electron network model for conjugated systems. I. Theory. *The Journal of Chemical Physics*, 21(9):1565–1581, 1953.

[30] A.G. Hankin and A.M. North. D.C. conductivity of some linear conjugated polymers. *Transactions of the Faraday Society*, 63:1525–1536, 1967.

[31] B.E. Davydov, G.P. Karpacheva, T.G. Samedova, and M.M. Yandarova. On certain peculiarities of polyconjugated systems. *European Polymer Journal*, 7(11):1569–1574, 1971.

[32] Y. Tan, Q. Zhang, J. Yu, X. Zhao, Y. Tian, Y. Cui, X. Hao, Y. Yang, and G. Qian. Solvent effect on two-photon absorption (TPA) of three novel dyes with large TPA cross-section and red emission. *Dyes and Pigments*, 97(1):58–64, 2013.

[33] J. McMurry. *Organic Chemistry, 5th Edition*. Brooks/Cole, 2000.

[34] W. Rettig and B. Zietz. Do twisting and pyramidalization contribute to the reaction coordinate of charge-transfer formation in DMABN and derivatives? *Chemical Physics Letters*, 317(3-5):187–196, 2000.

[35] P. R. Andrews, S. L. A. Munro, M. Sadek, and M. G. Wong. The hybridization state of nitrogen as a conformational variable in biologically active molecules. *Journal of the Chemical Society, Perkin Transactions 2*, pages 711–718, 1988.

[36] W. Schuddeboom, S. A. Jonker, J. M. Warman, U. Leinhos, W. Kuhnle, and K. A. Zachariasse. Excited-state dipole-moments of dual fluorescent 4-(dialkylamino)benzonitriles - influence of alkyl chain-length and effective solvent polarity. *Journal of Physical Chemistry*, 96(26):10809–10819, 1992.

[37] W. Rettig, D. Braun, P. Suppan, E. Vauthey, K. Rotkiewicz, R. Luboradzki, and K. Suwinska. Molecular-conformation and excited-state dipole-moments of di-methylaminobenzonitrile and tetramethylaminobenzonitrile (DMABN and TMABN). *Journal of Physical Chemistry*, 97(51):13500–13507, 1993.

[38] C. Ma, B. Zhang, Z. Liang, P. Xie, X. Wang, B. Zhang, Y. Cao, X. Jiang, and Z. Zhang. A novel n-type red luminescent material for organic light-emitting diodes. *Journal of Materials Chemistry*, 117:9858–9861, 2002.

[39] E. Lippert. *Zeitschrift für Naturforschung A*, 19:315–318, 1955.

[40] N. Mataga, Y. Kaifu, and M. Koizumi. The solvent effect on fluorescence spectrum, change of solute-solvent interaction during the lifetime of excited solute molecule. *Bulletin of the Chemical Society of Japan*, 28(9):690–691, 1955.

[41] N. Mataga and T. Kubota. *Molecular interactions and electronic spectra*. M. Dekker, New York, 1970.

[42] J. M. Drake, Michael L. Lesiecki, and Donald M. Camaioni. Photophysics and cis-trans isomerization of DCM. *Chemical Physics Letters*, 113(6):530–534, 1985.

[43] M. Meyer, J.C. Mialocq, and B. Perly. Photoinduced intramolecular charge transfer and trans-cis isomerization of the DCM styre dye. *Journal of Physical Chemistry*, 94:98–104, 1990.

[44] W. Rettig. Charge separation in excited-states of decoupled systems - TICT compounds and implications regarding the development of new laser-dyes and the primary processes of vision and photosynthesis. *Angewandte Chemie - International Edition in English*, 25(11):971–988, 1986.

[45] J.C. Mialocq and M. Meyer. Photophysical properties of the DCM and DFSBO styryl dyes consequence for their laser properties. *Laser Chemistry*, 10(5-6):19, 1990.

[46] Z. R. Grabowski, K. Rotkiewicz, and A. Siemiarczuk. Dual fluorescence of donor-acceptor molecules and the twisted intra-molecular charge-transfer (TICT) states. *Journal of Luminescence*, 18-9(Jan):420–424, 1979.

[47] Z. R. Grabowski, K. Rotkiewicz, A. Siemiarczuk, D. J. Cowley, and W. Baumann. Twisted intra-molecular charge-transfer states (TICT) - new class of excited-states with a full charge separation. *Nouveau Journal De Chimie - New Journal of Chemistry*, 3(7):443–454, 1979.

[48] Z.R. Grabowski and J. Dobkowski. Twisted intramolecular charge-transfer (TICT) excited-states - energy and molecular-structure. *Pure and Applied Chemistry*, 55(2):245–252, 1983.

[49] S. Biswas, I. Avan, A. K. Basak, N. E. Abo-Dya, A. Asiri, and A. R. Katritzky. Photophysics of novel coumarin-labeled depsipeptides in solution: Sensing interactions with SDS micelle via TICT model. *Amino acids*, 45(1):159–170, 2013.

[50] J. Catalan. On the dual emission of p-dimethylaminobenzonitrile and its photophysical implications. *Physical Chemistry Chemical Physics*, 15(22):8811–8820, 2013.

[51] C. Singh, R. Ghosh, J. A. Mondal, and D. K. Palit. Excited-state dynamics of a push-pull stilbene: A femtosecond transient absorption spectroscopic study. *Journal of Photochemistry and Photobiology A: Chemistry*, 263:50–60, 2013.

[52] H.K. Zhang, M. Ren-Lan, N. Er Pin, and G. Chu. Behaviour of the laser dye 4-dicyanomethylene-2-methyl-6-dimethylaminostryryl-4h-pyran in the excited singlet state. *Journal of Photochemistry*, 29:397–404, 1985.

[53] H. Zhang, A. Jonkman, P. Muelen, and M. Glasbeek. Femtosecond studies of the charge separation in photo-excited DCM in liquid solution. *Chemical Physics Letters*, 224:551–556, 1994.

[54] S. Pal, D. Sukul, D. Mandal, S. Sen, and K. Bhattacharyya. Solvation dynamics of DCM in micelles. *Chemical Physics Letters*, 327:91–96, 2000.

[55] D. Birch, G. Hungerford, R. Imhof, and A. Holmes. The fluorescence properties of DCM. *Chemical Physics Letters*, 178:177–184, 1991.

[56] M. Martin, P. Plaza, and Y. Meyer. Ultrafast intramolecular charge transfer in the merocynanine dye DCM. *Chem. Phys.*, 192:367–377, 1995.

[57] J.R. Lakowicz. *Principles of Fluorescence Spectroscopy, 3rd Edition*. Springer London, Limited, 2009.

[58] C. Chang, Y. Kao, and E. Diau. Fluorescence lifetime and nonradiative relaxation dynamics of DCM in nonpolar solvent. *Chemical Physics Letters*, 374:110–118, 2003.

[59] W. Rettig, B. Bliss, and K. Dirnberger. Pseudo-Jahn-Teller and TICT-models: a photophysical comparison of meta- and para-DMABN derivatives. *Chemical Physics Letters*, 305(1-2):8–14, 1999.

[60] A.L. Sobolewski and W. Domcke. Charge transfer in aminobenzonitriles: Do they twist? *Chemical Physics Letters*, 250(3-4):428–436, 1996.

[61] Van Tassle, A., Prantil, M., Fleming, G. Investigation of the excited-state structure of DCM via ultrafast electronic pump/vibrational probe. *Journal of Physical Chemistry B*, 110:18989–18995, 2006.

[62] J. Franck and E. G. Dymond. Elementary processes of photochemical reactions. *Transactions of the Faraday Society*, 21:536–542, 1926.

[63] E. Condon. A theory of intensity distribution in band systems. *Physical Review*, 28:1182–1201, Dec 1926.

[64] M. Maroncelli and G. R. Fleming. Picosecond solvation dynamics of coumarin-153 - the importance of molecular aspects of solvation. *Journal of Chemical Physics*, 86(11):6221–6239, 1987.

[65] G. Dutier, V. De Beaucoudrey, J. Zyss, and S. Brasselet. Photo-induced rotation of single molecules. In C. Burda and R. J. Ellingson, editors, *SPIE - The International Society for Optical Engineering*, volume 5929 of *Physical Chemistry of Interfaces and Nanomaterials IV*, pages 1–8, 2005.

[66] P. Debye. *Polar molecules*. Dover, New York, 1929.

[67] J. R. Mehaffey and Robert I. Cukier. Kinetic-theory derivation of the stokes-einstein law. *Physical Review Letters*, 38(19):1039, 1977.

[68] E. Vauthey. Picosecond transient grating study of the reorientation dynamics of nile red in different classes of solvent. *Chemical Physics Letters*, 216(3-6):530–536, 1993.

[69] D. R. Bessire and E. L. Quitevis. Effect of temperature and viscosity on rotational diffusion of merocyanine-540 in polar-solvents. *Journal of Physical Chemistry*, 98(49):13083–13092, 1994.

[70] W. Demtröder, A. Kamal, E. Mehdizadeh, G. Persch, Th. Weyh, and D. Zevgolis. Time-resolved molecular spectroscopy and molecular dynamics. In Baldassare Bartolo and Giulio Gambarota, editors, *Ultrafast Dynamics of Quantum Systems*, volume 372 of *NATO Science Series: B:*, pages 73–86. Springer US, 2002.

[71] L.E. Hargrove, R.L. Fork, and M.A. Pollack. Locking of HeNe laser modes induced by synchronous intracavity modulation. *Applied Physics Letters*, 5:4, 1964.

[72] H.W. Mocker and R.J. Collins. Mode competition and self-locking effects in a q-switched ruby laser. *Applied Physics Letters*, 7:270–273, 1965.

[73] A.J. De Maria, D.A. Stetser, and H. Heynau. Self mode-locking of lasers with saturable absorbers. *Applied Physics Letters*, 8:174–176, 1966.

[74] C. Spielmann, F. Krausz, T. Brabec, E. Wintner, and A.J. Schmidt. Femtosecond pulse generation from solid-state lasers. In *Institute of Physics Conference Series*, volume 126, pages 9–16, 1991.

[75] D.E. Spence, P.N. Kean, and W. Sibbett. 60-fsec pulse generation from a self-mode-locked Ti:sapphire laser. *Optics Letters*, 16:42–44, 1991.

[76] C. Rulliere. *Femtosecond Laser Pulses: Principles and Experiments*. Advanced Texts in Physics. Springer, 2005.

[77] B.R. Suydam. Self focusing in laser materials. *Proceedings of IEEE Reg 6 Conf (West USA) on Optoelectronics and Laser Technology*, pages 34–42, 1974.

[78] A. P. Piskarskas. Parametric generators and amplifiers of ultrashort light pulses. *Pacific Rim Conference on Lasers and Electro-Optics, CLEO - Technical Digest*, page 371, 2000.

[79] A. Penzkofer. Short pulse solid state lasers. *Proceedings of SPIE - The International Society for Optical Engineering*, 1277:14–28, 1990.

[80] J.P. Zhou, C.P. Huang, D. Garvey, M.T. Asaki, M.M Murnane, and H.C. Kapteyn. Ultrashort-pulse generation and amplification in Ti:sapphire. *Conference Proceedings - Lasers and Electro-Optics Society Annual Meeting*, pages 821–822, 1993.

[81] L. W. Coleman. Ultra-fast streak cameras for laser diagnostics. *IEEE Reg 6 Conf (West USA) on Optoelectronics and Laser Technology*, pages 9–12, 1974.

[82] J.W. Houghton, S.W. Thomas, and L.W. Coleman. Ultra-fast streak camera for optical pulse measurements. *Proceedings of the International Conference on Instrumentation Automation*, 29, 1974.

[83] M. Martin, P. Plaza, P. Changenet, and Y. Meyer. Investigation of excited-state charge transfer with structural change in compounds containing anilino subunits by subpicosecond spectroscopy. *Journal of Photochemistry and Photobiology A: Chemistry*, 105:197–204, 1997.

[84] G. Khitrova and P.R. Berman. Theory of pump-probe spectroscopy. *Journal of the Optical Society of America B*, 5:160–170, 1988.

[85] G. Stock and W. Domcke. Theory of femtosecond pump-probe spectroscopy of ultrafast internal conversion processes in polyatomic molecules. *Journal of the Optical Society of America B*, 7(9):1970, 1990.

[86] M. Bellini. Supercontinuum and high-order harmonics: Extreme coherent sources for atomic spectroscopy and attophysics. In P. Hannaford, editor, *Femtosecond Laser Spectroscopy*. Springer, New York, 2005.

[87] M. Ziolek, R. R. Naskrecki, and Karolczakm J. Some temporal and spectral properties of femtosecond supercontinuum important in pump-probe spectroscopy. *OC*, 41:131–134, 1978.

[88] S. A. Kovalenko, A. L. Dobryakov, J. Ruthmann, and N. P. Ernsting. Femtosecond spectroscopy of condensed phases with chirped supercontinuum probing. *Physical Review A*, 59(3):2369–2384, 1999.

[89] D. L. Wang, H. B. Jiang, S. J. Wu, H. Yang, Q. H. Gong, J. F. Xiang, and G. Z. Xu. An investigation of solvent effects on the optical properties of dye ir-140 using the pump supercontinuum-probing technique. *Journal of Optics A - Pure and Applied Optics*, 5(5):515–519, 2003.

[90] A. L. Dobryakov, S. A. Kovalenko, A. Weigel, J. L. Perez-Lustres, J. Lange, A. Muller, and N. P. Ernsting. Femtosecond pump/supercontinuum-probe spectroscopy: Optimized setup and signal analysis for single-shot spectral referencing. *Review of Scientific Instruments*, 81(11), 2010.

[91] H. Zhang, J. Cheng, J. Si, H. Liu, L. Yan, F. Chen, and X. Hou. Superior method for measuring chirp structure of femtosecond supercontinuum pulse. *IEEE Photonics Technology Letters*, 25(3):261–263, 2013.

[92] M. A. Duguay. The ultrafast optical kerr shutter. In E. Wolf, editor, *Progress in Optics*, volume 14 of *Progress in Optics*, pages 161 – 193. Elsevier, 1977.

[93] Ed. Dean, J.A. *Lange's Handbook of Chemistry, 15th Ed. [Online].* McGraw-Hill, New York, 1999.

[94] C. Yaws. *Chemical Properties Handbook: Physical, Thermodynamics, Environmental Transport, Safety & Health Related Properties for Organic &*. Chemical engineering books. McGraw-Hill Education, 1999.

[95] S. Bourquin, R.P. Prasankumar, F.X. K*ä*rtner, J.G. Fujimoto, T. Lasser, and R.P. Salath*é*. High-speed femtosecond pump-probe spectroscopy with a smart pixel detector array. *Optics Letters*, 28(17):1588–1590, 2003.

[96] P. V. Kumar and M. Maroncelli. Polar solvation dynamics of polyatomic

solutes - simulation studies in acetonitrile and methanol. *Journal of Chemical Physics*, 103(8):3038–3060, 1995.

[97] T. Gustavsson, P. Hebert, G. Baldacchino, S. Pommeret, R. Naskrecki, and J. C. Mialocq. Effect of the charge of the solvent probe on the solvated electron. *Journal De Chimie Physique Et De Physico-Chimie Biologique*, 93(1):117–127, 1996.

[98] B. M. Ladanyi and M. Maroncelli. Mechanisms of solvation dynamics of polyatomic solutes in polar and nondipolar solvents: A simulation study. *Journal of Chemical Physics*, 109(8):3204–3221, 1998.

[99] J. L. Dela Cruz and G. J. Blanchard. Reorientation dynamics of rhodamine 640 in normal alcohols: Measurement of the length and time scale of transient local heating in solution. *Journal of Physical Chemistry A*, 105(41):9328–9335, 2001.

[100] D. B. Siano and D. E. Metzler. Band shapes of the electronic spectra of complex molecules. *Journal of Chemical Physics*, 51(5):1856, 1969.

[101] M. A. Kahlow, W. Jarzeba, T. J. Kang, and P. F. Barbara. Femtosecond resolved solvation dynamics in polar solvents. *The Journal of Chemical Physics*, 90(1):151–158, 1989.

[102] P. Meulen, H. Zhang, A. Jonkman, and M. Glasbeek. Subpicosecond solvation relaxation of 4-(dicyanomethylene)-2-methyl-6-(p-(dimethylamino)styryl)-4h-pyran in polar liquids. *Journal of Physical Chemistry*, 100:5367–5373, 1996.

[103] M. Maroncelli. The dynamics of solvation in polar liquids. *Journal of Molecular Liquids*, 57(0):1 – 37, 1993.

[104] E.W. Castner, M. Maroncelli, and G.R. Fleming. Subpicosecond resolution

studies of solvation dynamics in polar aprotic and alcohol solvents. *Journal of Chemical Physics*, 86(3):1090, 1987.

[105] G. Beddard. Molecular photophysics. *Reports on Progress In Physics*, 56:63–171, 1993.

[106] Bernd Wilhelmi. Influence of solvent viscosity on excited-state lifetime and fluorescence quantum yield of dye molecules. *Chemical Physics*, 66(3):351 – 355, 1982.

[107] J. Cataln and C. Reichardt. Is the LE→TICT process in the s1 excited-state of 9,9-bisanthracenyl influenced by the viscosity or the dipolarity of the solvent? *Journal of Luminescence*, 143:635–639, 2013.

[108] L. Onsager. Electric moments of molecules in liquids. *Journal of the American Chemical Society*, 58, 1936.

[109] K. Rotkiewicz and W. Rettig. The TICT excited-state of secondary aromatic-amines. *Journal of Luminescence*, 54(4):221–229, 1992.

[110] G. Kohler, K. Rechthaler, K. Rotkiewicz, and W. Rettig. Formation and stabilization of twisted intramolecular charge transfer states in binary mixed solvents. *Chemical Physics*, 207(1):85–101, 1996.

[111] S. Delmond, J. F. Letard, R. Lapouyade, and W. Rettig. Photoinduced intramolecular charge transfer in planar vs. twisted donor-acceptor terphenyls. *Journal of Photochemistry and Photobiology A - Chemistry*, 105(2-3):135–148, 1997.

[112] X. F. Xu, R. Q. Zhang, Z. X. Cao, and Q. Zhang. Intramolecular charge transfer and photoisomerization of the DCM styrene dye: A theoretical study. *Journal of Theoretical & Computational Chemistry*, 7(4):719–736, 2008.

[113] P. Gedeck and S. Schneider. Numerical self-consistent reaction field study of intramolecular charge transfer in p-(dimethylamino)-benzonitrile. *Journal of Photochemistry and Photobiology A - Chemistry*, 105(2-3):165–181, 1997.

[114] P. van der Meulen, A.M. Jonkman, and M. Glasbeek. Simulations of solvation dynamics using a nonlinear response approach. *Journal of Physical Chemistry*, 102:1906–1911, 1998.

[115] S. J. V. Frankland and M. Maroncelli. Molecular-dynamics simulations of solvent effects on the C-H stretching raman bands of cyclohexane-d(11) in supercritical CO_2 and liquid solvents. *Journal of Chemical Physics*, 110(3):1687–1710, 1999.

[116] R. Tommasini, C. Root, M. Braun, P. Gilch, W. Zinth, and E. Fill. Ultrafast X-ray diffraction studies on Si(111) and DMABN crystals using Cu-K alpha radiation. *Laser-Generated and Other Laboratory X-Ray and EUV Sources, Optics, and Applications*, 5196:311–318, 2003.

[117] S. Techert and K. A. Zachariasse. Structure determination of the intramolecular charge transfer state in crystalline 4-(diisopropylamino)benzonitrile from picosecond x-ray diffraction. *Journal of the American Chemical Society*, 126(17):5593–5600, 2004.

[118] H. J. Moon, J. H. Yi, J. Lee, S. B. Lee, J. H. Lee, and J. S. Chang. Observation of the wavelength shift in the lasing spectrum from a deformed liquid jet. *Journal of the Korean Physical Society*, 33(3):265–269, 1998.

[119] S. Kholova, N. Lebedev, S. Bondarev, V. Knyukshto, A. Turban, V. Mikhailova, and A. Ivanov. Electronic structure of laser dye DCM and its derivatives. *International Journal of Quantum Chemistry*, 104:189–196, 2005.